# A TRIDENT SCHOLAR
# PROJECT REPORT

### NO. 234

"AN ANALYSIS INTO THE UNCERTAINTY OF STIFFENED PANEL
ULTIMATE STRENGTH"

## UNITED STATES NAVAL ACADEMY
## ANNAPOLIS, MARYLAND

| REPORT DOCUMENTATION PAGE | | Form Approved OMB no. 0704-0188 |
|---|---|---|

| 1. AGENCY USE ONLY (Leave blank) | 2. REPORT DATE<br>15 May 1995 | 3. REPORT TYPE AND DATES COVERED |
|---|---|---|

**4. TITLE AND SUBTITLE** An analysis into the uncertainty of stiffened panel ultimate strength

**5. FUNDING NUMBERS**

**6. AUTHOR(S)**

Robert H. Vroman

**7. PERFORMING ORGANIZATIONS NAME(S) AND ADDRESS(ES)**

U.S. Naval Academy, Annapolis, MD

**8. PERFORMING ORGANIZATION REPORT NUMBER** USNA

Trident report; no. 234 (1995)

**9. SPONSORING/MONITORING AGENCY NAME(S) AND ADDRESS(ES)**

**10. SPONSORING/MONITORING AGENCY REPORT NUMBER**

**11. SUPPLEMENTARY NOTES**

Accepted by the U.S. Trident Scholar Committee

**12a. DISTRIBUTION/AVAILABILITY STATEMENT**

This document has been approved for public release; its distribution is UNLIMITED.

**12b. DISTRIBUTION CODE**

**13. ABSTRACT (Maximum 200 words)** The objective of this project is to determine the level of uncertainty associated with the ultimate strength predictions generated by the standard design algorithm used in stiffened panel design of ship structures. This investigation into the modes of ultimate failure of stiffened panels is divided into three approaches: experimental tests of grillages in the USNA Ship Structures Laboratory, analysis of historical stiffened panel test data found in the literature, and non-linear finite element analysis. By comparing the predicted failure stress and deflections between the various methods, the level and areas of uncertainty can be recognized and quantified. Three tests were conducted in the USNA Ship Structures Laboratory. The data from these tests were compared to the historical tests found in the literature. A statistical data analysis was conducted to determine the most important factors influencing the modeling bias associated with stiffened panel ultimate strength. The non-linear finite element analysis of the USNA grillage was able to model the buckling of the panel but could not solve for the post-buckling behavior. Further experimental tests and finite element models need to be tested in order to confirm the validity of some of the predicted values and the overall reliability of the method.

**14. SUBJECT TERMS** stiffened panels; ultimate strength; ship structures; non-linear finite element analysis; reliability-based design

**15. NUMBER OF PAGES**

**16. PRICE CODE**

| 17. SECURITY CLASSIFICATION OF REPORT | 18. SECURITY CLASSIFICATION OF THIS PAGE | 19. SECURITY CLASSIFICATION OF ABSTRACT | 20. LIMITATATION OF ABSTRACT |
|---|---|---|---|
| UNCLASSIFIED | UNCLASSIFIED | UNCLASSIFIED | UNCLASSIFIED |

Standard Form 298 (Rev.2-89)

U.S.N.A. --- Trident Scholar report project; no. 234 (1995)

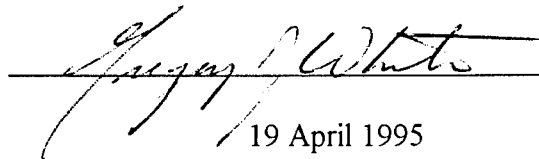# "AN ANALYSIS INTO THE UNCERTAINTY OF STIFFENED PANEL ULTIMATE STRENGTH"

by

Midshipman Robert H. Vroman, Class of 1995
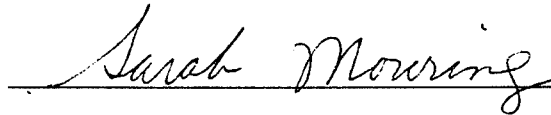United States Naval Academy
Annapolis, Maryland

_(signature)_

Certification of Advisers Approval

Professor Gregory J. White
Department of Naval Architecture, Ocean, and Marine Engineering

_(signature)_

19 April 1995

Assistant Professor Sarah Mouring
Department of Naval Architecture, Ocean, and Marine Engineering

_(signature)_

19 April 1995

Acceptance for the Trident Scholar Committee

Associate Professor Joyce E. Shade
Chair, Trident Scholar Committee

_(signature)_

15 May 95

USNA-1531-2

## Abstract

*The objective of this project is to determine the level of uncertainty associated with the ultimate strength predictions generated by the standard design algorithm used in stiffened panel design of ship structures.*

*This investigation into the modes of ultimate failure of stiffened panels is divided into three approaches: experimental tests of grillages in the USNA Ship Structures Laboratory, analysis of historical stiffened panel test data found in the literature, and non-linear finite element analysis. By comparing the predicted failure stress and deflections between the various methods, the level and areas of uncertainty can be recognized and quantified.*

*Three tests were conducted in the USNA Ship Structures Laboratory. The data from these tests were compared to the historical tests found in the literature. A statistical data analysis was conducted to determine the most important factors influencing the modeling bias associated with stiffened panel ultimate strength.*

*The non-linear finite element analysis of the USNA grillage was able to model the buckling of the panel but could not solve for the post-buckling behavior. Further experimental tests and finite element models need to be tested in order to confirm the validity of some of the predicted values and the overall reliability of the method.*

## Keywords

# Table of Contents

## Acknowledgements

I would like to thank the following people for their assistance with my Trident Project:

# List of Figures

## List of Tables

# Nomenclature

| | |
|---|---|
| a, L | length of panel, length of grillage |
| a/b | panel aspect ratio |
| A | cross sectional area of beam column |
| $A_{tr}$ | transformed area of beam column |
| b | width of panel |
| E | modulus of elasticity |
| $f$ | nodal force vector(matrix) |
| $f_w$ | stiffener flange width |
| h | stiffener height of web |
| I | moment of inertia of beam column |
| $I_{tr}$ | transformed moment of inertia of beam column |
| $k$ | stiffness coefficient matrix |
| $M_o$ | maximum bending moment induced by lateral load without effect of axial load |
| $M_p$ | plastic moment |
| $P_f$ | probability of failure |
| Q | load in limit state equation for panel strength |
| $r_\tau$ | shear reduction factor |
| $R_o$ | experimental strength ($\frac{\sigma_{ULT}}{\sigma_{Ys}}$) |
| S | statistical strength |
| t | thickness of plating |
| $t_f$ | thickness of stiffener flange |
| $t_w$ | thickness of stiffener web |
| T | transformation factor based on secant modulus or tangent stiffness ($\frac{E_s}{E}$) |
| $u, v$ | nodal displacement vector(matrix) |
| $u_x, u_y, u_z$ | nodal displacement in global coordinates |
| $y_f$ | distance from centroidal axis of beam column cross section to mid-thickness of stiffener flange (taken to be negative) |
| $\alpha$ | eccentricity/residual stress factor |
| $\beta$ | plate slenderness ($\frac{b}{t}\sqrt{\frac{\sigma_{Yp}}{E}}$) |
| $\gamma_{st}$ | stiffener area parameter ($A_s$/bt) |
| $\Delta$ | initial eccentricity of stiffener |
| $\Delta_P$ | assumed eccentricity in loading due to shifting of neutral axis after loss of effective plating |

| | |
|---|---|
| $\delta_o$ | deflection induced by lateral load only |
| $\eta_e$ | eccentricity ratio |
| $\epsilon_x, \epsilon_y, \gamma$ | strain (x, y direction), shear strain |
| $\lambda_c$ | column slenderness ($\frac{a}{\rho \pi}\sqrt{\frac{\sigma_{Yf}}{E}}$) |
| $\rho_{tr}$ | transformed radius of gyration |
| $\rho$ | radius of gyration |
| $\sigma_a$ | applied compressive stress |
| $\sigma_{a,T}$ | tripping stress |
| $(\sigma_a)_{cr}$ | critical buckling stress |
| $\sigma_{ay,u}$ | ultimate transverse stress |
| $\sigma_{ax}, \sigma_{ay}$ | transverse and longitudinal applied stress |
| $\sigma_{exp}$ | experimental failure/collapse stress |
| $\sigma_E$ | Euler buckling stress ($\frac{\pi^2 E I}{A a^2}$) |
| $\sigma_F$ | failure stress |
| $\sigma_{PU}$ | maximum stress on load versus end-shortening curve |
| $\sigma_r$ | residual weld stress |
| $\sigma_{ULT}$ | ultimate compressive stress |
| $\sigma_Y, \sigma_{Ym}$ | yield stress, mean yield stress |
| $\sigma_{Yp}, \sigma_{Ys}$ | yield stress of plating, yield stress of stiffener |
| $\sigma_Q$ | "quasi"-yield stress of plate; defined to be the point where the line with a slope equal to Young's Modulus has a strain equal to the yield strain of the plate (eq. 2.7) |
| $\tau$ | shear stress |
| $\phi_{exp}, \phi_{th}$ | experimental, theoretical strength ratio ($\frac{\sigma_{ULT}}{\sigma_{Ym}}$) |
| $\Phi$ | magnification factor due to axial compressive stress (Euler Buckling Stress) |
| $\phi_x, \phi_y, \phi_z$ | nodal rotations about global axes |
| $\phi(x)$ | rotation of stiffener in tripping |
| $\lambda, \mu, \eta, \phi, \zeta, R$ | non-dimensional parameters for standard algorithm (Hughes, 1988) |

## 1.1 Background

Long, slender vessels, such as warships, are designed so that the bottom and deck structures have enough compressive and/or tensile strength to withstand vertical bending of the entire hull. Typically, this type of loading is simplified in design by theoretically placing the ship in a static condition where a ship is balanced longitudinally on a wave in either a hogging or sagging condition (Figure 1.1).
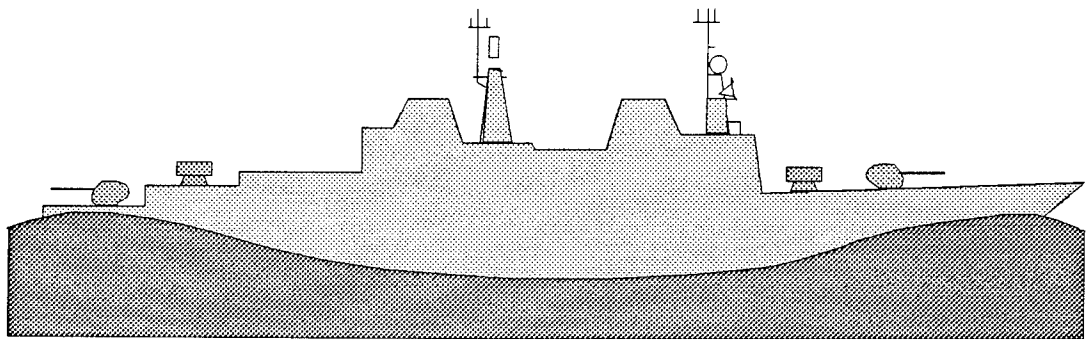
**Excess Weight Amidships  -  Excess Buoyancy on the Ends**

**Compression**

**Tension**
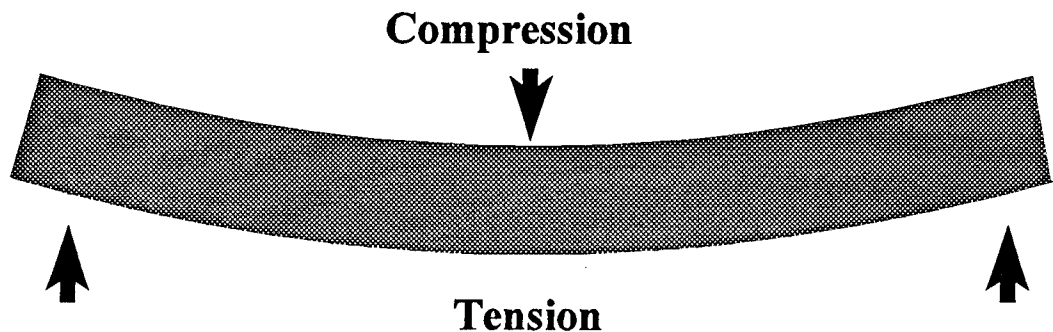
Figure1.1:   Ship balanced on a longitudinal wave placing the hull in a sagging condition.

In order to provide enough longitudinal strength to counteract the hull bending, long vessels, such as warships and tankers, are longitudinally framed. A longitudinally-framed ship typically has closely spaced longitudinal stiffeners and larger, wider-spaced transverse

members attached to the hull and deck plating (Figure 1.2). The stiffeners can be T-beams, angles, bulbs, or flat-bars. The transverse frames are typically T-beam sections. This type of structural configuration is commonly referred to as a cross-stiffened panel or grillage[1]. Cross-stiffened panels are found in decks, hull plating, bottoms, bulkheads, etc. Cross-stiffened panels, much like the ones found in ship structures, are also found in large suspension bridges where they are incorporated into a box-girder with walls constructed of stiffened panels.

Long'l Girder

Keel
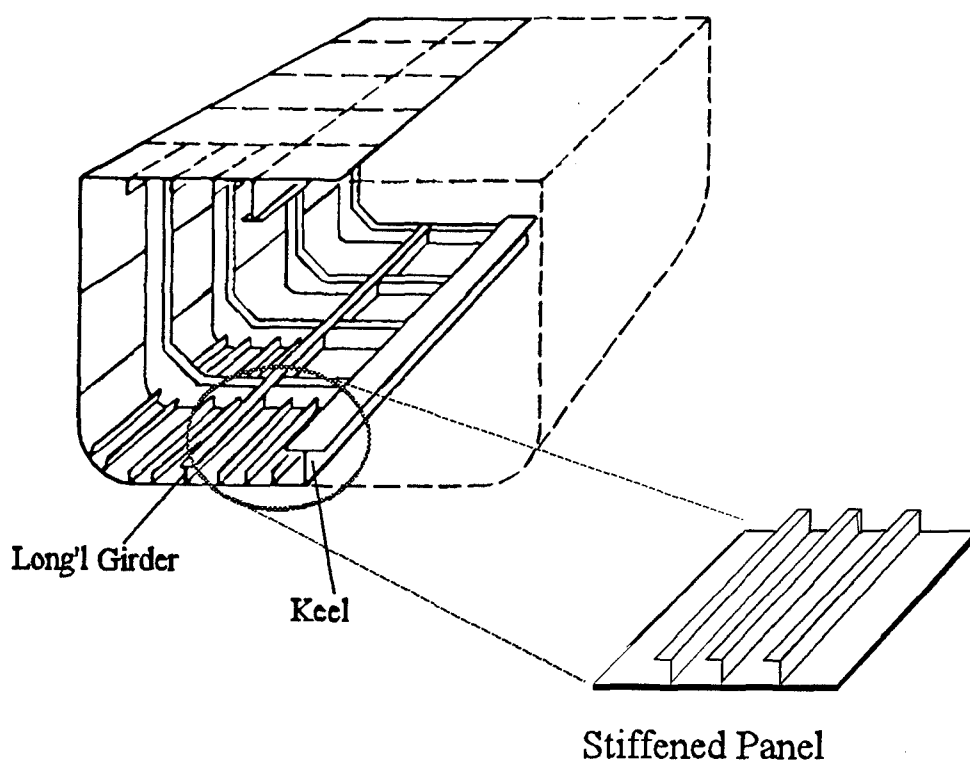
Stiffened Panel

Figure 1.2: Stiffened panel grillage as part of overall ship structure (Hughes, 1988)

---

[1]

Each area of plating between adjacent longitudinal stiffeners and transverse frames will be referred to as a panel.

Research into the longitudinal compressive strength of stiffened panels was first documented when the U.S. Navy began developing its Design Data Sheets (Sweeney, 1933(a) and 1933(b)). These deterministically-based design guidelines, in one form or another, have been the basis for U.S. Navy warship design until now. Interest into stiffened panel design and strength was renewed in the early 1970's following several catastrophic box-girder bridge failures in Europe and Australia (Smith, 1975). These disasters led to the extensive Merrison Committee (1973) report on the, "Inquiry into the Basis of Design and Method of Erection of Steel Box Girder Bridges", which set forth exhaustive design guidelines and justification for design of cross-stiffened panels in civil engineering structures. Today, the design of cross-stiffened panels is important to the future of structural design in both civil engineering and naval architecture, where reliability-based design is poised to replace the older deterministic methods currently in use.

In principle, reliability-based design is quite simple. All variables in the design algorithm for load and strength are treated as random variables. In order to develop and implement reliability-based design codes, the engineer needs statistical information (distribution type and variation) of load and strength. The load, or the seaway, can be statistically characterized by the naval architect. The strength, on the other hand, relies upon two types of uncertainties: statistical and modeling. Statisitcal uncertainty includes such design uncertainties as material yield stress, sizing uncertainty, etc. The statistical uncertainties associated with panel design have been found or are easy to find in the laboratory. Modeling uncertainty is the bias associated with the standard design algorithm

used in stiffened panel design. The modeling uncertainty is the one unknown in the development of a reliability-based design code.

It is usually more likely that the compressive failure stress of a stiffened panel is greater than the yield stress of the material. The structure typically has more strength beyond the structural material's yield stress. As such, the mechanism of collapse in a stiffened panel is a complex, inelastic process. However, the theoretical method of modeling the collapse relies upon many simplified, linear relationships. The accuracy of the standard theoretical algorithm (Hughes, 1988) for stiffened panel design depends upon the ability of these simplified relationships to model a complex process. In this report, the three approaches which endeavor to quantify the modeling bias or uncertainty associated with the standard design algorithm are: experimental tests in the USNA Ship Structures Laboratory testing rig, a parametric historical data analysis, and non-linear finite element analysis (FEA).

## 1.2 Approach

A brief summary of each of the three approaches follow. More detailed descriptions are included in chapters two through five.

1.    The objectives of the experimental tests are twofold: one, to add to the stiffened panel test database and two, to collect data and gain an understanding of the mechanism of stiffened panel collapse in order to validate/invalidate the FEA results. The three tests conducted in the laboratory increased the database of multi-bay tests by over 25% (Smith, 1975).

Three experimental tests were conducted in the USNA Ship Structures Laboratory. Each of the grillages tested comprised of three bays with four longitudinal stiffeners. All of the grillages were tested under axial load only. Extensive pre-test surveys were taken of the initial deformations as well as of the residual weld stresses in the grillage. During the testing, several loadings and unloadings were performed on the grillages to determine the degree of permanent set induced in the panel. Strain gages were monitored on both the plate and the stiffeners. Dial gages and string potentiometers measured deflections during the testing. All three grillages were tested well beyond the level of ultimate load. Post-test surveys of the plate and stiffener deformations were made.

2.     The objective of the historical data analysis is to quantify the level of uncertainty and bias associated with different parameters in the stiffened panel algorithm. This analysis provides statistical parameters which could ultimately be used in reliability-based design. Experimental results are compared to the theoretical predictions and the mean and variance of each of the parameters are found. The statistical mean and variance associated with the modeling bias can be used to determine a partial safety factor to account for the limitations of the theoretical algorithm.

This comparative analysis also demonstrates the relative merits of single-bay versus multi-bay testing, pinned-end versus fixed-end conditions, and the effects of combined lateral and axial loads. With this information, recommendations can be made to design future experimental tests which better emulate what would be seen in reality.

3.     The overall objective of the non-linear finite element analysis (FEA) is to develop a

numerically-based computer method to model the pre and post-buckling ultimate strength behaviors of a stiffened panel. This modeling method could be used to develop a database of tests at much less cost than actual experimental tests. The USNA grillage is modeled and tested using the fintie element program ABAQUS. Then, the FEA results are compared to the experimental results by looking at the grillages' load versus end-shortening, stress, and vertical displacement relationships. Once the results of the USNA model are verified, other tests can be used to validate or invalidate the effectiveness of the finite element method.

## 2.1 The Standard Algorithm

Cross-stiffened panels are typically strong enough that the critical buckling stress $(\sigma_a)_{cr}$ is greater than the yield stress of the material, $\sigma_Y$. As such, the mode of collapse of a stiffened panel under compression is not elastic, but a more complex inelastic process. When designing the structural grillage of a ship, the designer must consider two levels of grillage collapse:

1. Interframe collapse or collapse of individual panels between the transverse frames.

2. Gross structural collapse of the entire grillage. (Hughes, 1988)

Gross structural collapse is a catastrophic failure that involves a large portion of the ship's structure. If the structure of a ship is to fail, it is desirable for it to fail under local, interframe collapse. The members which prevent gross panel buckling and drive interframe collapse in a stiffened panel are the transverse web frames. These deep transverse members provide nearly undeflecting support and stiffness to the entire grillage. Cross-stiffened paneling is typically designed so that it will fail under interframe collapse before any gross panel buckling occurs. Design of cross-stiffened paneling which fails first by interframe collapse is the only mechanism of collapse that will be considered in the following discussion.

Stiffened panel design is performed based upon several modeling assumptions. A typical panel is bound on each end by a transverse structure (frame) that has large stiffness in the plane of the lateral load. On each side, the panel is bound by a structural member that resists bending and axial loading in the longitudinal direction (Figure 1.2). Under

compressive loading, the boundary condition for a panel in a ship's grillage is assumed to be simply supported on all four bounded edges. The simply supported condition permits rotation and, in this case, the ends are free to move in the plane of the grillage. This assumption models the most conservative case.

For longitudinally stiffened panels, there are three types of loading that must be considered. For this analysis, bending moment in the panel is positive when it causes compression in the plating and tension in the stiffener flange. In-plane loads are defined to be positive when in compression (Figure 2.1). An applied lateral load causes a bending moment, $M_o$, and deflection, $\delta_o$. In beam-column theory, these moment and deflection expressions are based upon an ideal column which is assumed to be pin-ended.

1. Lateral load causing negative bending of the panel.

2. Lateral load causing positive bending of the panel.

3. In-plane compression resulting from hull girder bending.

Initial eccentricities are defined to be positive when the deflection is in the direction of the stiffeners. By definition, there can be either positive or negative bending moments due to the lateral load. Intuitively, then, it would seem that there are four modes of collapse -- the plate in either tension or compression or the stiffener in either tension or compression. However, in reality, the plating will never fail in tension because the neutral axis of the combined stiffened plate is so close to the plate (Hughes, 1988). The remaining three possibilities are the modes of panel collapse that will be considered in greater detail.
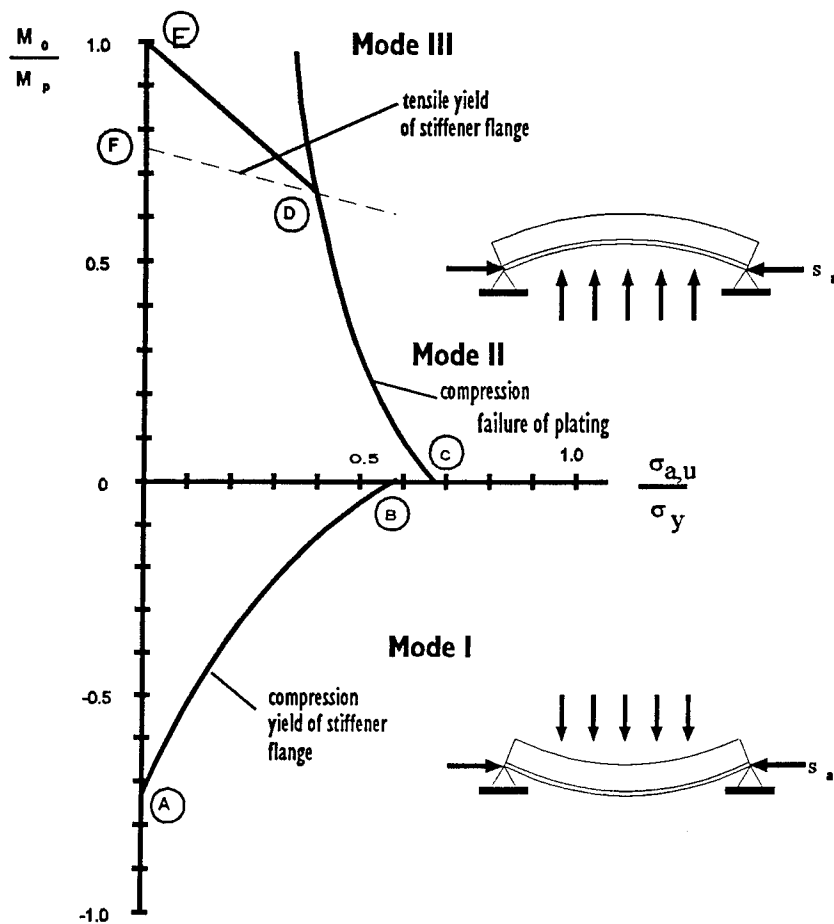
Figure 2.1: Interaction diagram for collapse mechanism of stiffened panels under in-plane and lateral loads (Hughes, 1988)

## 2.2 Mode I: Compression Failure of the Stiffener:

An interaction diagram (Figure 2.1), which relates the relative loading (axial and lateral) to the type of failure, facilitates an understanding of the effects of applied moments

and loading on the panel failure mode. Collapse in Mode I results from compressive failure of the stiffener flange when the plate and stiffener both reach a full plastic moment or when the stiffener flange reaches yield in compression. The lower half of the curve illustrates a Mode I failure as the grillage adopts a half-wave deflection towards the plating (Figure 2.1). This type of deflection in the plate is defined to be negative bending.

When there is considerable axial compressive stress, the stiffener flange approaches its yield stress faster than any other part of the stiffened plate because the negative bending of the plate forces the flange into compression. The tensile stress in the plating is reduced because the stiffener provides most of the stiffened panel's strength. As a result, the stiffener flange yields first while the plate experiences a "delay" until the stiffener failure occurs. At the point of stiffener failure, the panel loses most of its stiffness and the plate alone is unable to compensate for the loss of the stiffener strength. Once the stiffener yields, plate collapse follows quickly. Typically, the actual cause of the failure can be attributed to and observed as a formation of a local, plastic hinge and the resulting lateral deflection and rotation in the stiffener.

Under the axial compression and negative bending of Mode I, the stiffener may also fail by tripping or flexural torsional buckling. Tripping occurs when the stiffener buckles by twisting about its line of attachment to the plating. For a more detailed discussion of tripping, please refer to Appendix A-1, where this mode of failure is explained further. Tripping will be the dominant mode of failure if the magnitude of the stress necessary to cause tripping, $\sigma_{a,T}$, is less than the yield stress of the stiffener, $\sigma_{Ys}$. If $\sigma_{a,T}$ is less than $\sigma_{Ys}$, $\sigma_{a,T}$ replaces the yield stress in all design equations as the failure stress

of the plate or grillage, $\sigma_F$.

$$\sigma_F = MIN[\sigma_Y, \sigma_{a,T}] \qquad (2.1)$$

The process of Mode I failure can be described by the beam column theory. This theory is discussed in greater detail in Hughes (1988), Chapter 14 and the Merrison Committee's Report on Steel Box Girder Bridges (1973), Section 13.1. This equation is expressed as an inequality to represent the interaction between the applied and induced terms on the right-hand side of the equation to the failure stress, $\sigma_F$, described earlier. If the right side is greater than or equal to the failure stress, then the panel will fail in Mode I:

$$\sigma_F \leq \sigma_a + \frac{M_o y_f}{I} + \frac{\sigma_a A(\delta_o + \Delta) y_f}{I} \Phi \qquad (2.2)$$

where, $\Phi$, is the magnification factor due to the axial compressive stress:

$$\Phi = \frac{1}{1 - \frac{\sigma_a}{\sigma_E}} \qquad (2.3)$$

$where, \quad \sigma_E = \dfrac{\pi^2 EI}{A a^2} \quad is\ the\ Euler\ buckling\ stress$

This equation relates the failure mechanism of the beam-column to several components: the applied compressive stress, the stress due to bending, and the stress induced by deflections in the beam-column. The magnification factor accounts for the rapid loss of

strength in the panel as it approaches its yield point.

Hughes (1988), in his discussion on Mode I failure, derived several non-dimensional parameters for analyzing the stiffened panel in design in order to facilitate a solution for ultimate strength. These factors are obtained from the beam-column theory and are simple derivatives of the same: $\eta$ is essentially a restatement of the stress induced by the deflections, $\mu$ accounts for the stress due to bending, the $\lambda$ term accounts for the applied compression and magnification factor, and R is the strength ratio.

$$R = \frac{(\sigma_{a,tr})_{ult}}{\sigma_F} \qquad \eta = \frac{(\Delta + \delta_o)y_{p,tr}}{\rho_{tr}^2}$$

$$\mu = \frac{M_o y_{p,tr}}{I_{tr}\sigma_F} \qquad \phi = \frac{1}{1-\lambda^2 R} \tag{2.4}$$

$$\lambda = \frac{a}{\pi\rho_{tr}}\sqrt{\frac{\sigma_F}{E}} \qquad where: \quad \rho_{tr} = \sqrt{\frac{I_{tr}}{A_{tr}}}$$

When expressed in this non-dimensional form, equation(2.2) must be treated as an equality to be factored as a quadratic equation. Hughes (1988) suggests a solution for the applied compressive stress, $\sigma_a$, as R, a strength ratio. Expressed in other terms, his solution is:

$$R = \frac{\zeta}{2} - \sqrt{\frac{\zeta^2}{4} - \frac{1-\mu}{\lambda^2}} \qquad where: \quad \zeta = 1 - \mu + \frac{1+\eta}{\lambda^2} \tag{2.5}$$

The interactive collapse curve, shown in Figure 2.1, relates the amount of applied

compressive stress to the applied lateral load and indicates how they affect collapse in the

panel. The lower half of the diagram shows negative bending and what would

characterize a Mode I failure. As the amount of bending increases, the applied

compression necessary to cause failure in the panel decreases. If the mechanism of

collapse is tripping, the curve is slightly closer to the vertical axis.


2.3 Mode II Collapse: Compression Failure of the Plating

When the stiffened panel is subjected to a combination of in-plane compression and

small to moderate positive bending moment, Mode II failure will typically occur. Mode II
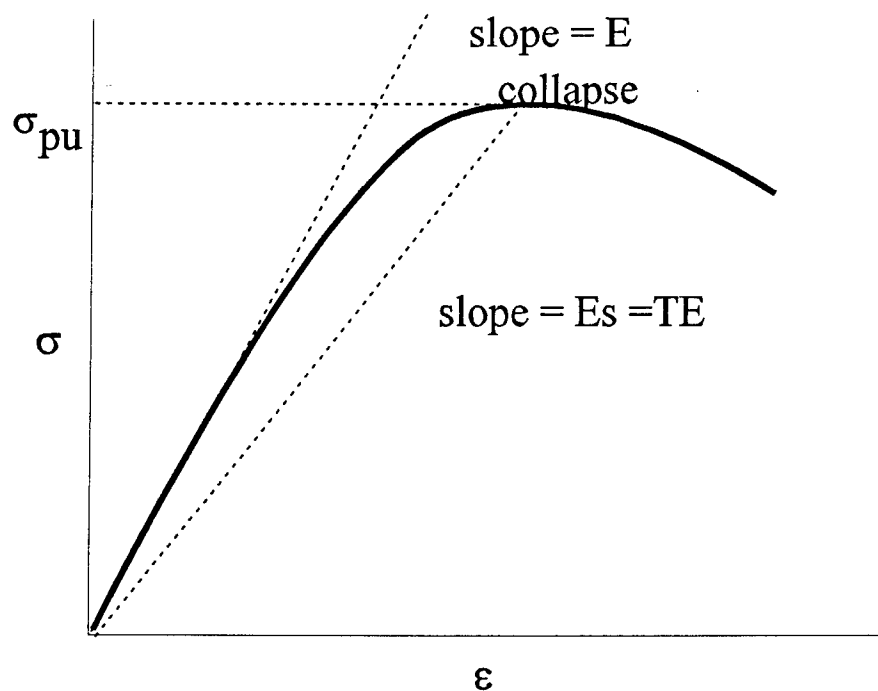


Figure 2.2: Hypothetical stress-strain curve showing the loss of panel strength prior to the ultimate stress point

failure is distinguished by compression failure of the plate (Figure 2.1). If the behavior of the stiffened plate was elastic throughout a loading sequence, the beam-column theory would be an adequate theoretical description of the panel collapse. However, as was stated earlier, the failure of a stiffened panel is usually a complex, inelastic process. On a typical compressive stress versus strain curve, the relationship becomes nonlinear before collapse occurs (Figure 2.2). The slope of the curve begins to decrease before the plate reaches failure. In contrast, on a typical tensile test of a specimen the plastic yield stress is usually not the ultimate or maximum tensile stress. The average stiffness over the range of loading can be described by the secant modulus, $E_s$ = TE. The secant modulus is the slope of the line connecting the origin to the point of plate failure. The secant modulus is given as (Chatterjee and Dowling, 1976):

$$T = \frac{E_s}{E} = 0.25 \ (2 + \xi - \sqrt{\xi^2 - \frac{10.4}{\beta^2}} \ ) \qquad \xi = 1 + \frac{2.75}{\beta^2} \qquad (2.6)$$

For collapse analysis, the behavior of the plate is only necessary at the point of failure.

Chatteerjee and Dowling (1976) found that for panels typically found in ship structures, the ultimate strength curve is similar to the curve for T, the transformation factor (equation (2.6)). The relationship they derived between the two curves was:

$$\frac{\sigma_{pu}}{\sigma_{Yp}} = (T - 0.1) \qquad (2.7)$$

Like the Mode I failure, Mode II relies on several simplified engineering

relationships to describe a complex collapse behavior (equation (2.2)). Again, beam column theory can be used to develop a collapse prediction. The one major difference in the expression is the introduction of a transformed section to account for the collapse behavior of the plate. The transformed section is only needed at one point in the collapse history, its failure point. The resulting expression is:

$$\sigma_F \le (\sigma_{a,tr})_{ult} + \frac{M_o y_{p,tr}}{I_{tr}} + \frac{(\sigma_{a,tr})_{ult} A_{tr}(\Delta + \delta_o) y_{p,tr}}{I_{tr}} \Phi \tag{2.8}$$

Again, the design relationship is a comparison (see equation (2.2)) between a material influenced factor and a geometry driven factor. This specific aspect of the design analysis will be discussed later.

The beam-column theory and its related derivative equations account only for longitudinal strength. A panel's transverse strength will have some effect on its ultimate strength, especially under large values of shear possibly attributable to bending and large compressive stresses. In fact, large in-plane shear stresses ($\tau$) tend to lower the strength of a panel in longitudinal compression. Failure due to shear in stiffened panels typically used in ship structures does not commonly occur because of the relatively low width to thickness ratio. However, shear will cause the panel to yield at a lower load. One way to account for this strength reduction due to shear is to introduce a reduced yield stress, $r_\tau \sigma_Y$ (Hughes, 1988).

$$r_\tau = \sqrt{1 - 3\left(\frac{\tau}{\sigma_{Yp}}\right)^2} \tag{2.9}$$

Similarly, if a compressive or tensile stress is applied transversely, there will be an effect on the ultimate collapse failure. The relationship between transverse and longitudinal stress, $\sigma_{ax}$ and $\sigma_{ay}$, depends on plate slenderness, $\beta$, and aspect ratio, a/b. The stouter the plate, the more strength that plate will exhibit before failure. As a result, the design equation accounts for the most conservative case, the slender plate. See Hughes (1988), Chapter 12 for more information.

If a panel is loaded axially in two orthogonal directions, both loading directions must be considered and are, in fact, significant to the strength of the panel. The primary stress direction, by definition, need not be in the direction of the greatest stress or in the longest length along the panel. It should be noted, however, that the interaction between the two loads is dependent mostly upon plate slenderness and aspect ratio. Therefore, the choice of primary stress direction will have an effect on the outcome of the resultant load[1]. Accounting for the transverse in-plane compression and in-plane shearing stress, the failure stress for the plating can be expressed as (Hughes, 1988):

$$\sigma_F = \frac{T\text{-}0.1}{T}\sigma_{Yp}\left(1-\frac{\sigma_{ay}}{\sigma_{ay,u}}\right)\sqrt{1-3\left(\frac{\tau}{\sigma_{Yp}}\right)^2} \qquad (2.10)$$

The term for $\sigma_F$ in Equation (2.10) must be less than the sum of the terms in Equation (2.8) in order for the panel not to yield.

---

[1] For all of the tests conducted in the USNA Ship Structures Laboratory and all of the tests found in the literature, no tests considered or tested the effects of a secondary loading direction. The addition of a secondary loading direction complicates the setup of the testing rig and poses unique testing problems beyond the scope of this project.

To account for the inelastic effect of the panel as it passes its yield point, each section of the beam-column is treated as a transformed section. The creation of a transformed section attempts to mirror the behavior of a plate in compression as the result of positive bending reaches and then passes its yield point. The secant modulus term, T, describes the material behavior after the specimen reaches its yield stress; the slope of the stress-strain curve begins to decrease continually. Instead of treating the plate flange in the beam column as a different material with a different Elastic Modulus, E, it becomes easier to treat the section with a loss of *effective* width in the flange. Hence, as the plate loses more effective width, it is also losing strength. The transformed section is derived by multiplying the original plate width by the transformation factor, T, to obtain an effective width. The properties of the transformed section are used in determining the panel's ultimate stress. The ultimate stress of the panel is defined by Hughes (1988) as:

$$R_{II} = \frac{(\sigma_{a,cr})_{ult}}{\sigma_F} = \frac{\zeta}{2} - \sqrt{\frac{\zeta^2}{4} - \frac{1 - \mu}{\lambda_c^2}} \qquad (2.11)$$

where the terms of this equation are:

$$\zeta = 1 - \mu + \frac{1+\eta}{\lambda_c^2} \qquad \lambda_c = \frac{a}{\pi \rho_{tr}} \sqrt{\frac{\sigma_F}{E}}$$

$$\mu = \frac{M_o y_{p,tr}}{I_{tr} \sigma_F} \qquad \eta = \frac{(\delta_o + \Delta) y_{p,tr}}{\rho_{tr}^2} \qquad (2.12)$$

$$\rho_{tr} = \sqrt{\frac{I_{tr}}{A_{tr}}} \qquad \eta_p = \frac{\Delta_p y_{p,tr}}{\rho_{tr}^2}$$

Ultimately, the failure stress, $\sigma_F$, is needed to find if the panel meets the design criteria. In order to accomplish this, the collapse stress, $\sigma_{a,u}$, must be calculated:

$$\sigma_{a,u} = (\sigma_{a,tr})_{ult} (\frac{A_{tr}}{A}) \qquad (2.13)$$

From the collapse stress, the failure stress is found to be (Hughes, 1988):

$$\sigma_F = \frac{\sigma_{a,u}}{R_{II}} (\frac{A}{A_{tr}}) \qquad (2.14)$$

## 2.4 Mode III - Combined Failure of the Stiffener and Plating

When the bending moment, $M_o$, becomes sufficiently large, the Mode II model of ultimate strength behavior does not describe the collapse properly. The large bending moment can cause a large tensile stress in the flange of the stiffener. The effect of the in-plane compressive stress reduces the tensile stress in the stiffener; however, if the bending

moment, $M_o$, gets large enough to negate this effect, there will be simultaneous tensile yielding in the stiffener flange and compressive failure in the plating. The point at which these simultaneous modes of failure begin to occur is indicated on the interaction diagram of Figure 2.1 as point D . For pure bending, the stiffener can yield throughout the whole section. When this occurs, the height of the effective neutral axis moves toward the plating. Ultimately, the effective neutral axis may enter the plating and place the plate partly in tension. The effect of tensile stress in the plating will allow it to absorb the full value of the compressive yield stress. In short, the panel will not exhibit collapse behavior until it reaches a plastic hinge condition (see Appendix A-2 for a discussion on the formation of a plastic hinge).

The analytical solution for Mode III is complicated by the interactive nature of the simultaneous stiffener and plating failure. The path that the interaction curve follows from the point where the simultaneous failure begins to occur to the point where the applied bending moment is equal to the full plastic moment is actually convex upwards. For simplification, this report assumes a more conservative case where the path followed by the collapse is a straight line (Figure 2.1), represented as DF. The method of finding this simultaneous failure point requires the solution of an equivalent beam-column theory expression for failure in the stiffener flange (Hughes, 1988):

$$-\sigma_{ys} = (\sigma_{a,tr})_{ult} + \frac{M_o y_{f,tr}}{I_{tr}} + \frac{(\sigma_{a,tr})_{ult} A_{tr}(\delta_o + \Delta) y_{f,tr}}{I_{tr}} \Phi + \frac{(\sigma_{a,tr})_{ult} A_{tr} \Delta_p y_{f,tr}}{I_{tr}} \qquad (2.15)$$

The yield stress in the stiffener is negative to represent the tensile yield stress of the

stiffener flange. Again, for ease in solving for $(\sigma_{a,tr})_{ult}$, the following non-dimensional

parameters are used:

$$R_{DF} = \frac{(\sigma_{a,tr})_{ult}}{-\sigma_{Ys}} \qquad \lambda_{DF} = \frac{a}{\pi\,\rho_{tr}}\sqrt{\frac{\sigma_{Ys}}{E}} \qquad \eta_{DF} = \frac{(\Delta + \delta_o)y_{f,tr}}{\rho_{tr}^2}$$

$$\eta_{p,DF} = \frac{\Delta_p y_{f,tr}}{\rho_{tr}^2} \qquad \mu_{DF} = \frac{M_o y_{f,tr}}{I_{tr}(-\sigma_{Ys})} \qquad \phi_{DF} = \frac{1}{1 + \lambda_{DF}^2 R_{DF}}$$

$$(2.16)$$

Equation (2.8) is the same as equation (2.15) with the magnification factor term amended

to account for the tensile stress present in the stiffener. It should also be noted that the

distance to the flange, $y_{f,tr}$, replaces the distance to the plating, $y_{p,tr}$ (in Equation 2.8) and

as a result, will be a negative value. Consequently, the values of $\eta_{DF}$ and $\eta_{P,DF}$ also will be

negative. Since the failure stress is negative, the strength ratio R will also be negative.

Solving for $R_{DF}$ yields:

$$R_{DF} = \frac{\zeta_{DF}}{2} \pm \sqrt{\frac{\zeta_{DF}^2}{4} - \frac{1 - \mu_{DF}}{(1 + \eta_{p,DF})\lambda_{DF}^2}}$$

$$(2.17)$$

$$where: \quad \zeta_{DF} = \frac{1 - \mu_{DF}}{1 + \eta_{p,DF}} + \frac{1 + \eta_{p,DF} + \eta_{DF}}{(1 + \eta_{p,DF})\lambda_{DF}^2}$$

The solution delineated above finds the level of stress at which the stiffener will

fail. It is necessary also to find the point where a Mode II failure occurs. Once this point

is found, the solution for the failure point at $(M_o)_D$ and $(\sigma_{a,u})_D$ can be solved iteratively,

such that:

$$R_{II}\sigma_F = -R_{DF}\sigma_{Ys} \tag{2.18}$$

The equation for the Mode III collapse line (where $\sigma_{a,u}/\sigma_Y=0$; $M_o/M_p=1$) can be expressed as:

$$(\frac{\sigma_{a,u}}{\sigma_Y})_{III} = \frac{M_P-M_O}{M_P-(M_O)_D} \frac{(\sigma_{a,u})_D}{\sigma_Y} \tag{2.19}$$

where $(\sigma_{a,u})_D = \sigma_F(\frac{A_{tr}}{A})R_{II}$ or $(\sigma_{a,u})_D = -\sigma_{Ys} \cdot (\frac{A_{tr}}{A})R_{DF}$

After solving for the Mode III equation line and plotting it on the interaction diagram, the feasibility of a Mode III failure can be determined.

Mode III collapse is not common for typical ship grillages. In most cases, the only way a stiffened plate may fail under a Mode III failure is when there is significant lateral load (large bending moment) applied to the grillage. It will be shown later that the application of a lateral load may not cause a Mode III failure, but instead, effectively strengthen the grillage for some time. Furthermore, for some ship panel geomtries and initial conditions, a Mode III collapse cannot be found or predicted by an analytical solution of this type.

## 3.1 USNA Ship Structures Laboratory Testing Rig

The grillage test fixture used in the USNA Ship Structures Laboratory is a specially designed rig developed by the Naval Surface Warfare Center at Carderock, Maryland. The design is based upon an earlier design used at Rhor Marine Inc., in San Diego, California, under NSWC sponsorship. The fixture is designed to apply both axial and lateral loads to a grillage. The axial load simulates the loading that would result from bending of a ship's hull. The application of a lateral load simulates a hydrostatic load on a ship's shell. A schematic diagram of the test fixture is presented in Figure 3.1.

Axial compression is applied to the grillage by a loading head which is pushed by a hydraulic cylinder. The hydraulic cylinder is attached to a fixed head. The hydraulic loading mechanism is capable of applying 1.513MN[1] (340,000 lbs) in compression. The end opposite the loading head is called the reaction head. The test specimen is bolted to both the reaction and the loading head, applying fixed end conditions at both ends of the grillage. The reaction and loading heads are able to withstand 96,075.7 N-m (850,000 in-lbs) of moment. This moment, which resists the deflected shape's tendency to rotate, constrains the ends in a fixed-end loading condition. The compression applied to the structure tends to push the reaction head and fixed head away from each other. The tension beams, which run longitudinally along the length of the fixture, provide the necessary resistive tension in the structure to allow it to be self-reacting. The grillage

---

[1]

All experiments were performed using the U.S. Customary system of measurement. All measurements presented in this report are given in U.S.C.S. and S.I. units. Most graphs are in S.I.
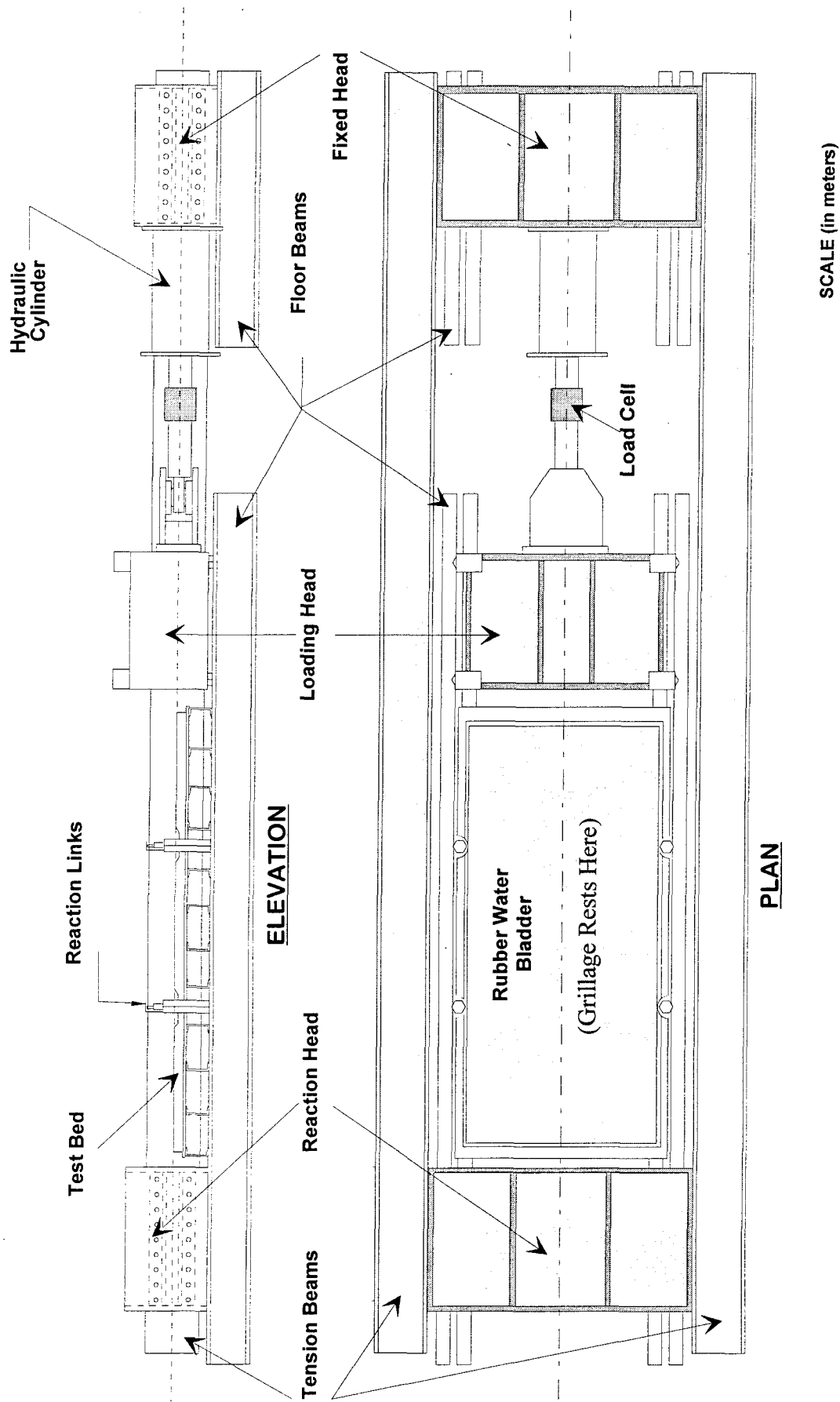
32

Figure 3.1: USNA Ship Structures Laboratory testing rig.

specimen is attached to four reaction links located at the ends of the transverse frames in the stiffened panel. These reaction links simulate the surrounding structure of the ship and also allow the ends of the transverse frames to translate and rotate longitudinally and transversely, but not move in the vertical plane nor rotate about the vertical axis. Each of the four reaction links is able to withstand 122.4 kN (27,500 lbs.) of loading.

The lateral pressure is applied to the test specimen by a rubberized water bladder which pushes against a steel pressure bed. The rubber diaphragm of the bladder pushes against the panel with a pressure equal to the water pressure in the bladder. The fixture is able to apply up to 276 kPa (40 psi) over a 0.94 m by 2.39 m (37" by 94") area. The four reaction links attached to the ends of the transverse webs of the test specimen also simulate the surrounding structure of the ship in the case of lateral pressure loading.

### 3.2 Load Control:

Load control is managed by a personal computer operating station. The PC Integrated Control Management (PCICM) System Model X8700, developed by Test Systems & Simulation, Inc. (TS&S), is able to monitor ram head position through a feedback control system. The PCICM acts as an interface between the user, parallel and serial communication, analog subsystem, and the TS&S Digital Closed Loop (DCL) Servo Controller. The X8700 system enables the user to set up DCL parameters for force or motion control. The DCL valve operates directly from the output of the PCICM. Communication is through an RS485 2-wire balanced serial bus. The DCL servo controller valve is capable of a supply pressure of 20,685KPa (3000 psi), with a minimum

pressure of 1380 KPa (200 psi). The DCL servo controller valve has a hysteresis of less than 2% and a threshold of less than 4%.

The hydraulic pressure necessary to produce loading in the hydraulic system is generated by a 7.457 kW (10Hp), 1745rpm, 440VAC, horizontal, centrifugal, positive displacement pump. The operating PC sends a signal with the desired head position from the servo synchro transmitter to a servo amplifier. The power transfer valve determines whether the head should be moved forward or backwards. The feedback synchro on the load head sends a feedback signal back to the servo amplifier and PC which tells the head whether to continue moving or to stop.

The magnitude of the lateral load applied by the water bladder is not monitored or controlled by the PC system. During testing, the pressure being applied must be vigilantly monitored on the data acquisition system through pressure transducers and by monitoring pressure gages in the supply water lines. In order to account for any variation in the pressure, there are needle valves in the water lines which allow the operator to maintain a constant lateral load.

## 3.3 Data Acquisition

The data acquisition system used in these experiments allows several types of data to be gathered with one system. Two NEFF 470 control panels convert the data signals from the various measuring instruments into a format usable by the computer system. Each NEFF 470 panel is capable of accommodating 64 channels. For the test setup, 124 channels are available for data acquisition and one card (four channels) is allocated for the

load cell.

The PC-based data acquisition program was developed by NSWC. This program is capable of acquiring information from strain gages, potentiometers, pressure transducers, and load cells. For the tests performed at USNA, only strain gages, string potentiometers, and load cells were used. Calibration of the gages and resistors is achieved by an on-screen monitor that displays the calibration values as each of the shunt resistors is manually adjusted. Moreover, the setup of the data system allows the characteristics of each individual strain gage or potentiometer (i.e. resistance) to be entered by the user.

The strain gages used in these tests were Micro-Measurements linear precision strain gages (model numbers CEA-13-250UW-350 and CEA-06-250UW-350). Each of the gages was attached with M-bond AE-10, a 100% solid epoxy system. This material has a 6% elongation capability and is essentially creep free. Each of the wires connecting the NEFF system to the individual strain gages was the same length. This reduces the error attributed to variable wire resistance. The key gage locations used for data analysis are shown in Figure 3.2. These gages are in the center panel of the bay between the transverse frames. At the longitudinal center of the panel, gages 35, 37, and 39 on the bottom of the plate, correspond to the gages 36, 38, and 40 at the top of the plate. Gages 32, 33, 34 and 42, 43, 44 on the top of the two centermost stiffener flanges are located at the longitudinal center of the grillage.
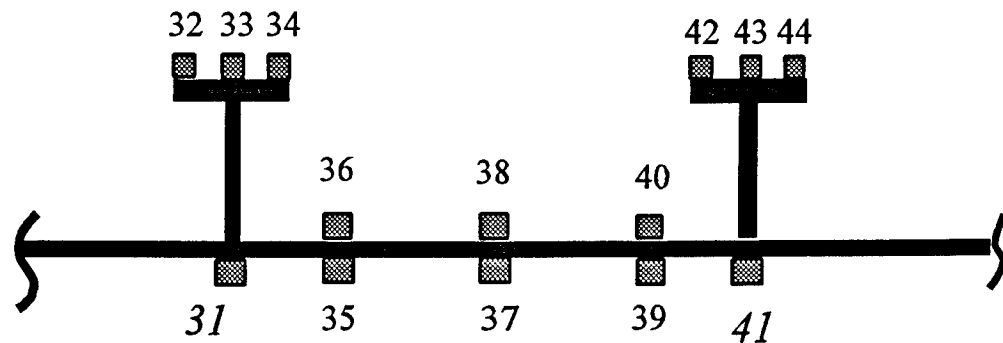
Figure 3.2: Major strain gage locations, viewed from loaded end (aft) looking towards the reaction head (forward). All gages in centerline row. Data from gages 31 and 41 are not used for this analysis.

The linear string potentiometers used to measure end shortening and panel displacements are scanned by the data acquisition computer every second during the loading and unloading processes. These potentiometers are attached to the NEFF 470 which scans and saves the data. The linear potentiometers used for this experiment worked well in one direction but showed a significant delay and error in unloading. After the first unloading, the data obtained from these potentiometers are suspect. The visual dial gages used to measure deflections did not exhibit any similar errors in unloading. However, the limitations of a visually-read analog dial gage are obvious when compared to computer-scanned potentiometers. Future tests need to include a more reliable method of displacement measurement. One such method might include the use of digital dial gages with an output fed into the NEFF 470 system.

The data acquisition program is a useful tool during testing. While acquiring data,

the acquisition program is capable of scanning each individual data point into a file or

scanning the entire test run into one large file. For these tests, the latter is preferred. Real

time analysis of the loading and the stress/strains in the grillage facilitates the

determination of the loading and unloading points during the testing. In addition, the

graphing function on the system aids in determining the linearity (or non-linearity) of

variables such as the loading/unloading of the grillage.

## 3.4 Details of the Test Structure

The configuration of the three steel USNA test grillages were planned to model a

typical main deck of a generic warship (Figure 3.3). The test grillages were nominally

identical structures (Table 3.1). In order to maintain relative uniformity between the test

grillages, the steel was carefully selected from a large batch to all exhibit similar strengths,

mean thicknesses, etc. The grillages were all constructed at NSWC. The quality of

construction in each of these grillages was intended to emulate normal shipyard standards.

However, the relatively small size of the grillages and the nearly ideal welding conditions

in the welding shop, yielded a finished product generally better than shipyard welding

standards.

| Table 3.1 -Grillage Dimensions (reported by NSWC) | | | | | | | |
|---|---|---|---|---|---|---|---|
| | | plating | stiffener | | | | |
| Griilage # | length of bay | thickness | width of bay | height of web | flange width | web thickness | flange thickness |
| | a | t | b | h | $f_w$ | $t_w$ | $t_f$ |
| 0494 | 914 (36.0) | 4.8 (0.1875) | 229 (9.0) | 71 (2.799) | 47 (1.844) | 2.9 (0.114) | 4.3 (0.171) |
| 0894 | 914 (36.0) | 4.8 (0.1875) | 229 (9.0) | 71 (2.799) | 47 (1.844) | 2.9 (0.114) | 4.3 (0.171) |
| 1094 | 914 (36.0) | 4.8 (0.1875) | 229 (9.0) | 71 (2.799) | 47 (1.844) | 2.9 (0.114) | 4.3 (0.171) |
| all measurements in mm. (inches); values expressed are for center bay | | | | | | | |

The grillages were designed to have the four longitudinal stiffeners pass through cutouts in the transverse frames. The connections between the stiffeners and the frame web are provided by small clips that are butt-welded to each side of the stiffener and lap-welded to the transverse web frame. Jigging was not used during the welding process of the T-stiffeners. One important design enhancement to the grillage selection was the choice of plating. In order to ensure that failure occurs first in the center bay, the plating in the two outer bays was designed to be slightly thicker. The plating in the center bay is 4.7625 mm. (3/16") thick steel. In contrast, the plating on the ends is 6.35 mm. (1/4") thick, but all of the other scantlings (structural members) are nominally identical. The transition between plate thicknesses occurs 25.4 mm from the transverse web frame towards the middle of the grillages. This is shown in Figure 3.3. Table 3.1 details the geometry of the structure.

The materials used to construct these grillages were all ordinary mild steel. This is the type of steel commonly used in most warship construction. Compressive coupon tests

were conducted at NSWC. The plates of different thicknesses showed different strength characteristics in yield and ultimate compressive strength. The strength of the stiffeners also varied from the plating. The results of the coupon tests are given in Table 3.2.

| Table 3.2 - Material Properties | | |
|---|---|---|
| Grillage # | mean yield stress(stiffener) | mean yield stress(plating) |
| 0494 | 383 kPa (55.5 ksi) | 305 kPa (44.2 ksi) |
| 0894 | 383 kPa (55.5 ksi) | 305 kPa (44.2 ksi) |
| 1094 | 383 kPa (55.5 ksi) | 305 kPa (44.2 ksi) |

Measurements of the residual weld stresses were taken at three phases of the fabrication by NSWC: when the plate was first cut with no welding, when grillage was tack-welded together, and when fabrication was complete. All measurements were taken with a Whitmore gage with a nominal gage length of 254 mm. (10"). A separate temperature compensation plate was maintained as a control. Measurements were taken on the plate side and on the stiffener side at equally spaced intervals of 70 mm. (2 3/4") starting at 19 mm. (3/4") from the edge. Residual stresses were only evaluated at the longitudinal center of the grillage. For purposes of this analysis only the center bay residual stresses were considered; at the ends, the residual stresses were higher because there was no tacking to keep the plate from moving during welding. Figure 3.4 shows the residual weld stress measurements. Table 3.3 summarizes the average residual weld stresses in the center bay.

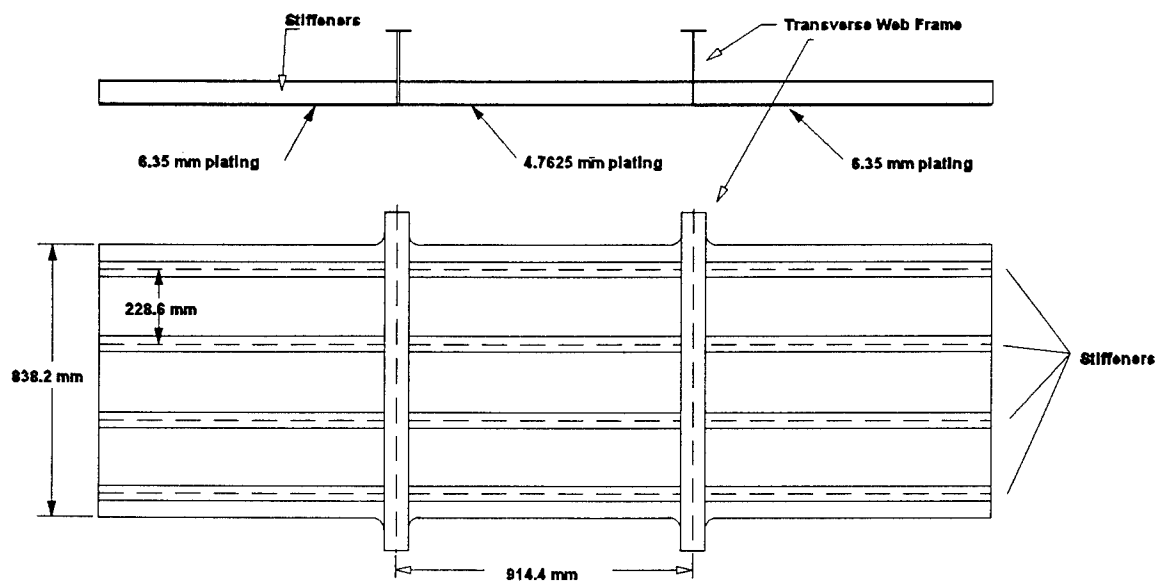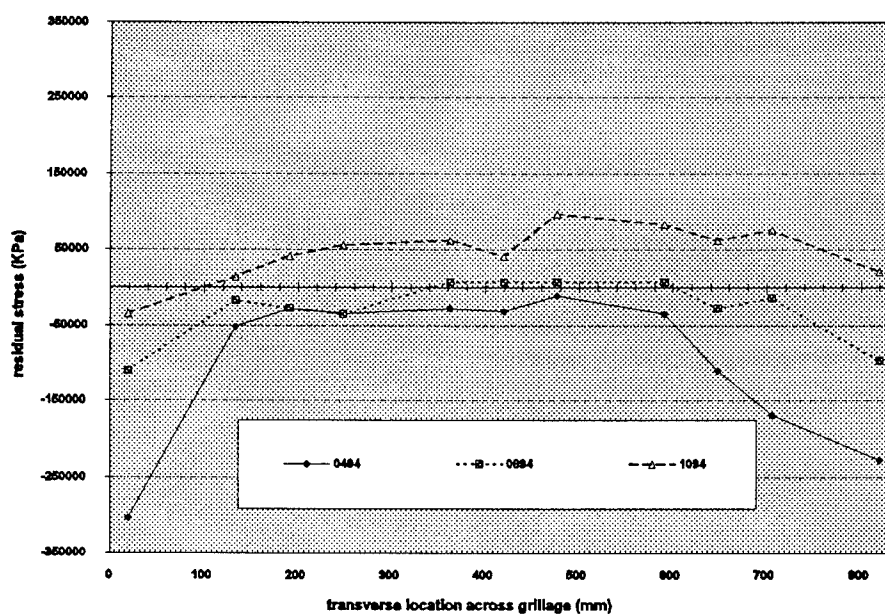| Table 3.3 - Residual Weld Streses as measured by NSWC (avg. of plate and stiffener) | |
| --- | --- |
| Grillage | residual stress / plate yield stress ($\sigma_r/\sigma_{Yp}$) |
| 0494 | 0.059 |
| 0894 | 0.014 (in tension) |
| 1094 | 0.231 (in tension) |

Figure 3.3: USNA Grillage.



Figure 3.4: Residual weld stress in plate (average axial only; bending stresses due to welding were found to be negligible).

## 3.5 Test Procedure

The grillage was placed into the fixture as level as possible. This reduces any effects of load eccentricities or induced bending. All four corners were surveyed and the vertical position of each corner was controlled by adjusting the length of the reaction link turnbuckle. The grillage was positioned vertically so that the line of action of the center of the hydraulic cylinder was midway between the elastic and plastic neutral axes of the grillage center bay section. Loading the grillage at the elastic neutral axis would work well with small loads. However, as the beam-column stress approaches the plastic hinge condition, the neutral axis moves into the plating. The inaccuracies induced by this correction can be reduced by increasing the number of bays in the test grillage (increase number of frames) as well as by loading between the plastic and neutral axes.

Once the grillage was levelled and attached to the testing rig, the initial deformations were surveyed at two-hundred sixty-six locations; twenty-four longitudinal points were measured along each of the stiffeners and seventy-two points were taken in the center bay. Table 3.4 details the maximum deflections measured in each of the grillages.

| Table 3.4 - Initial Deformations | | |
|---|---|---|
| Grillage # | stiffener | plating |
| 0494 | .0030556 | .0030303 |
| 0894 | .0058333 | .0045455 |
| 1094 | .0033333 | .0024242 |
| stiffener normalized by frame spacing (a); plating normalized by plate width(b) | | |

All three grillages were tested to collapse. As is shown in the time history plot of the loading sequence from test 1094 (Figure 3.5), several loading and unloadings of the grillage were performed. This procedure aids in determining the elasticity of the materials in the grillage (whether it has yielded or not) and also the magnitude of permanent set after certain loads are applied. The load versus end-shortening plot shows how yielding and material elasticity can be ascertained from monitoring these relationships during testing and during data analysis (Figure 3.6). After the first loading, all subsequent loading/unloadings show an offset loading line with nominally the same slope. Note that in this graph, some of the hysteresis from the string potentiometers was removed to facilitate a determination of the linearity of the load versus end-shortening relationship in the grillage. Permanent set is defined to be the amount a plastic deformation present in a material after it is stressed and unloaded. By comparing the vertical deflections from visual dial gages and string potentiometers at a common unloading point to the same point prior to loading, the magnitude of permanent deformation present at each unloading point can be determined (Figure 3.7). Although small amounts of permanent set may have only small effects on strength, any permanent set can be particularly undesireable in the outer shell of a ship where resistance may be greatly influenced by anomalies in the underwater hullform.
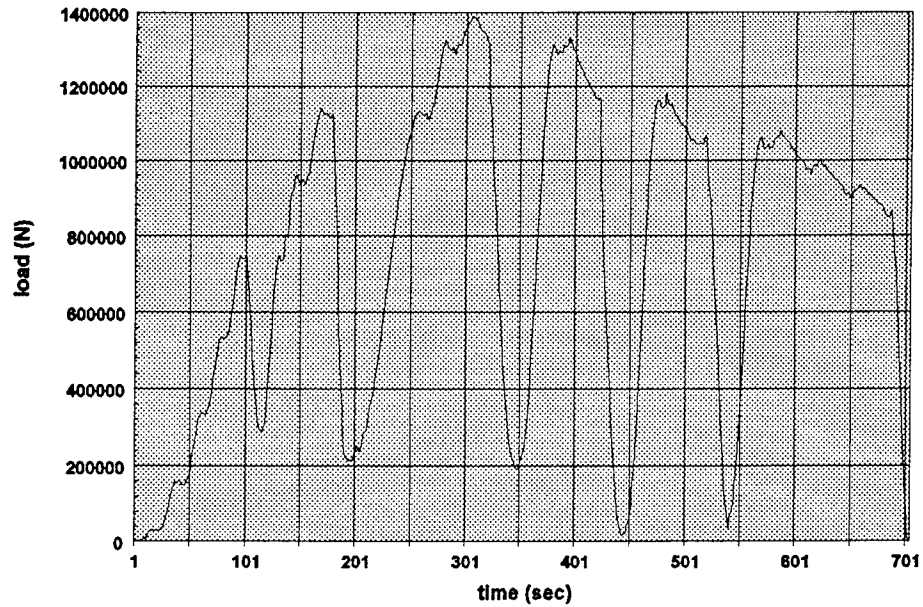
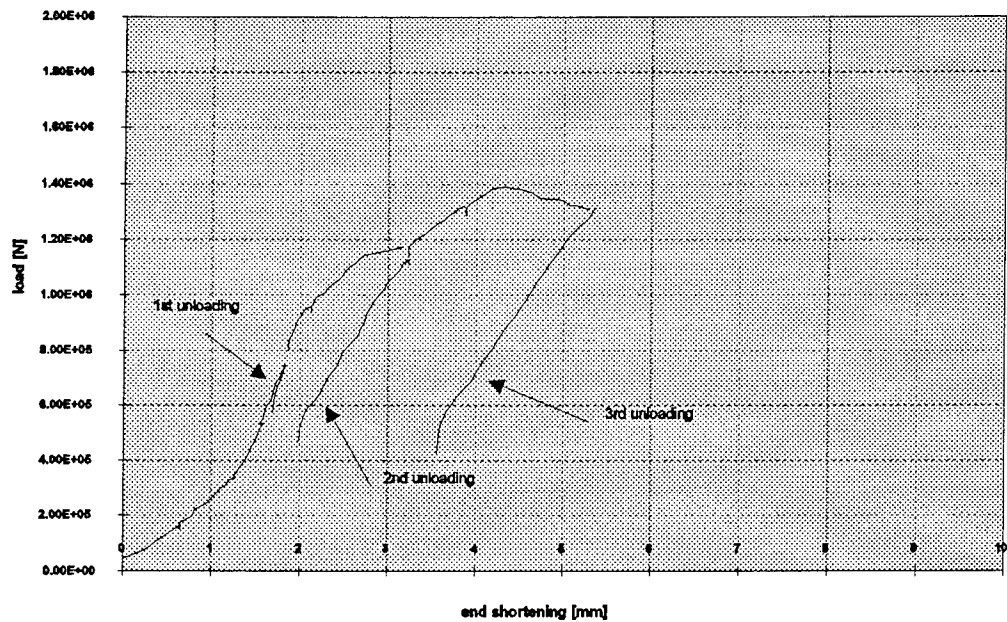Figure 3.5: Time history loading plot (1094).



Figure 3.6: Load versus end-shortening curve (1094). End displacement measurements taken with string potentiometers (data corrected for string potentiometer hysteresis).
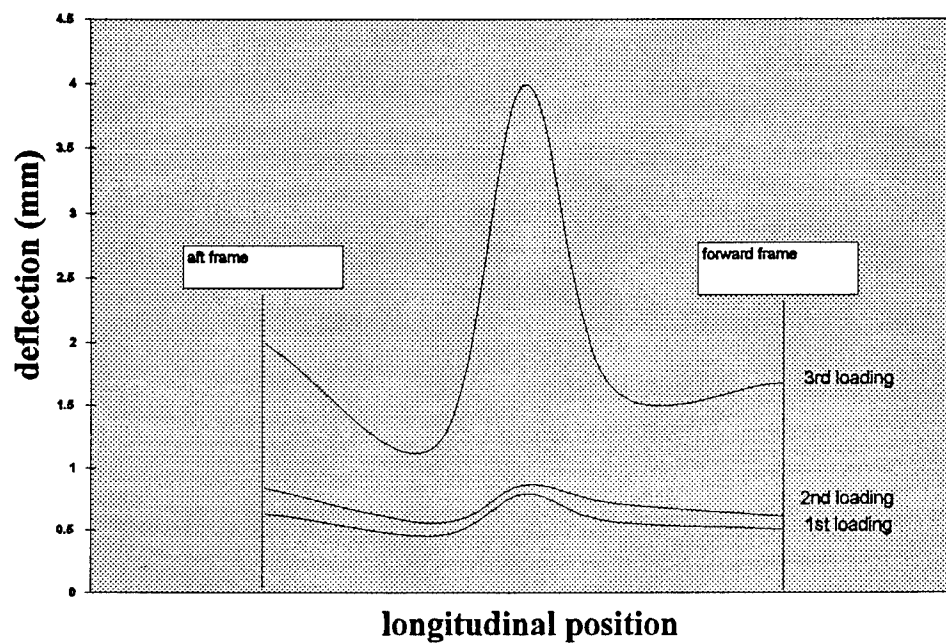
Figure 3.7:   Permanent set evaluation (1094) at every unloading.

### 3.6 Discussion of Results

With two types of loading possible, axial and lateral, the types of panel failure are limited to three modes. Mode I results from compressive failure of the stiffener flange when the plate and stiffener both reach a full plastic moment, or when the stiffener flange reaches yield in compression. The plate, in negative bending, deflects downward towards the plating. Mode II failure is distinguished by compressive failure of the plate in positive bending toward the stiffener flange. Mode III failure is not typically found in ship structures, but is the result of simultaneous failure of the stiffener flange in tension and the plating in compression. This mode is normally driven by a large magnitude lateral load on the structure. In addition, one other type of failure that is possible is lateral torsional buckling of the stiffeners, also known as tripping.

In the laboratory, the distinction between Mode I and Mode II failure is not readily apparent. Theoretically, Mode I occurs in negative bending and Mode II occurs in positive bending. However, determination of what element actually fails is not as simple as looking to see which direction the plate deflects. Data analysis of the mode of panel failure is accomplished by looking at a series of strain gages at set loading or time intervals. Whichever gage first shows equivalent strains that exceed the yield strain of the element will determine the type of failure mode. Mode I failure will first yield in the stiffener flange and Mode II will first show compressive yield of the plating. Because of the large amounts of bending present in the deformed panel, some elements will go into tension.

Tripping is defined as a rotation of the stiffeners about their attachment to the plating.

Tripping should not be confused with a characteristic Mode I or II failure. The stiffeners

in a Mode I and II failure adopt a local plastic mechanism which forces a failure similar in

appearance to tripping. Tripping, on the other hand, is typified by overall flange buckling.

The Mode I and II deflection(s) of the stiffener flange also adopts a local "s" shape in the

longitudinal direction; this shape is not seen in a tripping failure where the flange may

adopt some multiple of half-waves in deflection but nothing as concentrated as the local

"s" shape. Figure 3.8 is a photograph of the characteristic "s" shape in a Mode II failure.

A summary of grillage collapse stresses is given in Table 3.5. A brief summary of each

particular test is given below.

| Table 3.5 - Summary of Collapse Parameters | | | |
|---|---|---|---|
| | ultimate yield stress | $\sigma_{ult}/\sigma_{mean\ yield}$ | $\sigma_{ult}/\sigma_{yield\ of\ stiffener}$ |
| Griillage # | $\sigma_{ult}$ | $\phi_{exp}$ | $R_{exp}$ |
| 0494 | 254.9 kPa (36,958 psi) | 0.656 | 0.693 |
| 0894 | 235.2 kPa (34,117 psi) | 0.599 | 0.640 |
| 1094 | 244.3 kPa (35,433 psi) | 0.622 | 0.665 |

*Grillage 0494*

Grillage 0494 collapsed by Mode II failure, a compression failure of the plating. This

determination was made by an evaluation of the stress/strain relationships in the center

bay. At common loading increments, the plating was the first element to reach the yield

stress of the material. Figures 3.9 (a,b,c, and d) show the incremental stresses in the

plating and stiffener before and after failure. The experimental ultimate collapse stress

was 254.8 kPa (36,958 psi) with no applied lateral pressure. The collapse occurred

between the transverse frames in the center bay. As loading was increased, the plating

deformation progressed from a single longitudinal half-wave between frames to two half-waves between the frames (Figure 3.10). These figures are also useful tools in evaluating the amount of permanent set resulting from incremental loadings and unloadings. A characteristic positive bending of the grillage towards the stiffeners was observed. Photographs of fully developed collapse from above, below, and from the side of the grillage are shown in Figures 3.11(a, b, c, and d). Figure 3.11a is an illustration of the alternating positive and negative deflection nodes formed in the center bay. Figure 3.11b is a good example of the characteristic local "s" buckling of the stiffener flange in a Mode II failure. This photograph is of the center bay, looking aft. Note that in Figure 3.11a the deflection nodes induce an "s" type failure. When the deflection is positive towards the stiffener, the stiffener web deflects outward from the bay; when the deflection is negative, the web deflects towards the node. Figure 3.11c, the underside of the grillage, shows the characteristic deflections in the center bay. Note that in Figure 3.11d the failure is nominally in the center. Figure 3.12a and 3.12b summarize the values of final deformation in both the plating and the stiffeners as determined by a post-test survey.
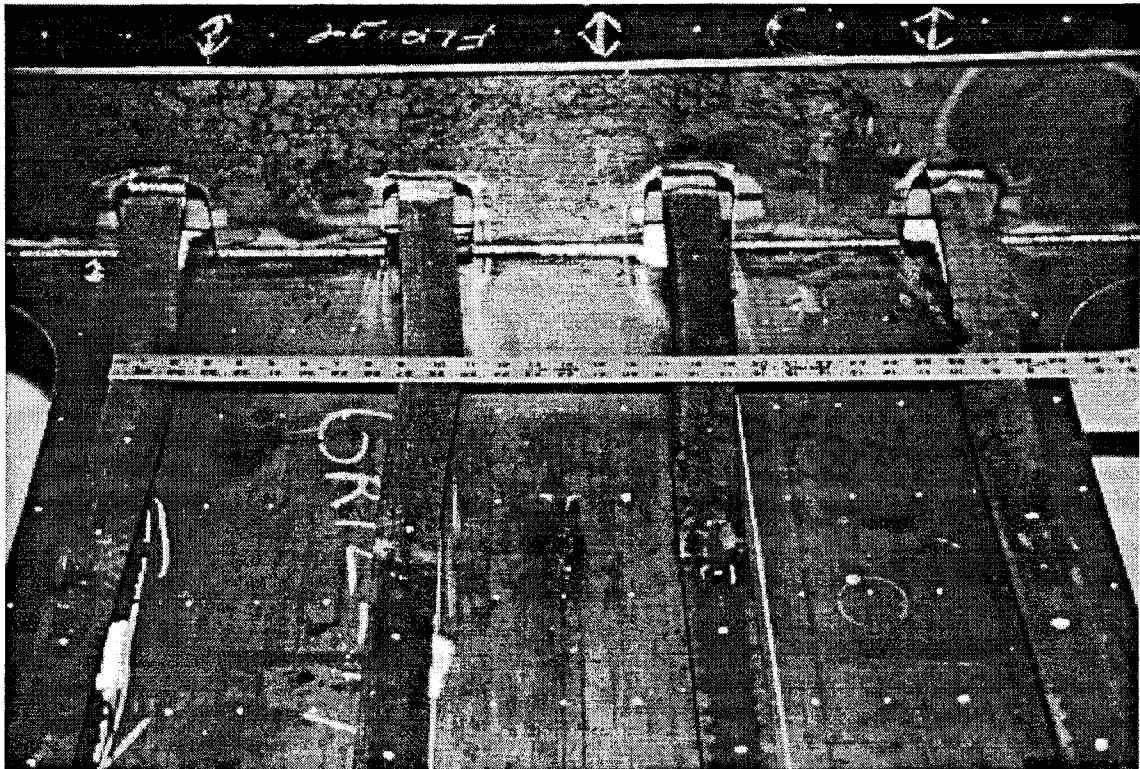
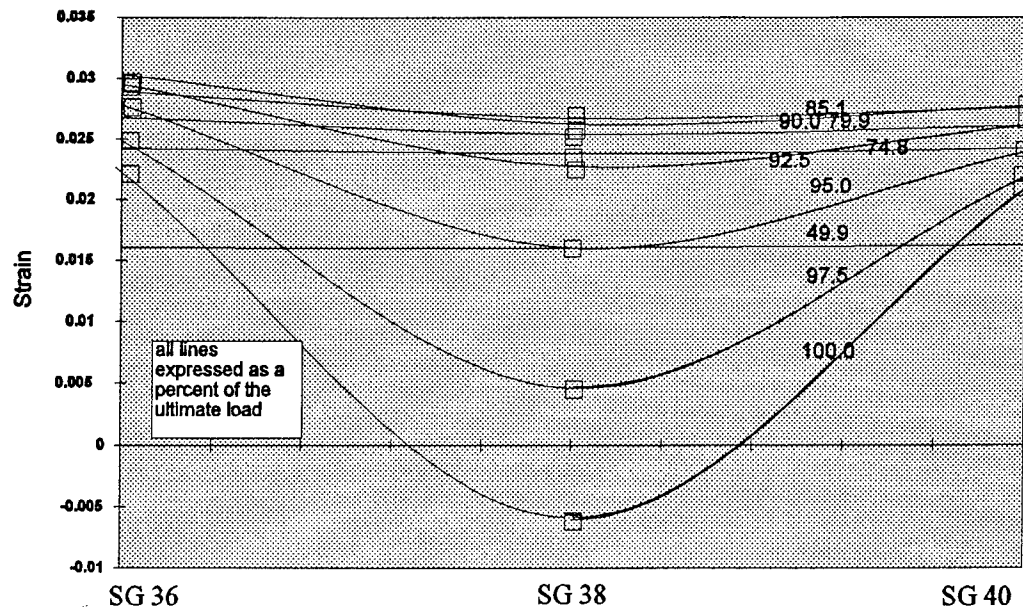Figure 3.8: S-shape development of stiffener on 0894 test.

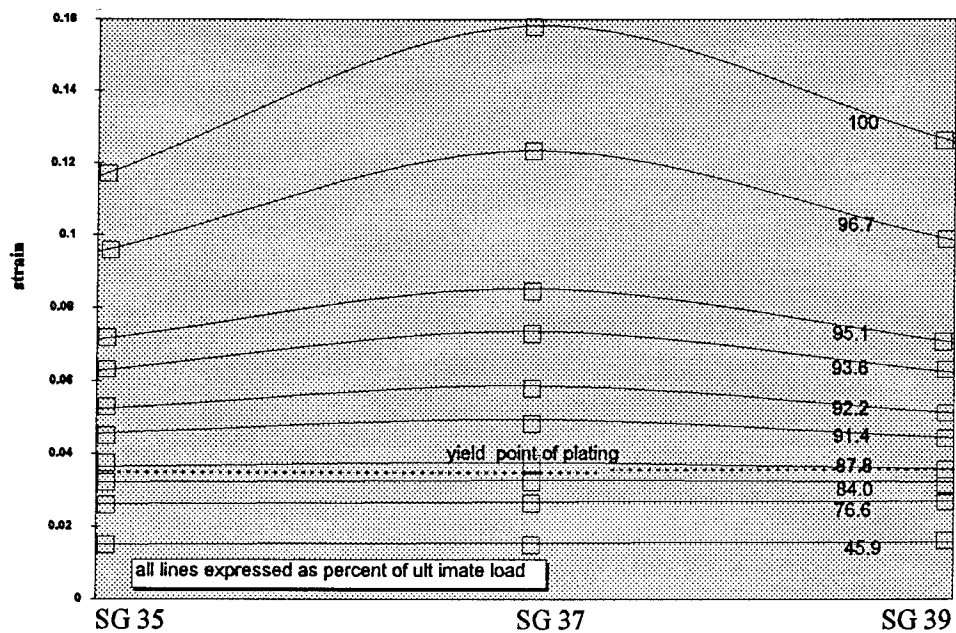Figure 3.9a: Incremental strain development for collapse mode determination in top of plate (0494).



Figure 3.9b: Incremental strain development for collapse mode determination in bottom of plate (0494).
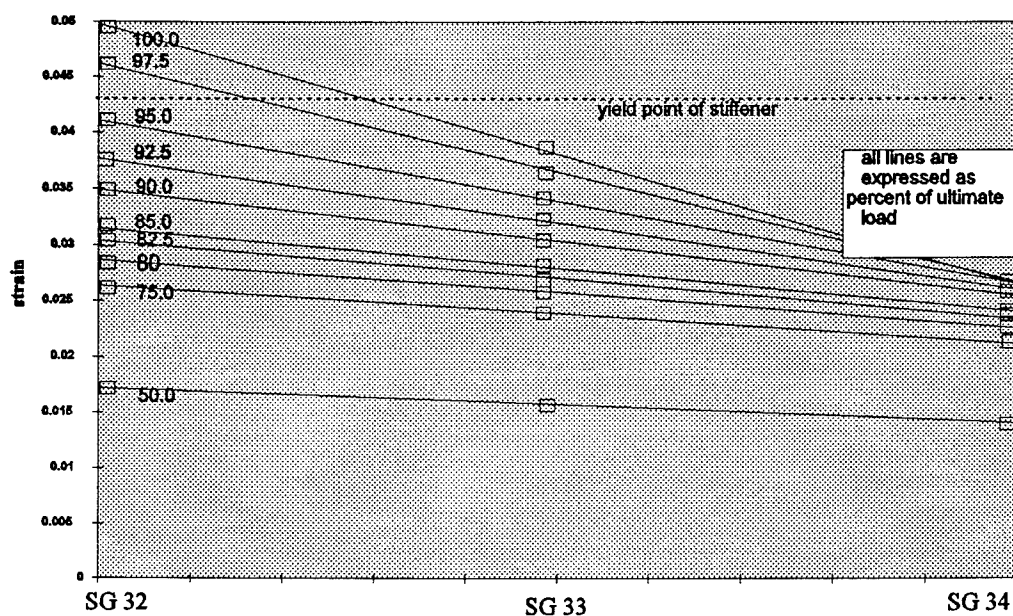
Figure 3.9c:   Incremental strain development for collapse mode determination in port stiffener (0494).
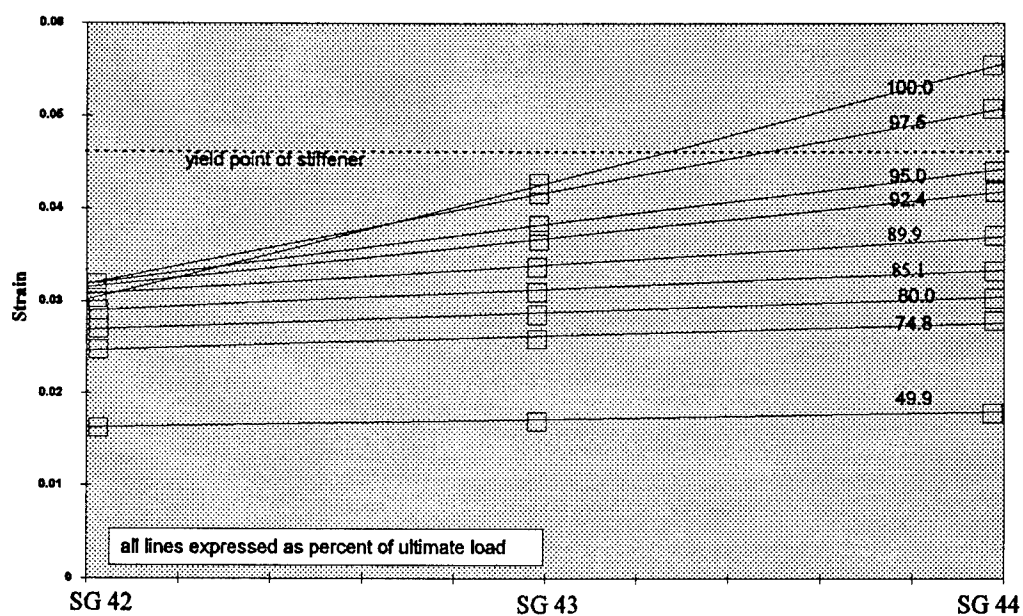


Figure 3.9d:   Incremental strain development for collapse mode determination in starboard stiffener (0494).
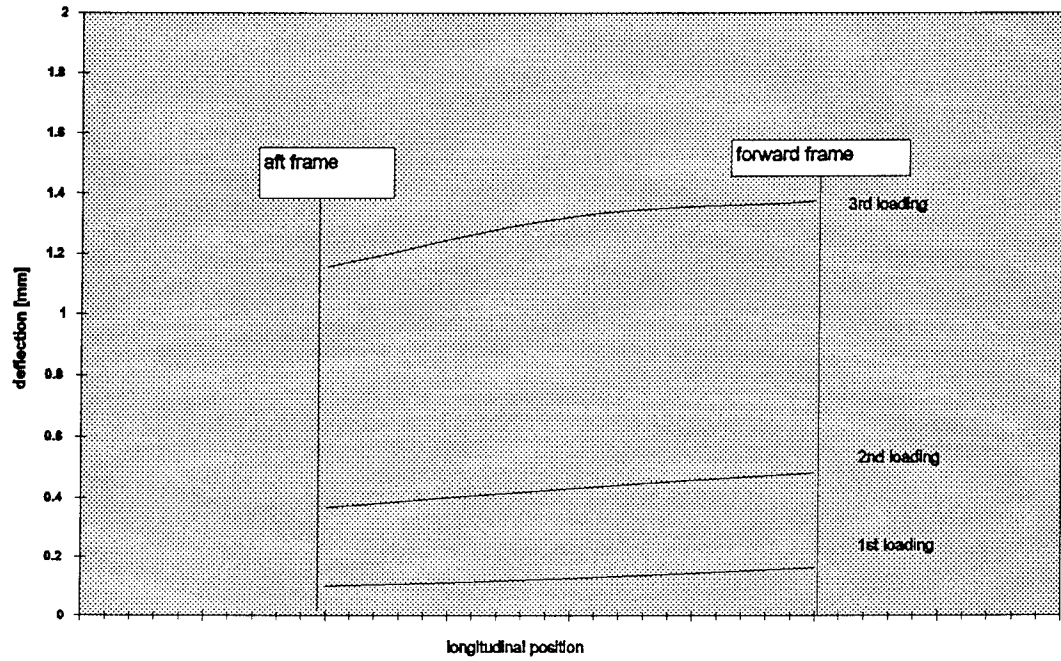
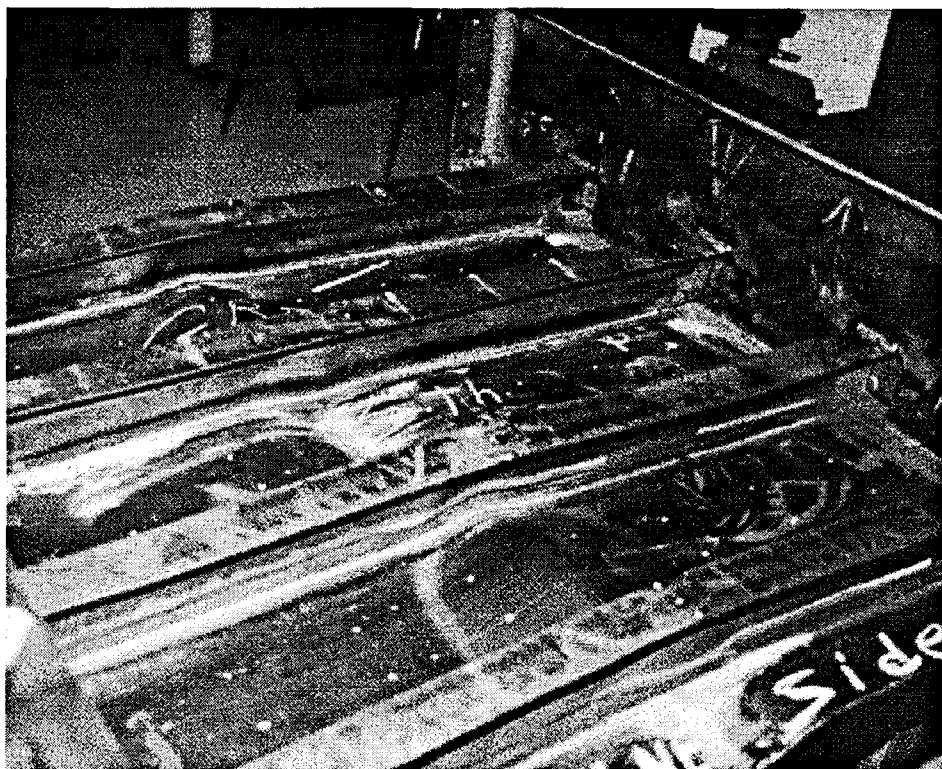Figure 3.10: Permanent set evaluation (0494).

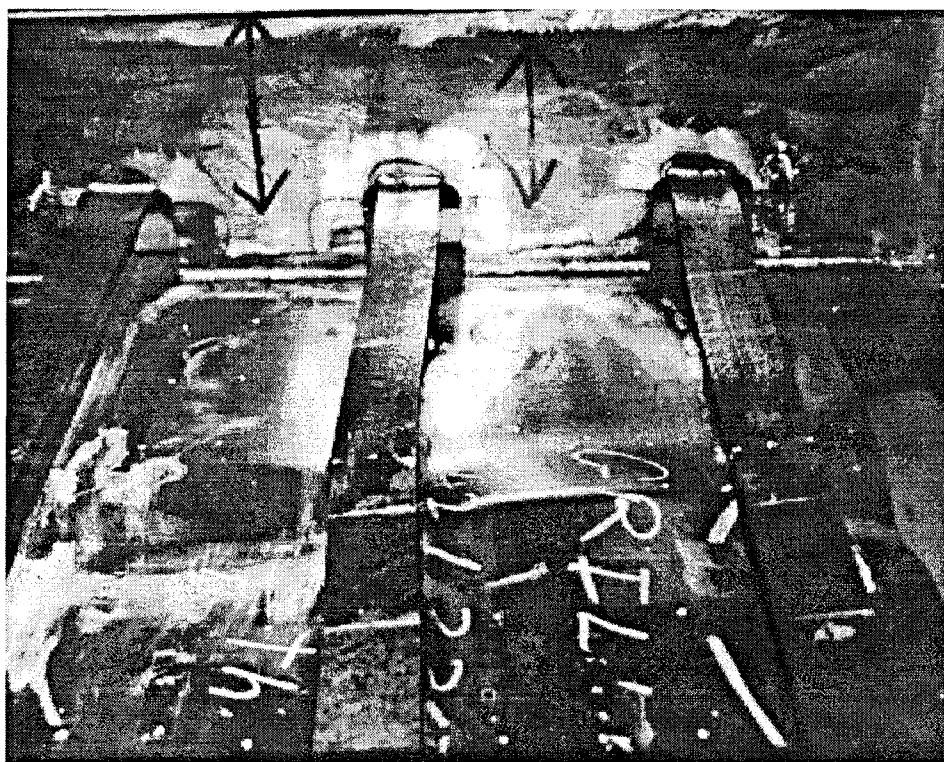Figure 3.11a: Top of grillage (alternating node patterns).



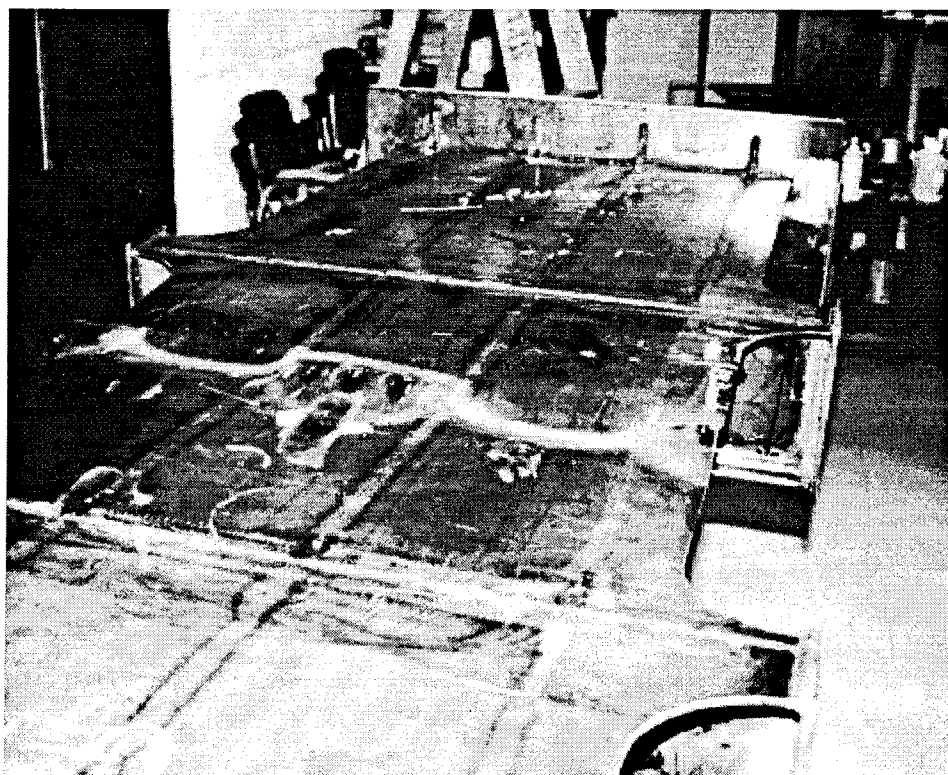Figure 3.11b: Top of grillage (detail of center bay, looking aft)
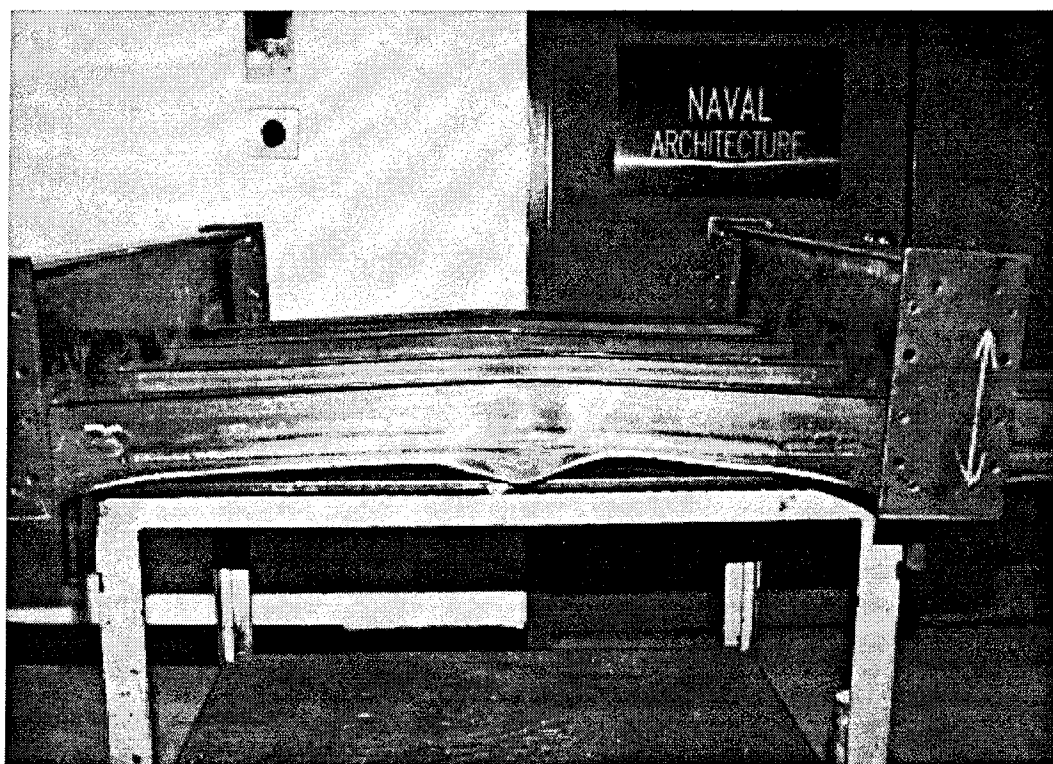
Figure 3.11c:   Underside of grillage



Figure 3.11d:   Side of grillage

Figure 3.12a:   Post-test survey of deformations (plate).
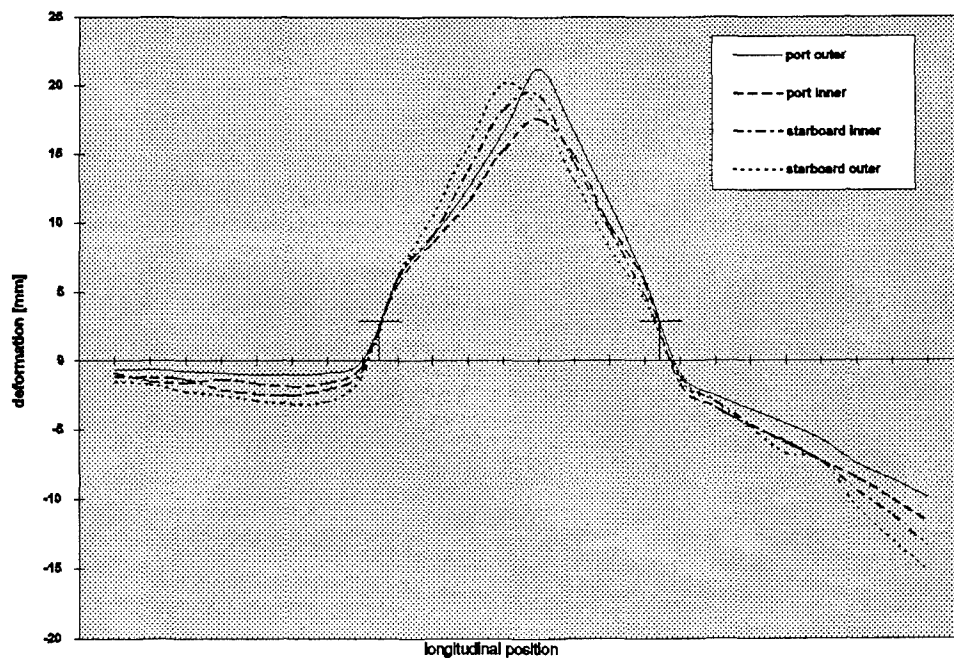


Figure 3.12b:   Post-test survey of deformations (stiffeners).

*Grillage 0894*

Grillage 0894 collapsed by Mode II failure, a compression failure of the plating (Figures

3.13 a, b, c, and d). This determination was made by an analysis of the strain gages in the

plate and stiffener during loading. The experimental ultimate collapse stress was

235.2 kPa (34,117 psi). No lateral pressure was applied. Collapse occurred first in the

center bay between the transverse frames. As loading was increased, the plating

deformation transformed between a single half-wave to two half-waves between the

frames (Figure 3.14). Positive bending towards the stiffeners was observed. Photographs

of the fully developed collapse are shown in Figures 3.15 (a, b, and c). Note that in

Figures 3.15a and c, the failure took place approximately 90 mm. forward of the midspan

in the center bay. Figure 3.8 shows local "s" buckling in the forward bay. The interaction

between these two reactions is related as stiffness was lost near the forward bay first and

the foward panel was forced to hold a greater load. Figures 3.16(a,b) show the post-test

surveys of the plate and stiffeners.

Figure 3.13a:   Incremental strain development for collapse mode determination in top of plate (0894).



Figure3.13b:   Incremental strain development for collapse mode determination in bottom of plate (0894)

Figure 3.13c: Incremental strain development for collapse mode determination in port stiffener (0894).



Figure 3.13d: Incremental strain development for collapse mode determination in starboard stiffener (0894).
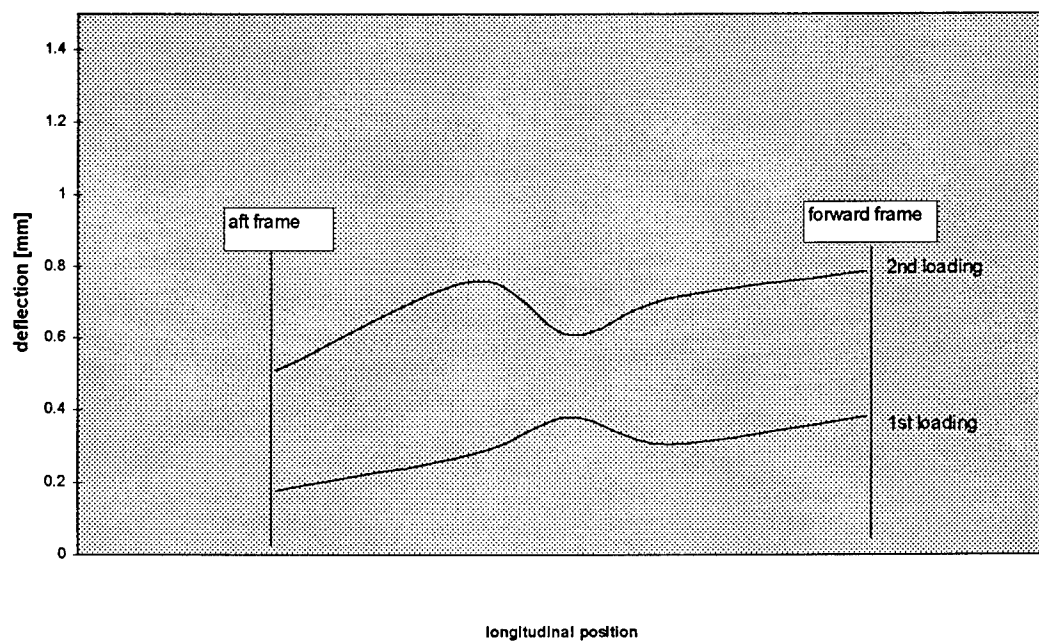
Figure 3.14: Permanent set evaluation (0894).
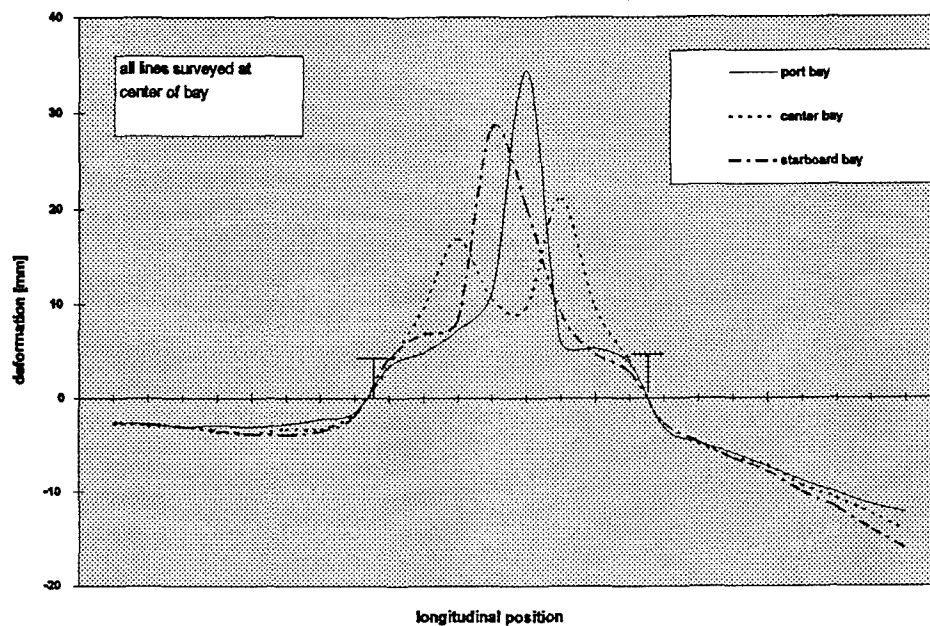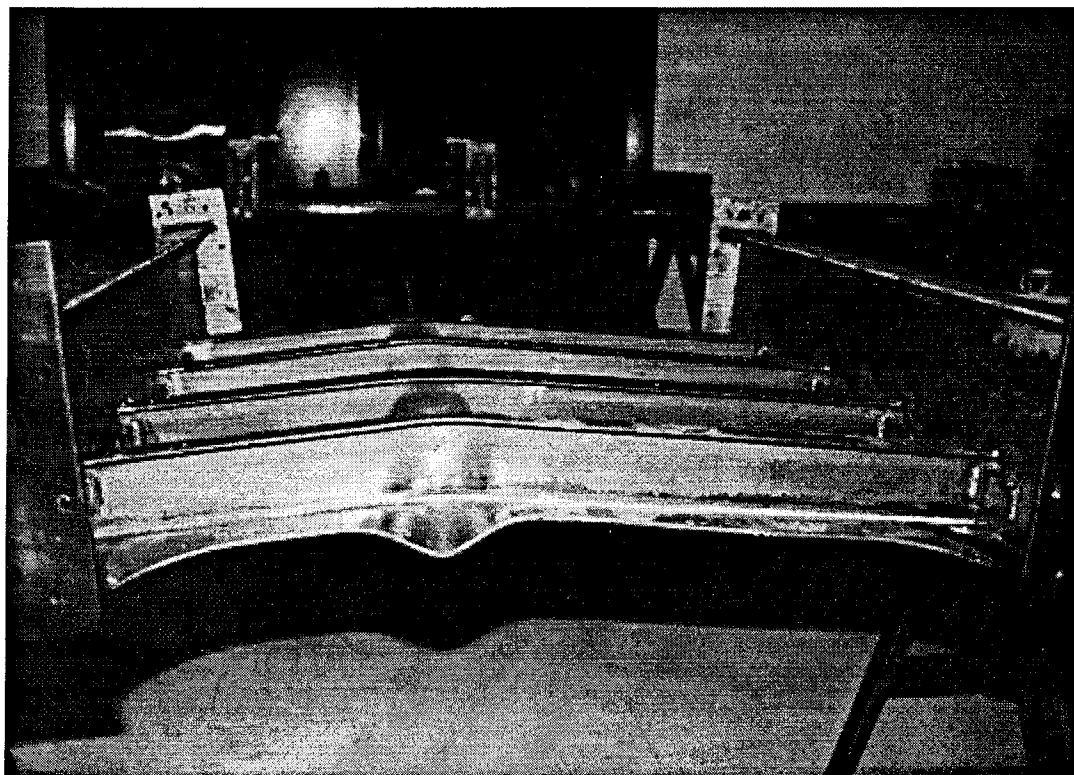
Figure 3.15a: Side of grillage.



Figure 3.15b: Side of grillage (turned over).
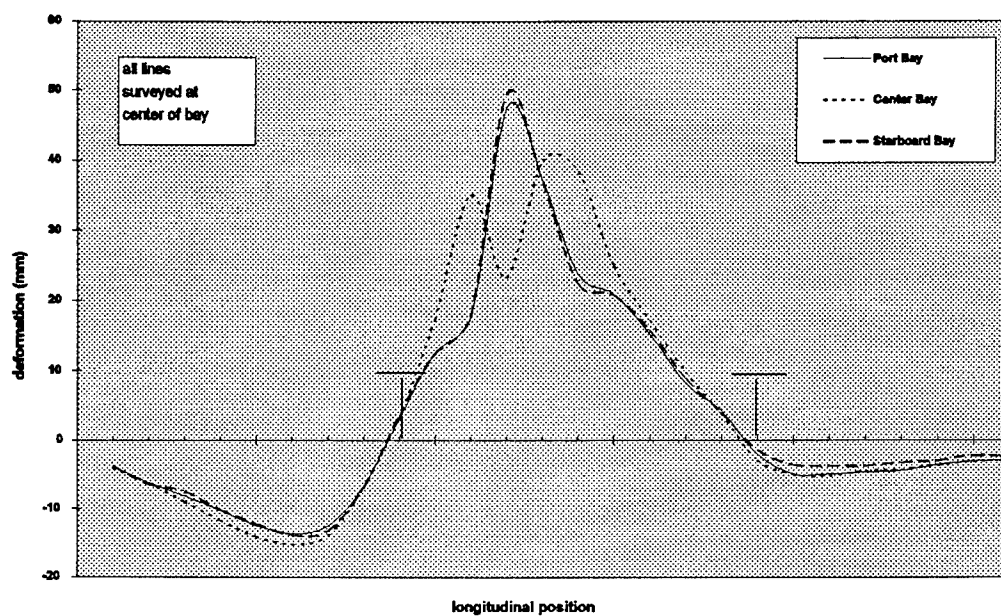
Figure 3.16a:   Post-test survey of deformations (plate).
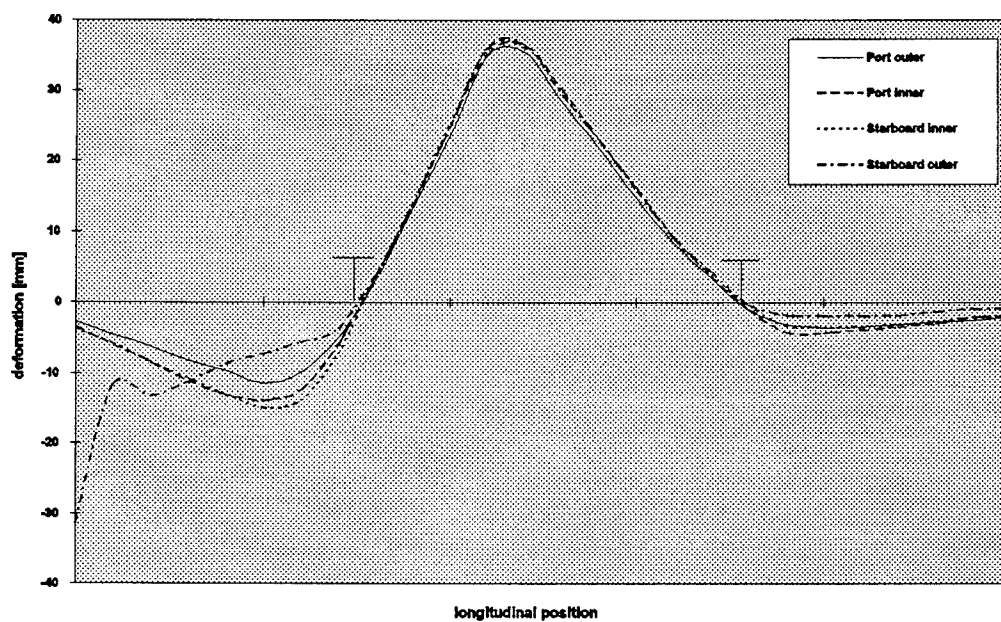


Figure 3.16b:   Post-test survey of deformations (stiffeners).

*Grillage 1094*

Grillage 1094 also collapsed by a Mode II failure (Figures 3.17 a,b,c,d). The ultimate collapse stress was 244.3 kPa (35,433 psi). No lateral pressure was applied. Collapse occurred in the center bay between the transverse frames. Progressive deformations changed from a single half-wave to two half-waves (Figure 3.18). Positive bending towards the stiffeners was also observed. Photographs of the collapse, Figures 3.19(a, b, and c) show results similar to the 0494 grillage. In Figure 3.19a, some local, "s" flange buckling is observed in the aft bay. As for grillage 0894, the stiffness was first lost in the aft bay and the aft panel was forced to hold a greater load. Figure 3.19b shows the nodes which formed almost exactly at the midspan of the center bay. Figures 3.20(a,b) show the post-test surveys of the plate and stiffeners.
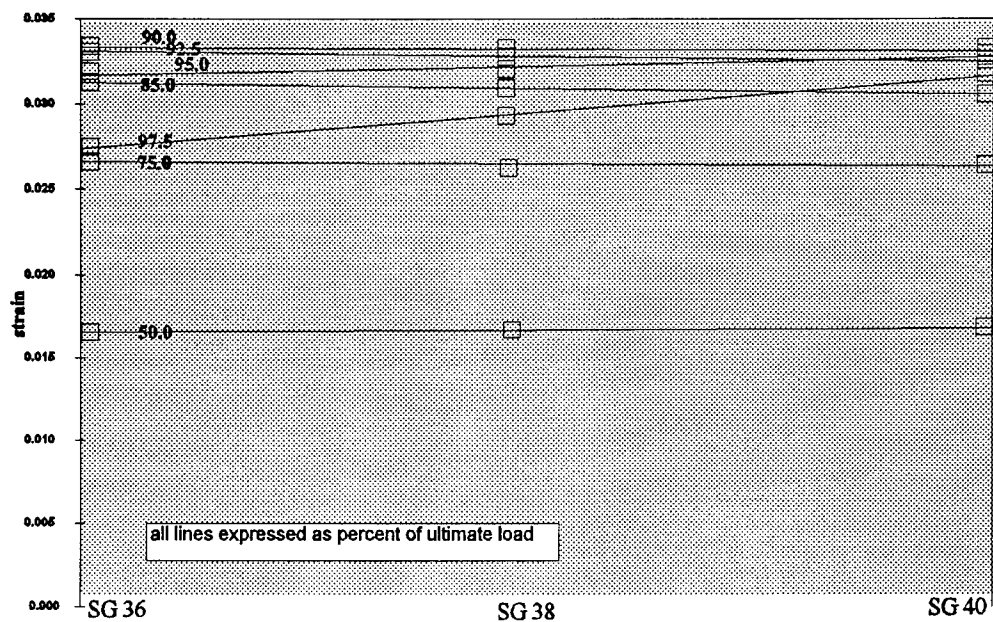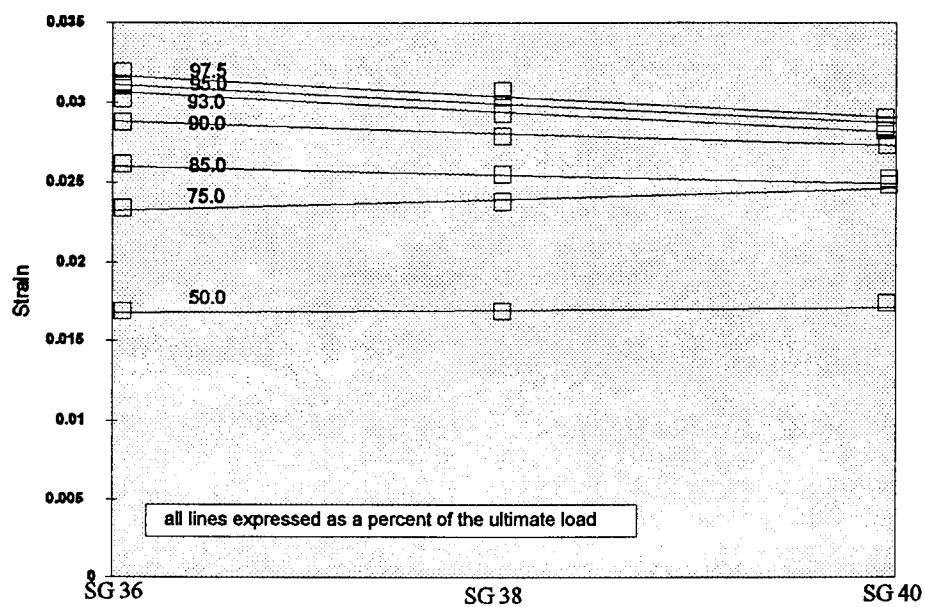
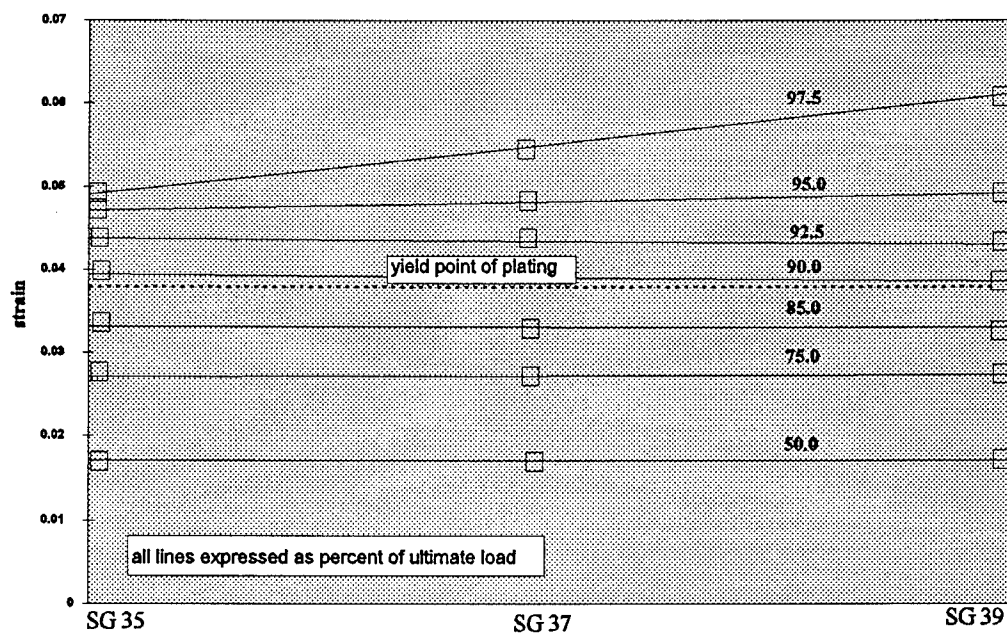Figure 3.17a:   Incremental strain development for collapse mode determination in top of plate (1094).
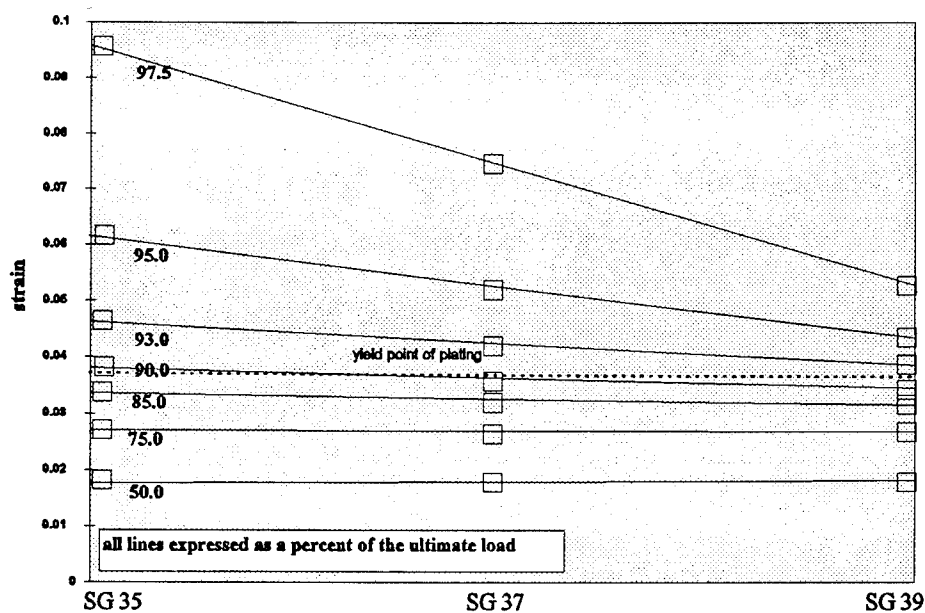


Figure 3.17b:   Incremental strain development for collapse mode determination in bottom of plate (1094).
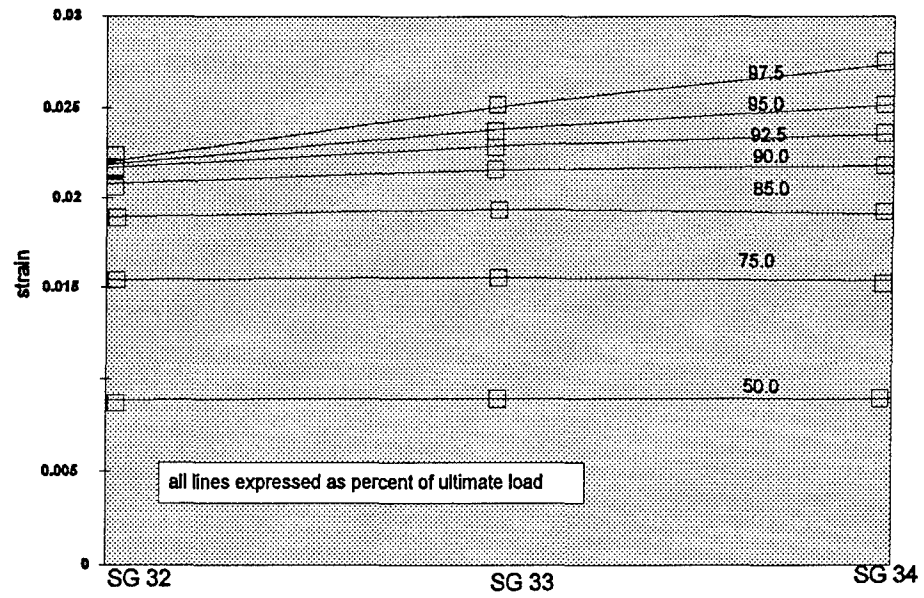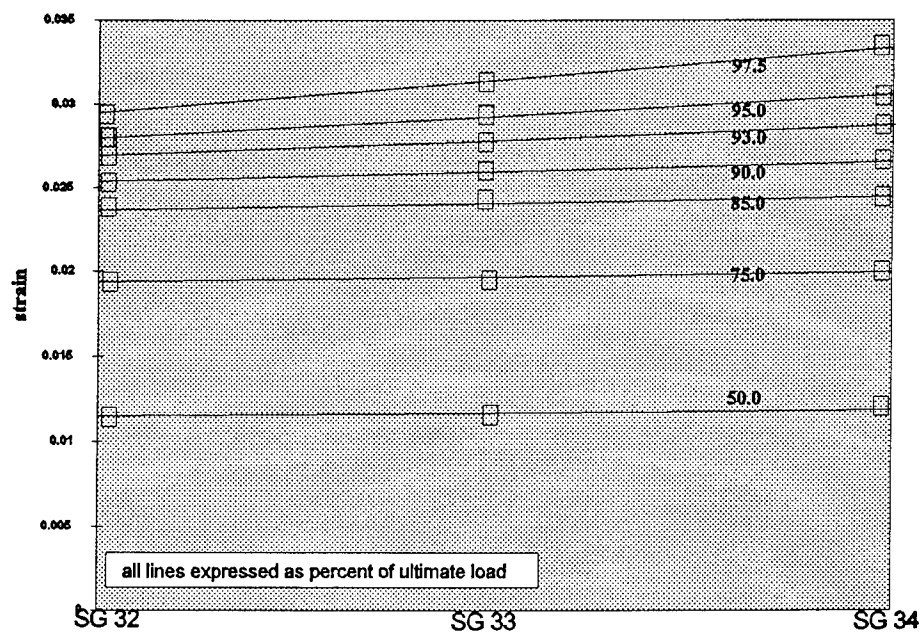
Figure 3.17c: Incremental strain development for collapse mode determination in port stiffener (1094).
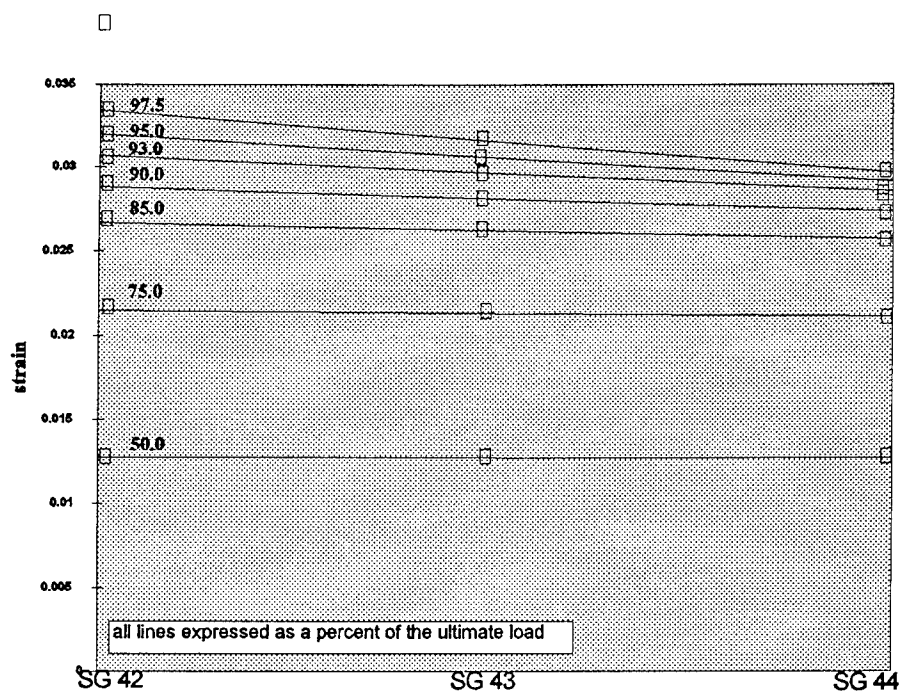


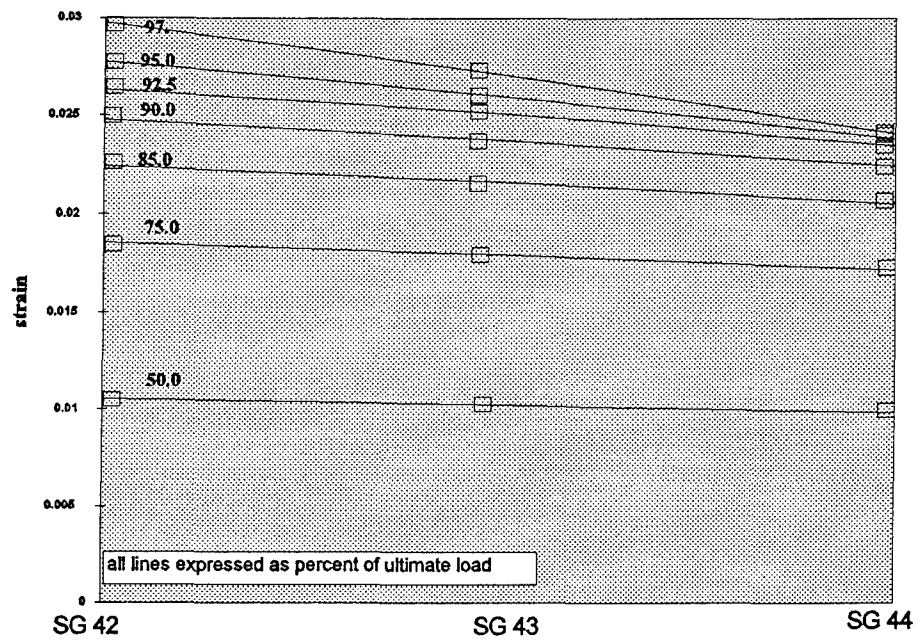Figure 3.17d: Incremental strain development for collapse mode determination in starboard stiffener (1094).

deflection (mm)



longitudinal position
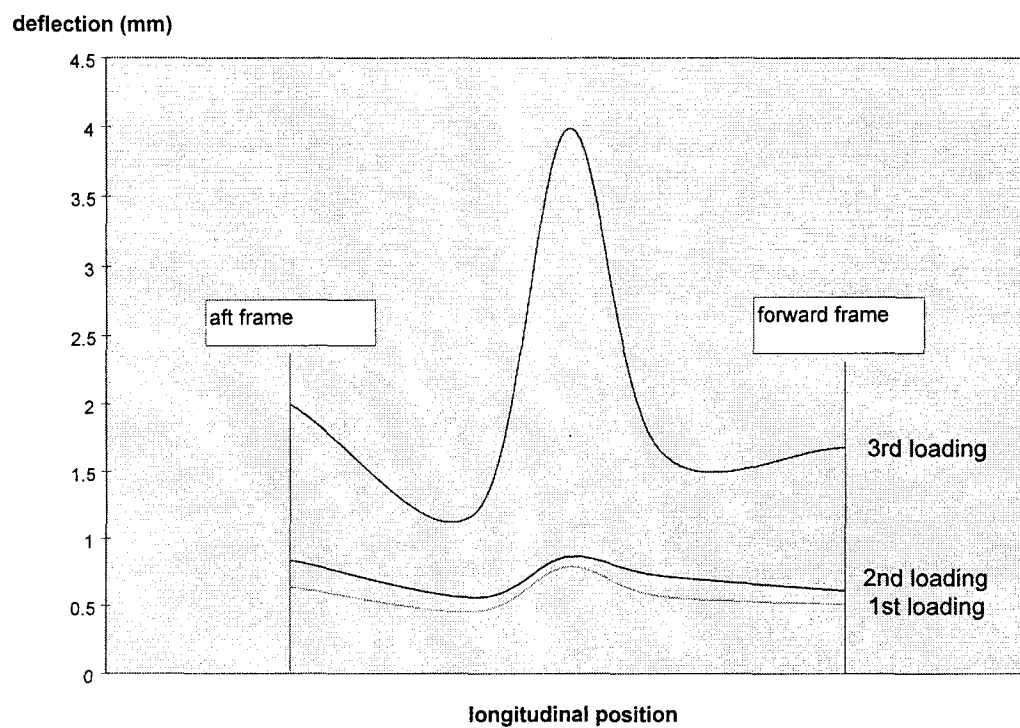
Figure 3.18:   Permanent set evaluation (1094).
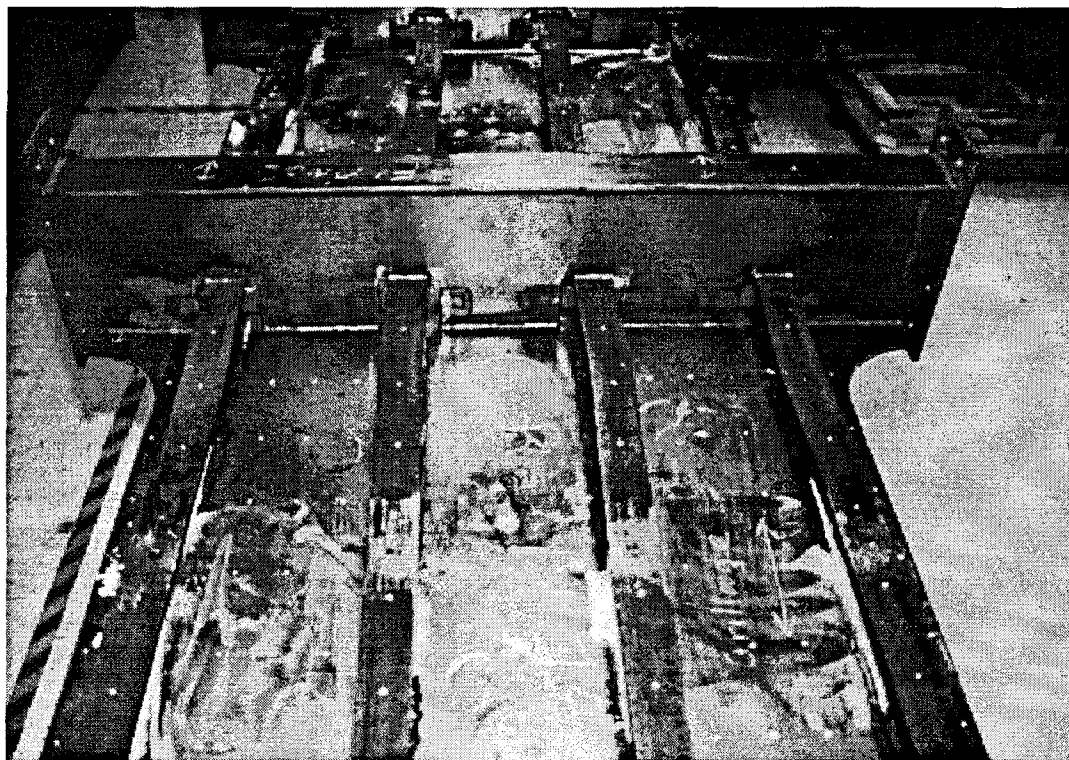


Figure 3.19a:   Top of grillage (aft and center bay).
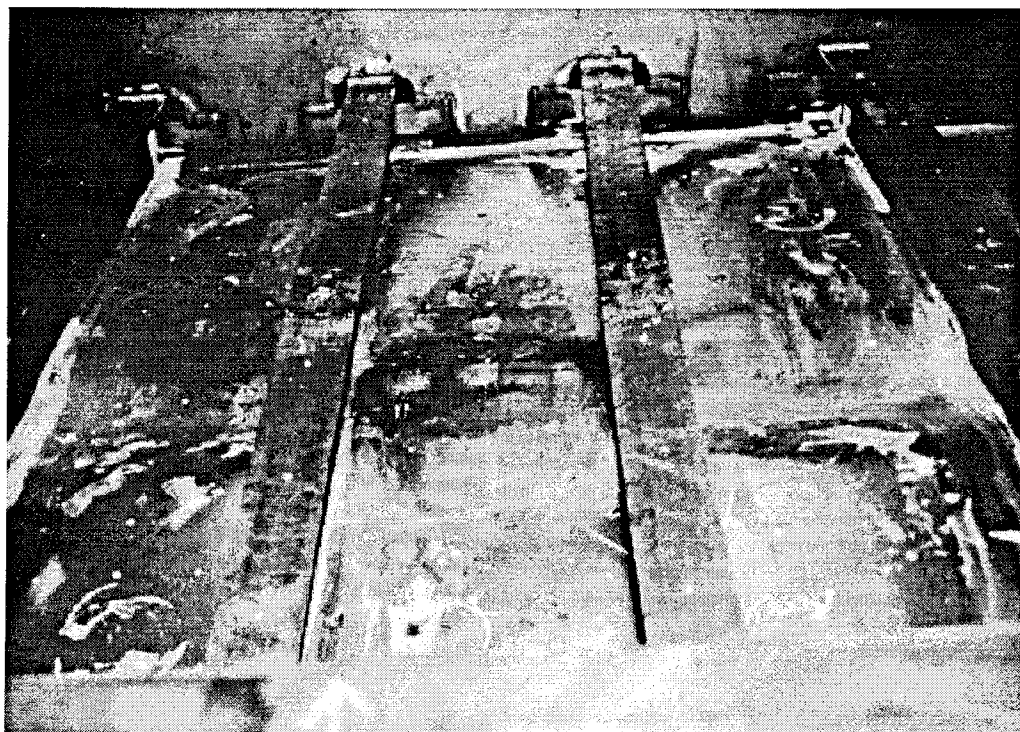
Figure 3.19b: Top of grillage (center bay).

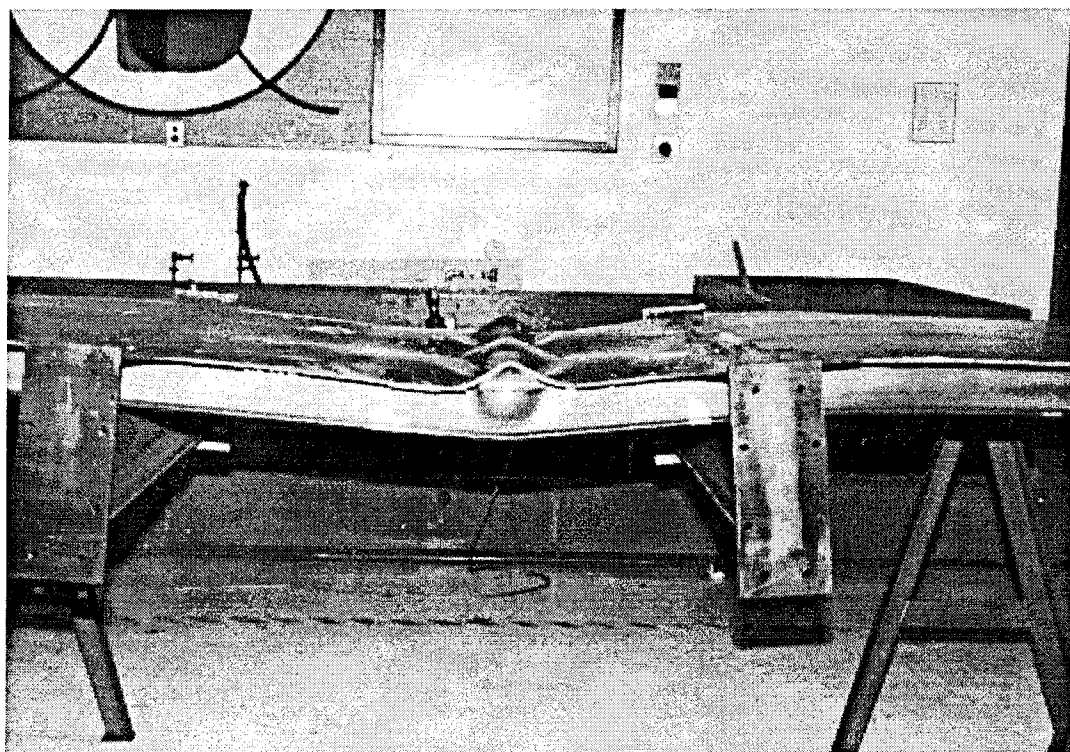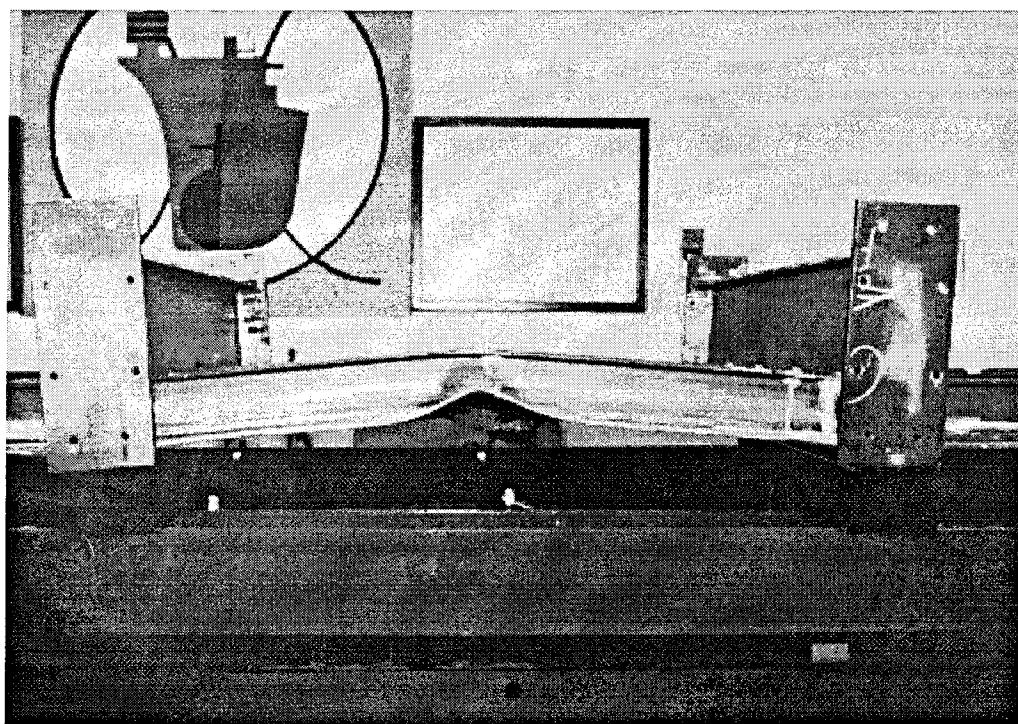

Figure 3.19c: Side of grillage.
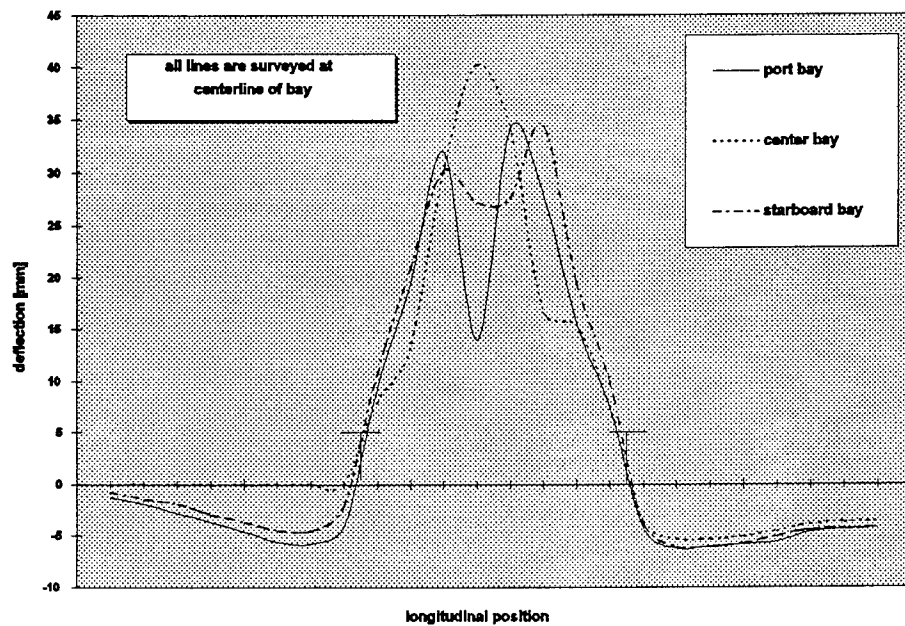
Figure 3.20a:   Post-test survey of deformations (plate).
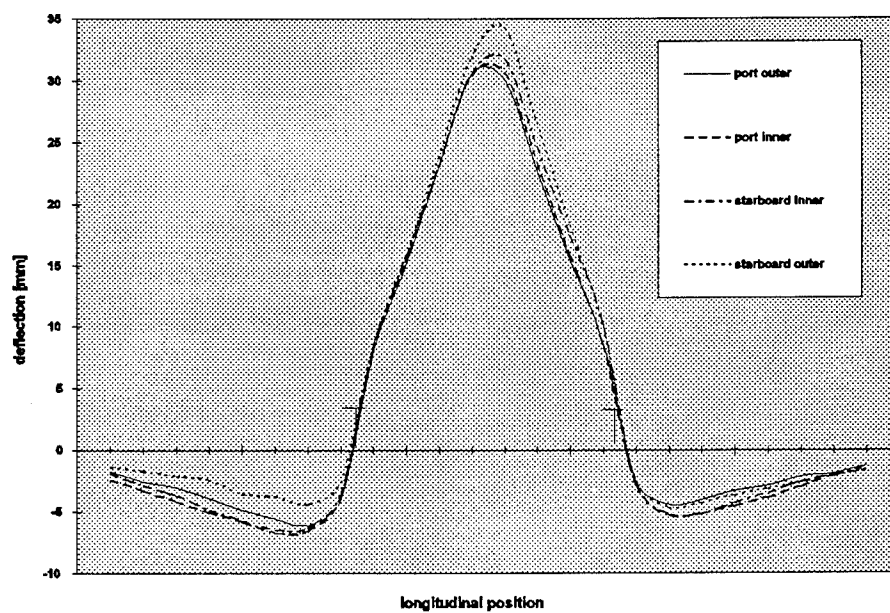


Figure 3.20b:   Post-test survey of deformations (stiffener).

## 3.7 Comparison of Experimental Results to Theory

A literature search of stiffened panel tests yielded nine separate series of tests conducted at six different facilities; the result of this search is a database of 86 separate tests[2] spanning a range of scantling sizes, material properties, and loading conditions. Faulkner (1977), Horne, et. al. (1977a), Horne, et. al. (1977b), Kondo, et. al. (1964), Rampetstreiter, et. al. (1962), Smith (1975), and Murray (1975) detail the particulars of each of these tests. Figure 3.21, shows the relationship between the predicted strength versus the experimental strength in the data analysis. The predicted strength of each grillage was estimated by the method explained in Hughes (1988) and is outlined under the theory section (2.0) of this paper. Figure 3.21, presupposes that the ideal relationship between the predicted and experimental strength is one-to-one, if the theory is accurate. The solid line represents a perfect correlation between experimental and theoretical results. Any data points falling below the solid line indicates a conservative theoretical estimate or a safe prediction. Note that the legends specify the different test series and experimental conditions (i.e., lateral pressure).

There are several important inferences that can be made from Figure 3.21 regarding stiffened panel testing, the theoretical algorithm, and the effects of geometry on panel strength. Each of the tests points to one or more important issues about stiffened panel design and strength. The following discussion will consider the relationships of end

---

[2]

Faulkner's (1977) student series were initially considered for this study but not included in this parametric analysis because of the suspect validity of the data. The Student's Series were conducted for demonstration purposes and not for data collection. In his paper, Faulkner issues a caveat about the data from the Student Series.
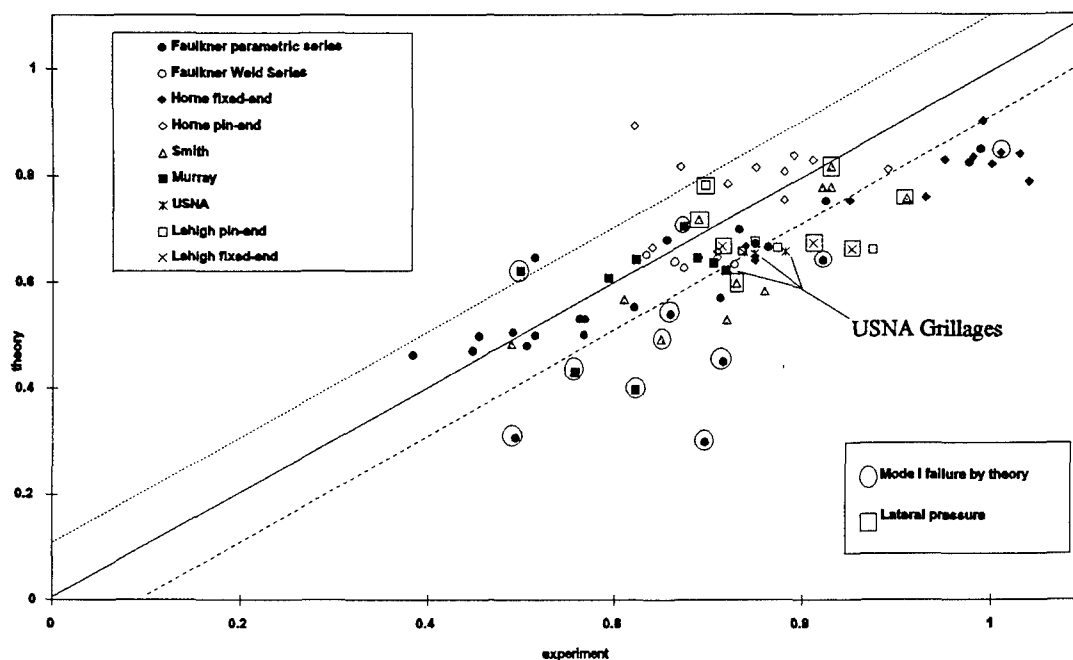
Figure 3.21: Predicted strength versus experimental strength (parametric study).

conditions, combined axial and lateral loading, the theoretical algorithm, and panel geometry to Figure 3.21.

Horne, et. al. (1977a) conducted their tests on single-bay panels using two approaches to boundary end conditions: half of the tests were conducted with fixed-end and the other half were pinned-end. The resulting relationships between these two procedures show that the strength of a pinned-end model is underpredicted by the standard algorithm whereas the strength of a fixed-end model is overpredicted by the standard design algorithm. In reality, the end boundary conditions of a panel in a ship's structure are neither entirely fixed nor pinned. Rather, an actual panel is somewhere between these two extremes; a simply supported end condition is used in the theoretical model for this very reason. Two similar series of tests were conducted at Lehigh University's Fritz Engineering Laboratory, one fixed-end and one pinned-end (Kondo, et.al., 1964 and Rampetstreiter, et.al., 1962). The delineation between these boundary conditions is not as distinct. However, this discrepancy should not discount Horne's results. Many of the Lehigh tests were subjected to combined lateral and axial loading. As will be discussed later in greater detail, the effect of lateral pressure on a stiffened plate tends to change the strength characteristics of a grillage.

The net result of the boundary condition data shows the necessity for multi-bay testing. In single bay testing, such as Horne's, the effects of the end restraints are influential on the strength of the panel. However, a three, four, or five bay grillage allows the experimenter to disregard the failure or data collected from the end bays and concentrate the analysis on the inner bays where the boundary conditions of the panel

more closely resemble the actual end conditions of a ship's panel in a continuum of panels in a ship's structure. The three USNA tests are good examples of a multi-bay test. Only the center bay and center panel were used for data analysis. The data show that the USNA tests yielded data with a good correlation between experiment and theory.

In elastic panel buckling, the application of lateral pressure on a panel causes the panel to buckle in a single longitudinal half-wave. However, the bending caused by the combined axial and lateral load does not usually induce a single longitudinal half-wave pattern seen in simple, elastic buckling. As is seen in failure under axial load only, the pattern of failure adopted by the grillage is several multiple half-waves. The effect of the lateral load induced single half-wave negates the panel's preferred failure mechanism of a multiple half-wave pattern. The net effect of this negation of the panel's preferred complex half-wave pattern is an effective strengthening of the stiffened panel. In Figure 3.21, there are eight panels subjected to a lateral load (four Lehigh tests and four Smith (1975) tests). The majority of these panels fall below the correlation line. It is altogether possible to see a loss of strength, especially in testing where only a single bay is used. This is one possible explanation why the pin-ended Lehigh test plots near the upper 10% margin line. The pin-end condition may facilitate the adoption of a single half-wave in a single bay test such as this one; in this case, the intuitive explanation of a laterally-induced single half-wave deflection and its effect on panel strength may prevail.

Eleven of the tests exhibited a Mode II experimental failure when the theoretical algorithm predicted a Mode I failure. For the most part, these predictions are extremely conservative, hence, the points are considerably lower on Figure 3.21 than any other tests.

Although there is no common cause which points to the reason behind these aberrations, there are several viable explanations. Four of the tests conducted by Murray (1975) reported nominally straight initial deformations in the grillage. Building a panel with zero initial deformations is impossible. The theoretical results can be significantly affected by the magnitude and direction of initial deformations. As a result, an assumption of zero initial deflections is unlikely to yield good correlation between theory and practice. In addition, the theoretical analysis of many of the panels in question shows a small difference between the values of a Mode I and Mode II failure. In these particular cases, a Mode II failure by theory could be equally correct. This explanation, however, does not account for the largely overconservative predictions of panel strength which would still remain. Moreover, many of the panels that showed this behavior also had relatively high initial deformations. For example, three of the four tests in Faulkner's parametric series had deformations of 1.78, 1.53, and 3.37 mm.; most of the other tests in the series had deformations less than 0.50 mm. All of the deformations in this series were towards the stiffeners, which would not tend to induce a Mode I failure.

Faulkner's parametric series was intended to investigate the effect of column slenderness($\lambda_c$), plate slenderness ($\beta$), and stiffener area parameter ($\gamma_{st}$) on panel strength. There is some scatter, as would be expected, but the relationship between experiment and theory is consistent for this series. However, this series of tests demonstrates that as the panel geometry is varied, the resulting panel strength can be significantly affected. The parametric series is the only series in this analysis of tests to cover such a wide range of

strengths. This is due in large part to the wide span of geometries that were used. Figure 3.22 shows the effect of plate slenderness, β, on panel strength.

Plate slenderness is the ratio of panel width to panel thickness and compressive yield stress to Young's Modulus:

$$\beta = \frac{b}{t}\sqrt{\frac{\sigma_{Yp}}{E}} \qquad (3.1)$$

Without any relationship to compare plate slenderness to panel strength, there seems to be a considerable amount of scatter of the data in Figure 3.22. However, graphs such as Figure 3.22 were preceded by the U.S. Navy's Design Data Sheets developed in the 1940's. The Vasta Method, which relates plate slenderness to plate strength was derived from these experiments conducted at the Experimental Model Basin (EMB) (Frankland, 1940):

$$\phi_{exp} = \frac{2.25}{\beta} - \frac{1.25}{\beta^2} \qquad (3.2)$$

The data plotted over the Vasta Method line show the characteristic relationship of plate strength to plate slenderness. Faulkner (1977) proposed an improvement to the Vasta method:

$$\phi_{exp} = \frac{2}{\beta} - \frac{1}{\beta^2} \qquad (3.3)$$

Most of the panels used in this study collapsed under a Mode II failure, compression

failure of the plating. Therefore, plate slenderness is most likely the driving geometric

parameter behind this collapse. As the width of the panel is decreased, the strength of the

panel increases. At a plate slenderness of 1.00, the strength ratio of the panel approaches

1.00. Below a plate slenderness of 1.00, the strength of the panel drops off significantly

according to both the Vasta and Faulkner methods and the experimental data. As the

plate slenderness becomes greater than 1.00, the plate strength, $\phi_{exp}$, decreases.

The relationship between panel strength, $\phi_{exp}$, and column slenderness, $\lambda_c$, is not so

direct. By disregarding the various lines on Figure 3.23, and paying attention only to the

data points, it seems that there is considerable scatter and no correlation between the two

factors. However, when the panel is treated as a column (beam-column), the relationship

between strength and column geometry is dependent upon other factors such as initial

deflections, residual stresses, and lateral loading. The Johnson Parabola, plotted on Figure

3.23, is the theoretical relationship recommended by the Column Research Council and the

American Institute for Steel Construction (A.I.S.C.) for calculating the ultimate strength

of a straight, pinned-end column, under no lateral load:

$$\textit{when } \lambda_c \leq \sqrt{2}$$

$$\frac{\sigma_{ult}}{\sigma_y} = 1 - \frac{\lambda_c^2}{4} \tag{3.4}$$

As is evident from Figure 3.23, almost all of the experiments did not behave like the

ideal described by the Johnson Parabola. Real life grillages are imperfect and have initial
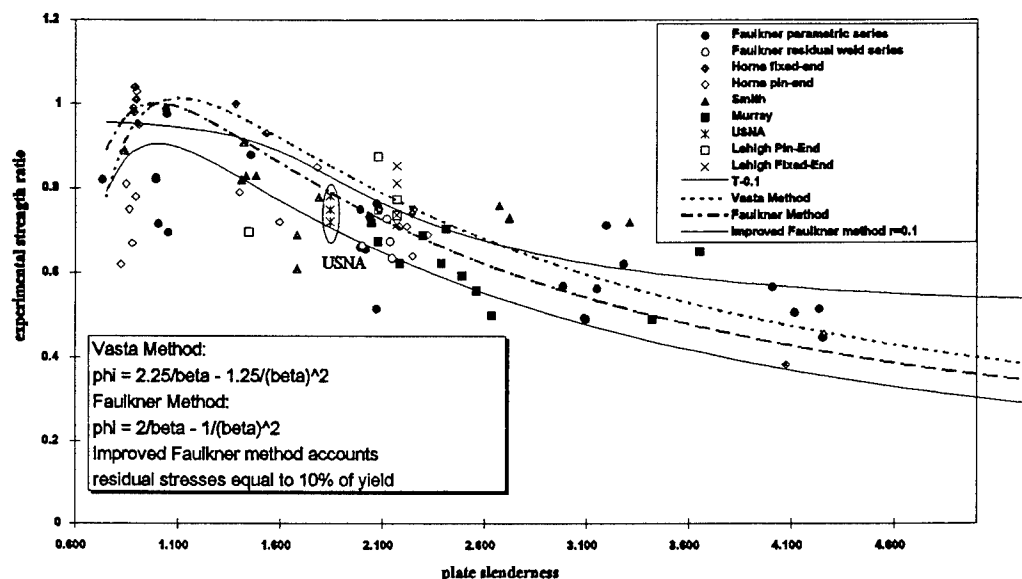
.Figure 3.22:  Experimental strength, $\phi_{exp,}$ versus plate slenderness,$\beta$.
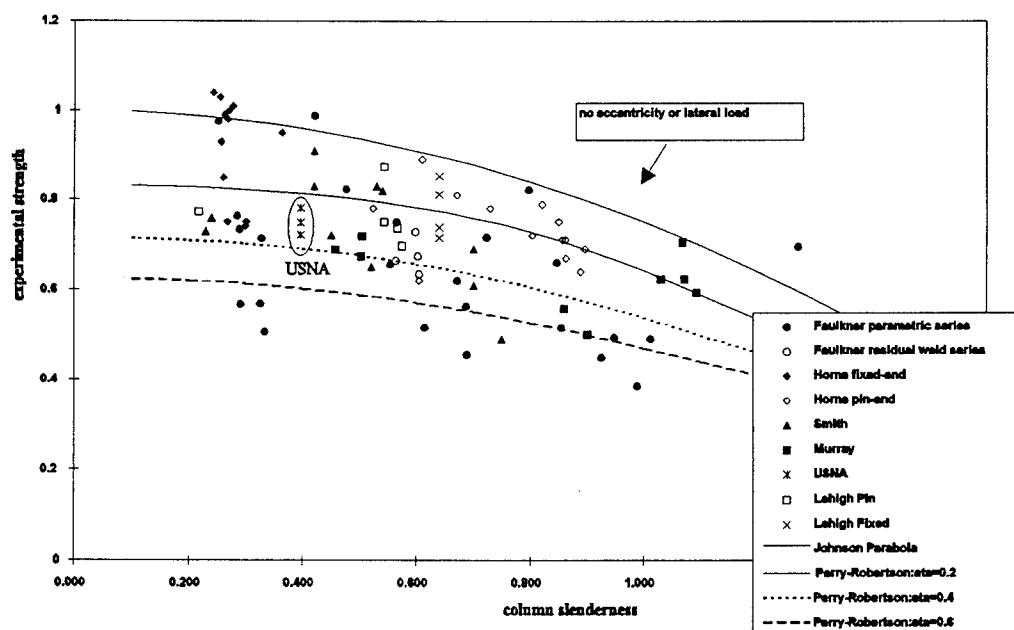


Figure 3.23:  Experimental strength, $\phi_{exp,}$ versus column slenderness, $\lambda_c$ (Perry-Robertson curves)

deformations. The Perry-Robertson Formula is a column design formula used to account for such imperfections in the ultimate strength of columns (see Appendix A-3). The varying values of the eccentricity ratio, $\eta_e$, will affect the ultimate strength of the panel. Figure 3.24 breaks the tests down in ranges of $\eta_e$ values and compares them to the values predicted by the Perry-Robertson formula. The two Horne series were not included because the values of initial deflection reported in the literature was 0, which yields $\eta_e=0.0$, a virtual impossibility. There is some disparity between experimental values of $\eta_e$ and their predicted location. One possible explanation is that the experimental values of $\eta_e$ were only derived from the initial stiffener deflections. The Perry Robertson formula attempts to model many other factors besides initial deflection. However, the accuracy of the data for the three USNA tests is known. As is denoted on the graph, these tests fell relatively close to where they should lie with respect to the Perry Robertson formula, with small losses in strength attributable to the effects of residual stress or other experimental uncertainties.

The seven tests used to compare the effects of residual weld stresses on panel strength consisted of: four from Faulkner's (1977) residual weld series and the three USNA tests. Although some of the experimentally measured values of residual weld stress were greater than 10 percent of the yield stress (Figure 3.25), all of the series fell near or well within the Faulkner improved method (with residual weld stress equal to ten percent of yield stress). Faulkner's improved method utilizes the tangent stiffness relationship for welded plate elements and the ratio of residual weld stress to yield stress to correct for the reduced strength due to weld stress:

$$\phi_{exp} = \frac{2}{\beta} - \frac{1}{\beta^2} - (\frac{E_t}{E})(\frac{\sigma_r}{\sigma_{Yp}})$$

(3.5)

This conclusion concurs with several of the assumptions made in the design equation.

Hughes (1988) corrects the secant modulus by subtracting 0.1 (equation 2.7) -- this

corresponds to the maximum assumed residual stress of ten percent presented in Faulkner

(1977) and Chatterjee, et. al. (1976). Although many of the residual weld stresses were

measured to be greater than ten percent of the plate yield stress, the residual stress design

assumption yields valid and accurate results. The possible reason why many of the points

for experimentally-measured residual stress do not fall in the expected positions on

Figure 3.25 is most probably due to the effect of initial deformations.
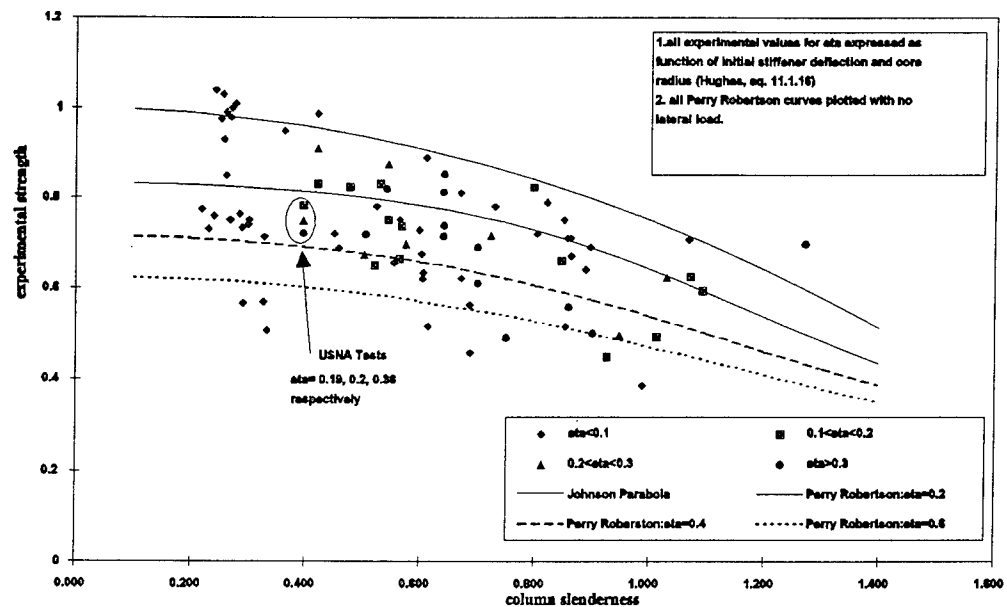
Figure 3.24: Experimental strength, $\phi_{exp}$, versus column slenderness, $\lambda_c$ (experimental $\eta_e$ values).
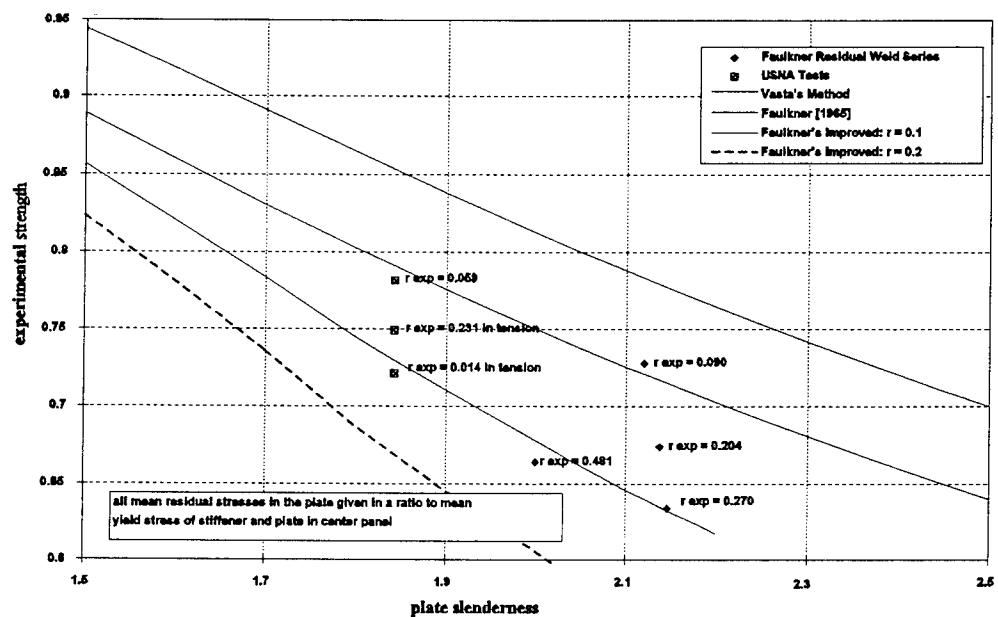


Figure 3.25: Experimental strength, $\phi_{exp}$, versus plate slenderness, $\beta$ (residual weld stresses).

## 4.1  The Finite Element Method

One of the most important aspect of finite element modeling is the subdivision of the structure into elements. Matrix analysis requires compatibility of the structure; two connecting nodes must displace equal amounts. In FEA, however, a shared or common boundary between two nodes may not have compatibility and a gap or overlap may occur (Figure 4.1). The interaction between adjacent elements typically tends to make the structure too stiff. For example, a beam element that is too long will be less likely to show the desired characteristic in bending than many shorter elements of the same total length. As such, one way to alleviate this problem is to break the structure down into smaller elements. However, smaller subdivisions complicate the analysis and require more computer solution time. Another way to reduce this error may be by the use a different type of element (i.e. increase the order of the element from a linear element to a quadratic element).
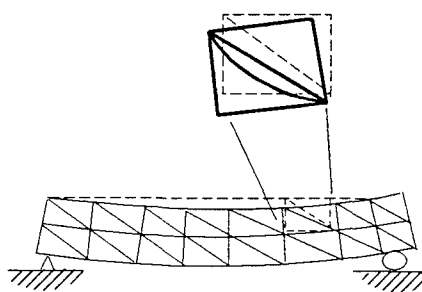
Figure 4.1: Interaction betweeen nodes and the deformation of elements (Hughes, 1988).

The problem becomes more complicated when the analysis involves a non-linear relationship such as plastic deformations in a stiffened panel. The requirements for modeling non-linear systems become more stringent. In order to avoid singularity errors in the computer solutions, the method of modeling must ensure that the solution is tractable; buckling analyses, for example, are particularly sensitive to material property definitions. As a result, the distinction between linearity and non-linearity is often vague. In compressive strength analyses, a grillage displaced past its yield point will experience some strain hardening, but eventually its stiffness will approach zero. The transition from linear to non-linear analysis is hard to define, but is usually found when the analysis encounters negative eigenvalues in the solution process. Often in non-linear FEA, the result is a solution that, at best, requires a large number of iterations or may not even converge. There are several ways to deal with this problem in FEA. The different approaches used for the USNA model will be presented in more detail later in the discussion.

## 4.2 Modeling

The finite element program used for the analysis is ABAQUS. The program has the capability for non-linear finite element stress analysis and modeling. Several simplifying assumptions were made in constructing the model. In the actual grillage there are fillets at the intersection between the frame tabs and the plate. Because the analysis is not concerned with this region, no detailed refinement was necessary and these areas were modeled as right angles. Additionally, several estimations had to be made when assigning

connections between different element types. These conditions attempt to model the behavior of the actual grillage as accurately as possible.

Figure 4.2 is the element subdivision for the plate. The plate is broken up into four-node rectangular elements; the majority of these nodes measure 76 mm. X 152 mm. (3 in. X 6 in.). At the location where there are tabs near the frames, a mesh refinement was necessary to model the geometry accurately. The element type used in the plate was S4R5, a four-node, doubly-curved shell element. This element allows for reduced integration and hourglass control using five degrees of freedom per node ($u_x$, $u_y$, $u_z$, and two in-surface rotations). The size of the plate element was common among both the 6.4 mm.-(1/4 in.) and 4.8 mm.-(3/16 in.) thick plates.

In each of the four stiffeners, there are 18 beam elements measuring 152 mm. (6 in.) in length. In the two frames, the beam elements are spaced every 76 mm. (3 in.). The element types used in the frames and stiffeners were the same. The B31 element allows bending, stretching, and torsion. The element is a two-node, linear beam in space. A node is located at each end of the beam element. All degrees of freedom are active in this beam: $u_x$, $u_y$, $u_z$, $\phi_x$, $\phi_y$, and $\phi_z$.

Multi-point constraints (MPCs) are used to model the attachment of one element to another. The interaction between elements is critical to the accuracy of the model. The two types of MPCs used in the model are links and beams. A link provides a pinned-rigid link between two nodes in order to keep the distance between the two nodes constant (Figure 4.3). A beam MPC provides a rigid beam between two nodes in order to constrain the displacement and rotation at the first node to the displacement and rotation
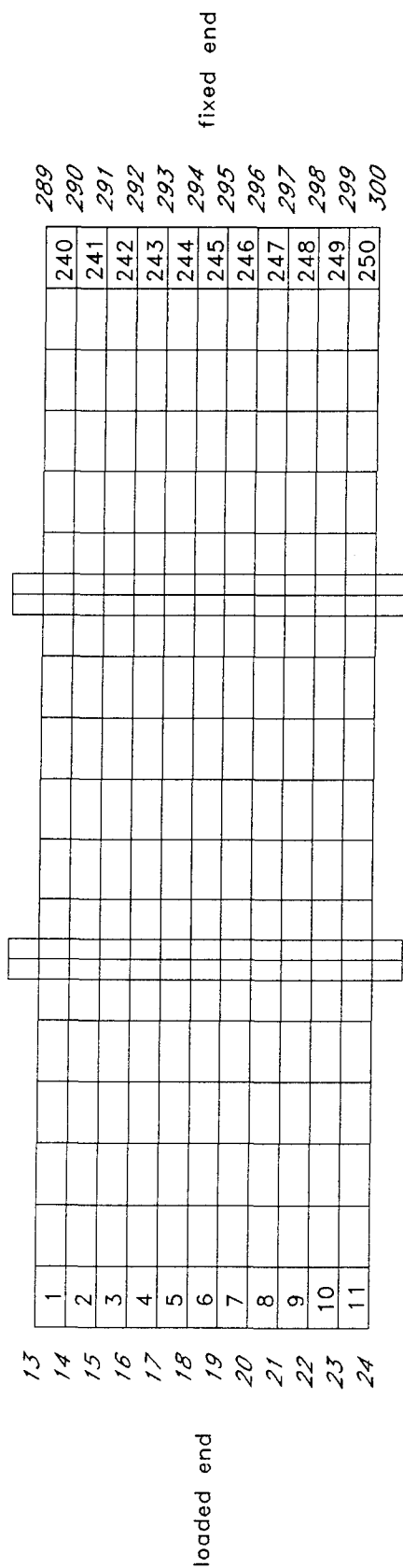
## Subdivision of Plate

element numbers

*node numbers*

Figure 4.2: Element subdivision of plate (nodes and elements). All nodes and elements shown are numbered consecutively.

at the second node. Beam MPCs were used sparingly in the model mostly because their characteristics tend to be too rigid. At several places in the model, beam MPCs were used to make the solution tractable or because additional rigidity was needed. At the loaded and reaction ends of the panel, beams were used to provide a rigid connection between the edge of the stiffener and the edge of the plate. Each end of the grillage is welded to a flat plate which induces a fixed-end type loading condition when it is bolted to the test fixture. Likewise, beam MPCs were used at the connection between the frames and the edge of the plate. Again, the edges of the frame and plate were welded and attached to the testing rig (Figure 4.4). In addition, because two different plating thicknesses were modelled, beam MPCs were used to connect the offset nodes of the end plates to the center plate. In all other cases, links were the primary MPC, most notably in attaching the remaining corresponding nodes of the stiffeners to the plates and of the frames to the plates.
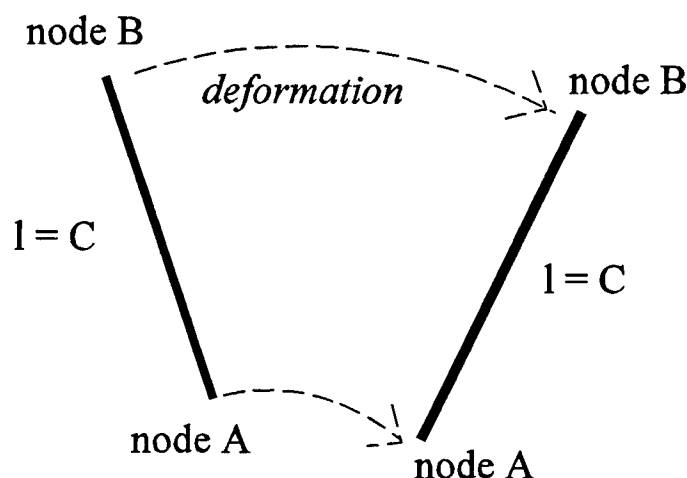


Figure 4.3: Link multi point constraint (MPC) (ABAQUS, *Users Manual, Volume II* 1994)

An EQUATION in ABAQUS is a method for the user to define a linear MPC. The MPCs in EQUATION take the form (ABAQUS:*Users Manual: Volume II*, 1994):

$$A_1 u_1 + A_2 u_2 + \ldots\ldots + A_N u_N = constant \qquad (4.1)$$

where the A values represent magnitudes and the u terms, active degrees of freedom. In the model, a two-term equation is used to model the interaction between the stiffener and the frame. The only constraint imposed by this MPC is an equivalent (in magnitude and direction) rotation of the stiffener about the z-axis when the frame rotates about the z-axis. This constraint attempts to model the rigid connection between the stiffener and frames; it also allows the stiffeners to adopt the characteristic "s"-rotated shape.

Boundary conditions are used to impose edge constraints on the model. These conditions model the points of attachment between the grillage and the test fixture. On the loaded edge of the plate, the end is bolted to the loading head; therefore, this edge of the plate in the model is constrained in all degrees of freedom except for $u_y$. At the fixed end attached to the reaction head, the model is given an fixed boundary condition where it is constrained in the $u_x$, $u_y$, $u_z$, $\phi_x$, $\phi_y$, and $\phi_z$ directions for both the stiffeners and the plate. At the tabs of the plate where the frames attach to the reaction links (see testing rig description), the edge of the plate is only modeled to be constrained in the $u_z$ direction. This condition allows the model to rotate about any axis and translate freely in the longitudinal and the transverse direction, very similar to the actual behavior of the reaction link (Figure 4.4)

For a non-linear buckling analysis, the proper definition of the material behavior of

the model is essential. In the elastic region, the element properties were defined to be equal to the nominal values for mild steel: Elastic Modulus (E) = 207 MPa and Poisson's Ratio (v) = 0.3. The material definitions for the plastic behavior of the elements were based upon compression coupon tests performed at NSWC. Refer to Figures 4.5(a,b) for the actual stress-strain diagrams obtained from NSWC. The behavior of mild steel in a compression test exhibits essentially an elastic/plastic behavior. As a simplification for modeling the stress strain curves were modeled to be linear to the point at which yielding occurred. After yield, the slope of the stress strain curve decreased slightly from the initial slope, E. This new slope line continued for only a small change of strain, after which the material went completely plastic (a horizontal line of E=0). The behavior of steel in compression complicates the solution process because at the point of buckling, the structure loses all of its strain hardening which ultimately leads to a collapse of the structure. As a result, a conventional solution cannot be used in this case and a new method must be adopted.

The FEA proved to be very complex. After the plate yielded and began to lose strength, the solution became complicated. Several methods were attempted which promised to characterize the post-buckling behavior of the grillage. The RIKS method was developed in the 1970's by Edward Riks and implemented for stress-displacement models in the early 1980's by Mike Crisfield (ABAQUS, 1993). A simple boundary-displacement loading condition and a RIKS analysis were the two primary solution methods adopted. The boundary-displacement method attempted to model the non-linear case by displacing the loaded-end some given distance. The maximum end-deflection
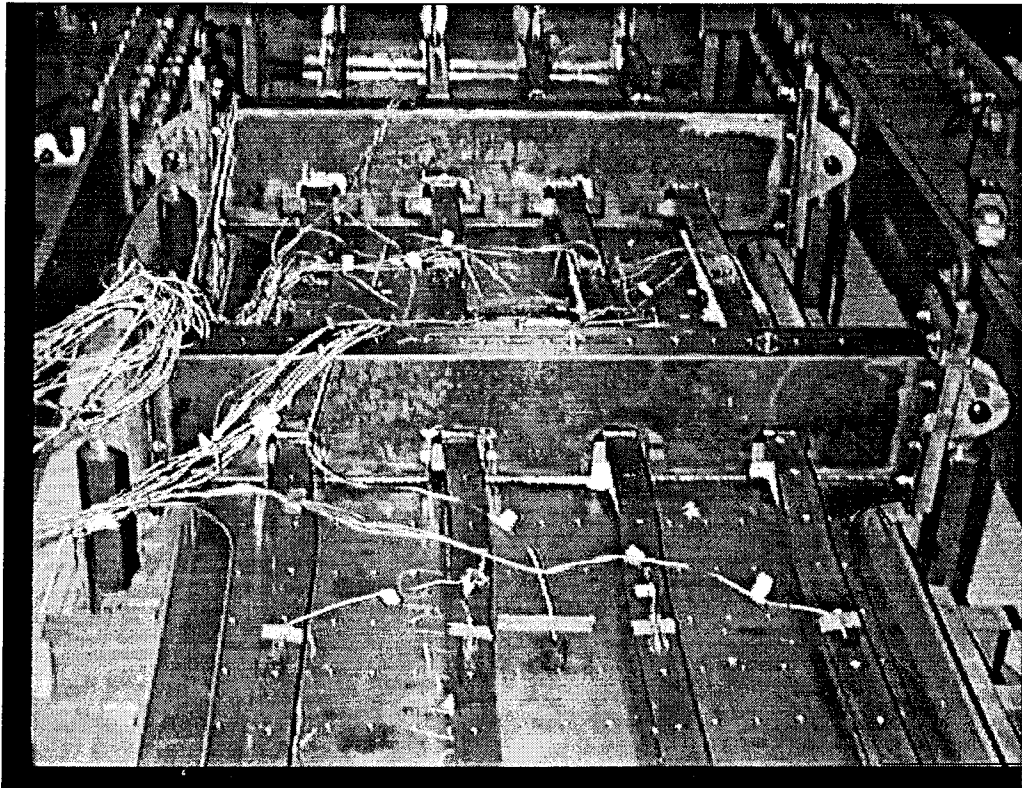
Figure 4.4:   Frame attachment to the reaction links, showing constraint conditions.
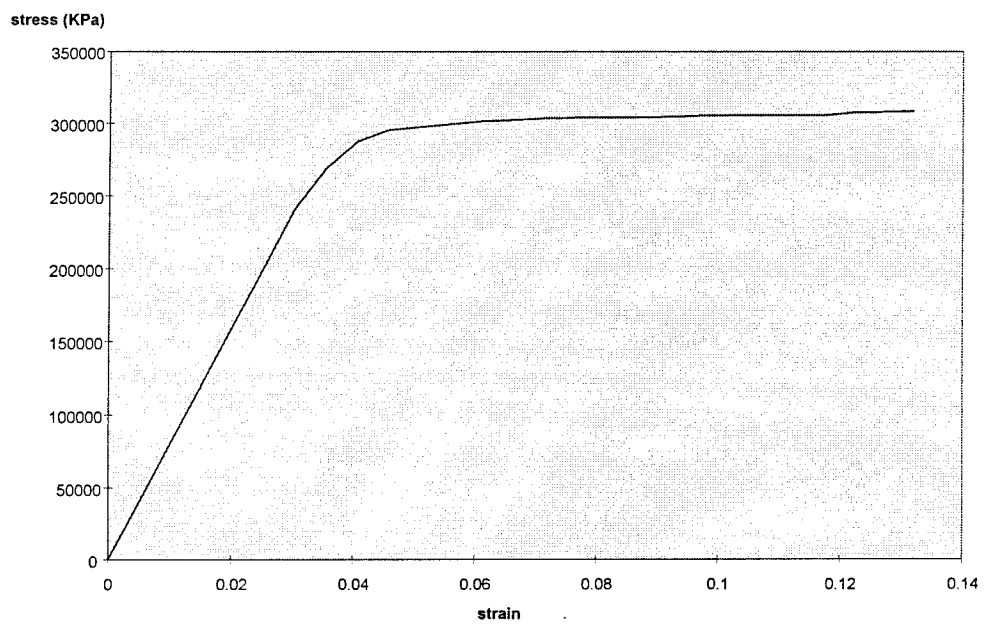


Figure 4.5a:   Compressive coupon test for center plate (NSWC).
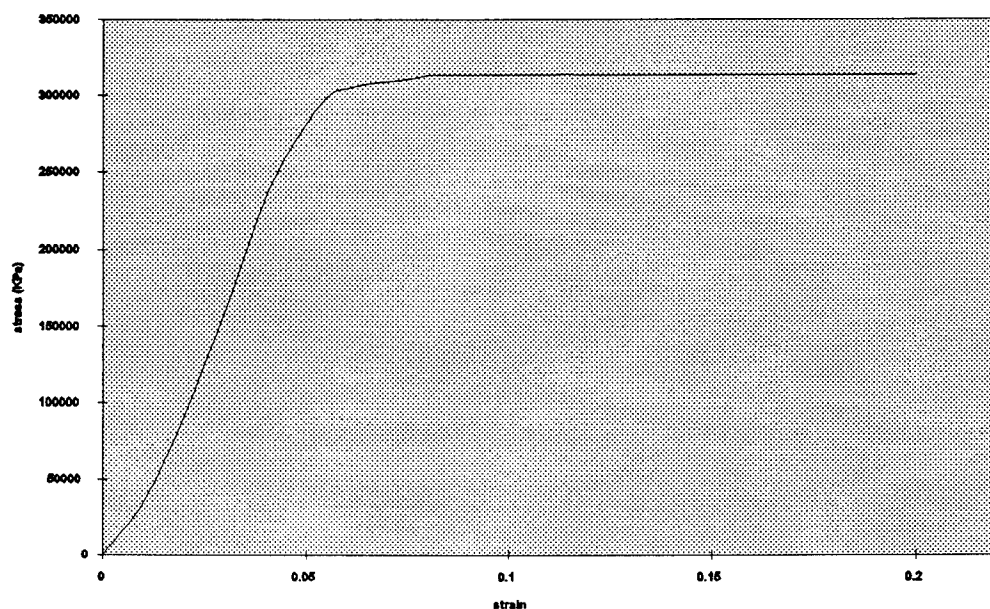
Figure 4.5b:   Compressive coupon test of end plates (NSWC).
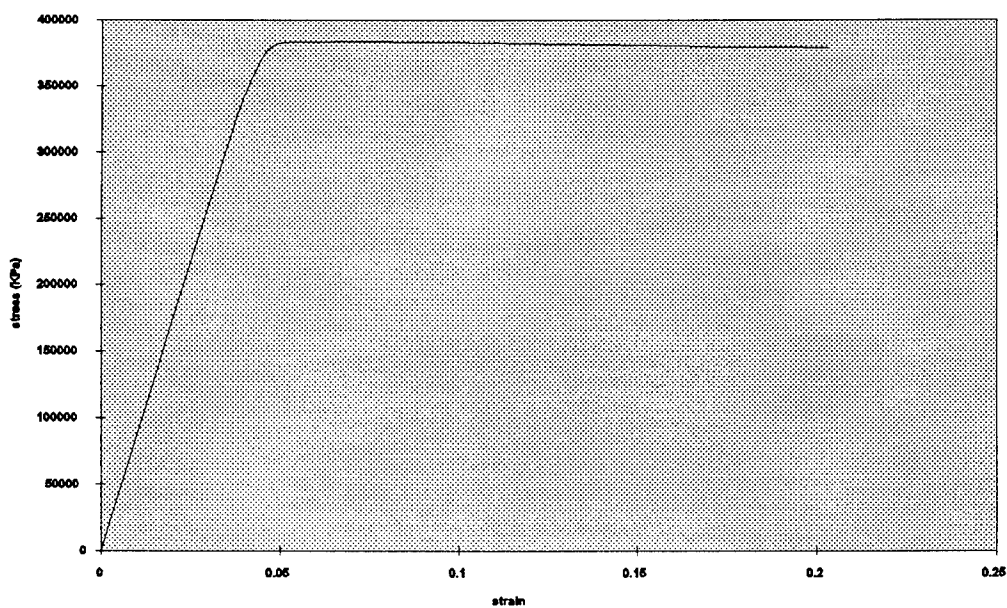


Figure 4.5c:   Compressive coupon tests of stiffeners (NSWC).

achieved through this approach was approximately 3.7 mm. (0.144 in.). The RIKS

algorithm solves simultaneously for load and displacement (see Appendix B1). RIKS

analysis is useful for non-linear analysis and is particularly sensitive to imperfections in the

model (a solution is usually not possible without some initial perturbations). Two

methods were used to perturb the mesh. First, a FORTRAN code was written that

perturbed the mesh into a single half-wave longitudinally and transversely with a maximum

deflection equal to $\frac{a\ (\ length\ \ of\ panel\ )}{750}$ (Antoniou, 1980). The second method used to

perturb the mesh was to preload the model in a separate step which created a perturbed

mesh before the RIKS step began. The best results obtained from RIKS did not displace

the model nearly as far as the boundary-displacement loading.

Neither method was able to effectively model the post-buckling behavior of the

grillage. Since the material is defined to be very nearly elastic-plastic, the model must then

deal with two non-linearities: geometric and material. At the point which corresponds to

the peak on the load versus end-shortening curve, the material goes very nearly plastic.

ABAQUS has difficulty modeling the strain-hardening of the grillage when the model

stiffness approaches zero. The model under the boundary-displacement loading reaches

the peak but cannot progress past this point where a reduction in loading and an increase

in end-shortening would occur.

Nevertheless, the fact that the analysis halts at this point is interesting in itself. It

suggests that the model is exhibiting the behavior that would be expected; however, the

FEA is unable to model any significant portion of the post-buckling behavior of the

grillage. Ideally, analyses such as this one could be used to predict the behavior of

structures under extreme loads. The structural designer, in this case, would be most concerned with the ultimate strength of the grillage (the peak on the load versus end-shortening curve). The post-buckling behavior of the grillage would not be important for design purposes. Therefore, the results obtained from this analysis would be useful for a structural designer concerned with designing for the ultimate strength behavior.

## 4.3 Finite Element Results

The results of the FEA matched the actual behavior of the grillage fairly well. The displaced shape of the grillage (magnified for presentation) is shown in Figure 4.6. The desired patterns of displacements and multiple half-wave patterns seen in the experimental tests were generated by the FEA. However, a more rigorous comparison is necessary to quantify the level of accuracy obtained by this method. The magnitudes of stresses and displacements and the relationship between them in the loading sequence are more indicative of the success and usefulness of the model.

Figure 4.7 represents the load versus end-shortening relationship for the nodes through the line of action formed by nodes 18 and 294 (all values on the results figures are expressed in U.S. Customary units). This load shown is the partial load carried by one node only. When the values of load for this node are multiplied by the twelve plate nodes across the loaded end and the effects of the load on the stiffeners are also considered, the total load when the solution fails at 3.66mm (0.144 in.) is 1.31 MN (293,000 lb). The average ultimate load for the three USNA tests was 1.39 MN. The percent difference between the FEA prediction and the average ultimate load was 6%. Figure 4.8 shows the maximum end-displacement of the loaded end of the grillage (upper-left end) equal to 0.144 inches or 3.66 mm, which corresponds to the maximum end-displacement of the load versus end-shortening curve. The prediction of the load versus end-shortening curve relationship is well within the expected tolerances for FEA for this project.

The values of the stresses at failure and their locations characterize the type of failure. In this case, theory and experiment will almost always result in a Mode II failure.

The maximum stresses in the center plate are 308 KPa (47,000 psi) and are located at the connection between the frames and the plate in the bays between the stiffeners (Figure 4.9). The stress in the center is 304 KPa (44,200 psi). Figures 3.9(a), 3.13(a), and 3.17(a) show the development of experimental stresses in the geometric center of the center panel at different increments during loading. Non-linear, plastic behavior is expected when the distribution of the stresses from gages 35, 37, and 39 become non-linear. The stresses at the point of non-linearity in the center of the middle panel match the FEA stress predictions at the center, with experimental stress values at 304 KPa (44,200 psi). Moreover, the experimental plots show approximately the same magnitude of loading at the point of buckling. The 0494 grillage, for example, has a corresponding load at the plastic point of approximately 1.32 MN (298,000 lbs).

Another indicator of the validity of the model results is the magnitude of vertical displacements as expressed in Figure 4.10. Each of the displacements is expressed on a contour plot relative to the initial frame of reference. The maximum positive deflection occurs at the longitudinal center of the plate in three locations between the stiffeners. On each edge, the displacement magnitudes are 0.406 mm (0.016 inches). At the geometric center, the vertical displacement is 0.361 mm (0.0142 inches). Between these maximum points across the width, the plate adopts a half-wave pattern but never drops below the frame of reference. No experimental results were collected that could validate or invalidate the displacement results quantitatively. Qualitatively, the patterns of displacements in the FEA match the multiple half wave patterns seen in the actual grillages.

Future experiments on actual grillages need to implement improved methods to validate or invalidate the vertical displacement predictions of the FEA. One experimental method to obtain this information would be to replace the dial gages with digital dial gages. An output from the digital gages could be fed into the NEFF 470 system and scanned by the data acquisition system. This method would allow the displacement magnitudes to be correlated to the exact level of ultimate load.

The results of this FEA show that non-linear FEA can be used as a practical method of predicting the ultimate strength of a stiffened panel. There are some limitations to the method, namely, the inability of the ABAQUS program to model any significant portion of the post-buckling behavior. The validity of the vertical displacement output data is still in question. A test conducted on a grillage with digital dial gage information may provide the information needed to increase confidence in the displacement output. Regardless, this type of FEA may be used to determine maximum permissible loads and stresses, not displacements. Therefore, the method should continue to be used and improved as a viable method of stiffened panel ultimate strength prediction.

One of the original goals of this FEA was to develop a model which could help increase the database of tests with different parameters (aspect ratio, plate slenderness, etc.). This goal was not fulfilled entirely. This particular analysis has proven that the model is able to predict the behavior of one particular grillage. More experimental grillages need to be modeled and tested with FEA. The data from the experiments can be compared to the FEA results. A larger database of comparisons between FEA prediction and actual testing will prove whether the method is valid for all types of grillages. If this

method of FEA proves to be a valid prediction method for all types of panels, it can ultimately be used to build a larger database of stiffened panel tests or as a first cut method in structural design.

DISPLACEMENT MAGNIFICATION FACTOR =    100.

TIME COMPLETED IN THIS STEP     86.7      TOTAL ACCUMULATED

ABAQUS VERSION: 5.3-1    DATE: 22-FEB-95   TIME: 14:28:24

STEP 1 INCREMENT 47
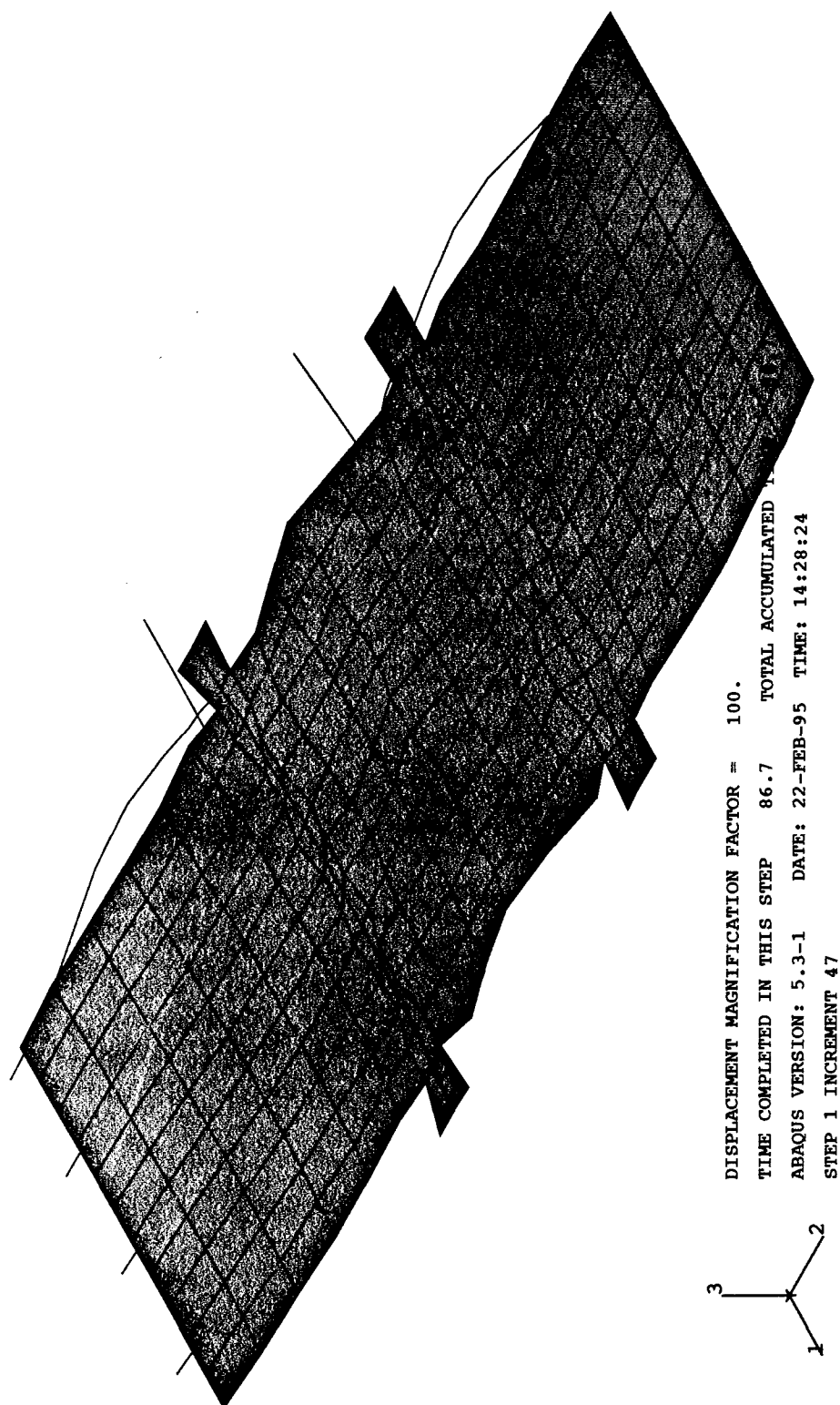
Figure 4.6:    FEA Results:    displaced shape (x100)
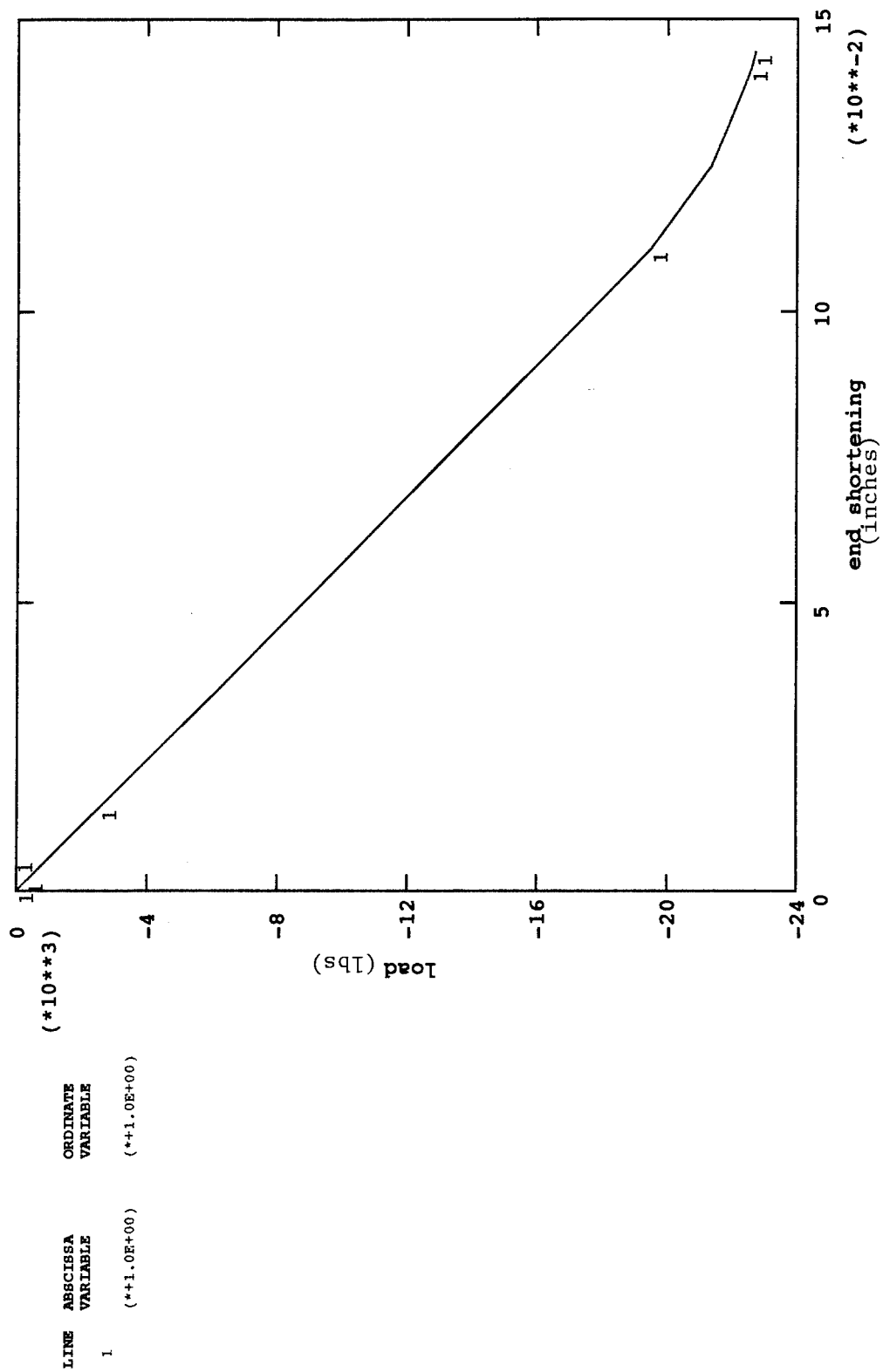
Figure 4.7:   FEA Results:  load versus end-shortening plot of nodes 18 and 294. (compression is defined to be negative).
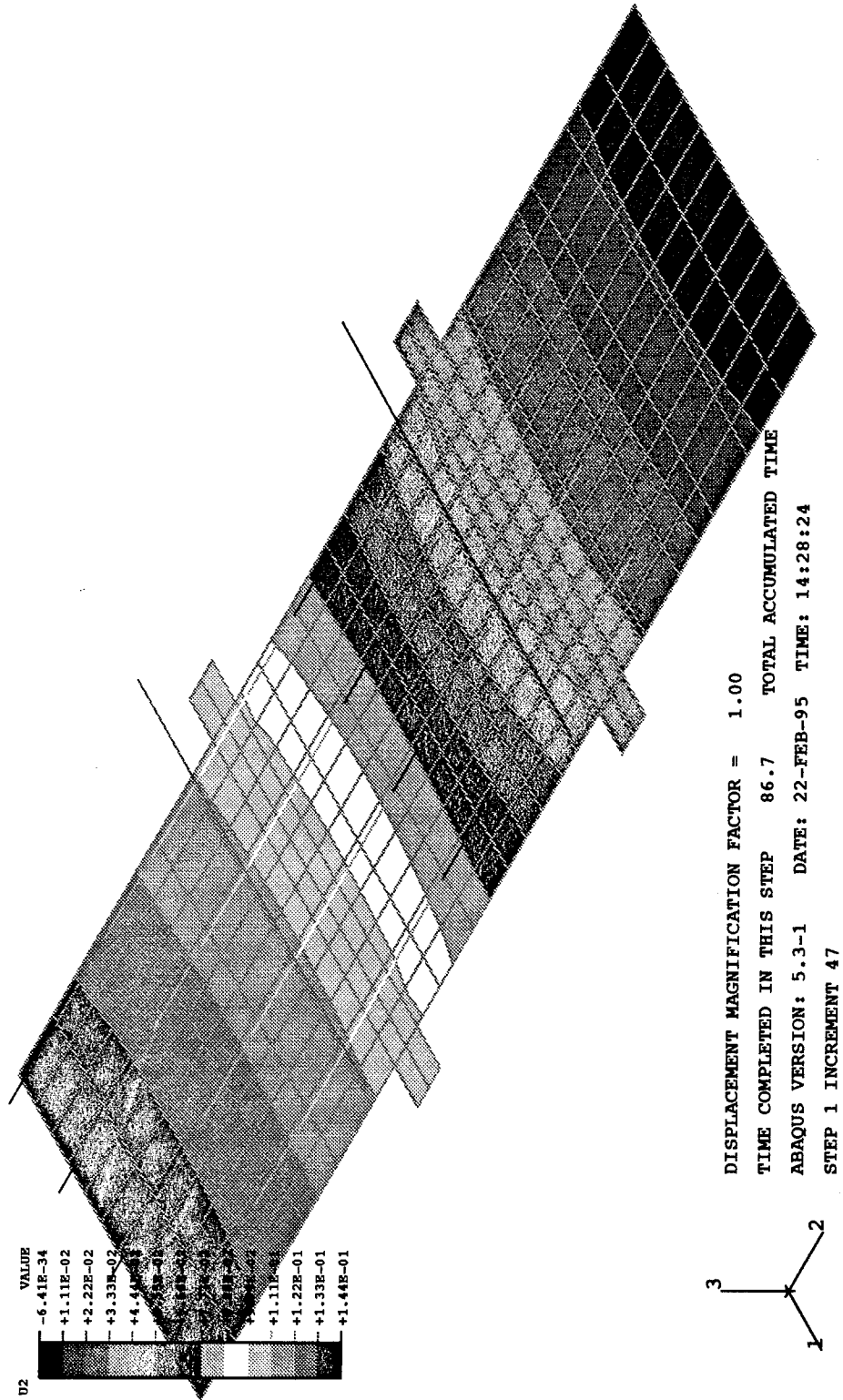
Figure 4.8:   FEA Results:   end displacement contour plot (u2).
(units in inches)
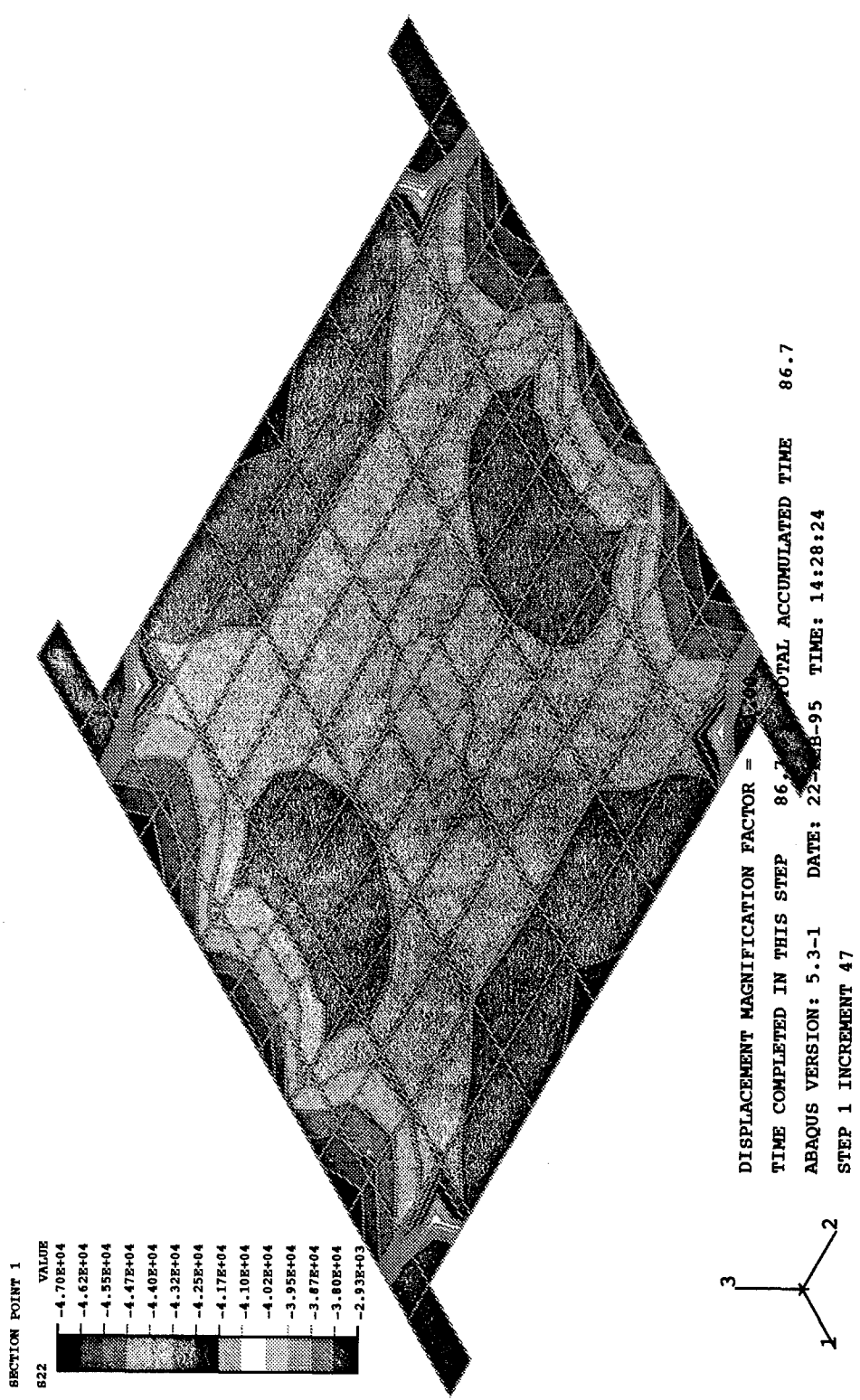
Figure 4.9: FEA Results: contour stress plots (s22).
(units in psi)

DISPLACEMENT MAGNIFICATION FACTOR = 1.00

TIME COMPLETED IN THIS STEP    86.7    TOTAL ACCUMULATED TIME    86.7

ABAQUS VERSION: 5.3-1    DATE: 22-FEB-95    TIME: 14:28:24

STEP 1 INCREMENT 47
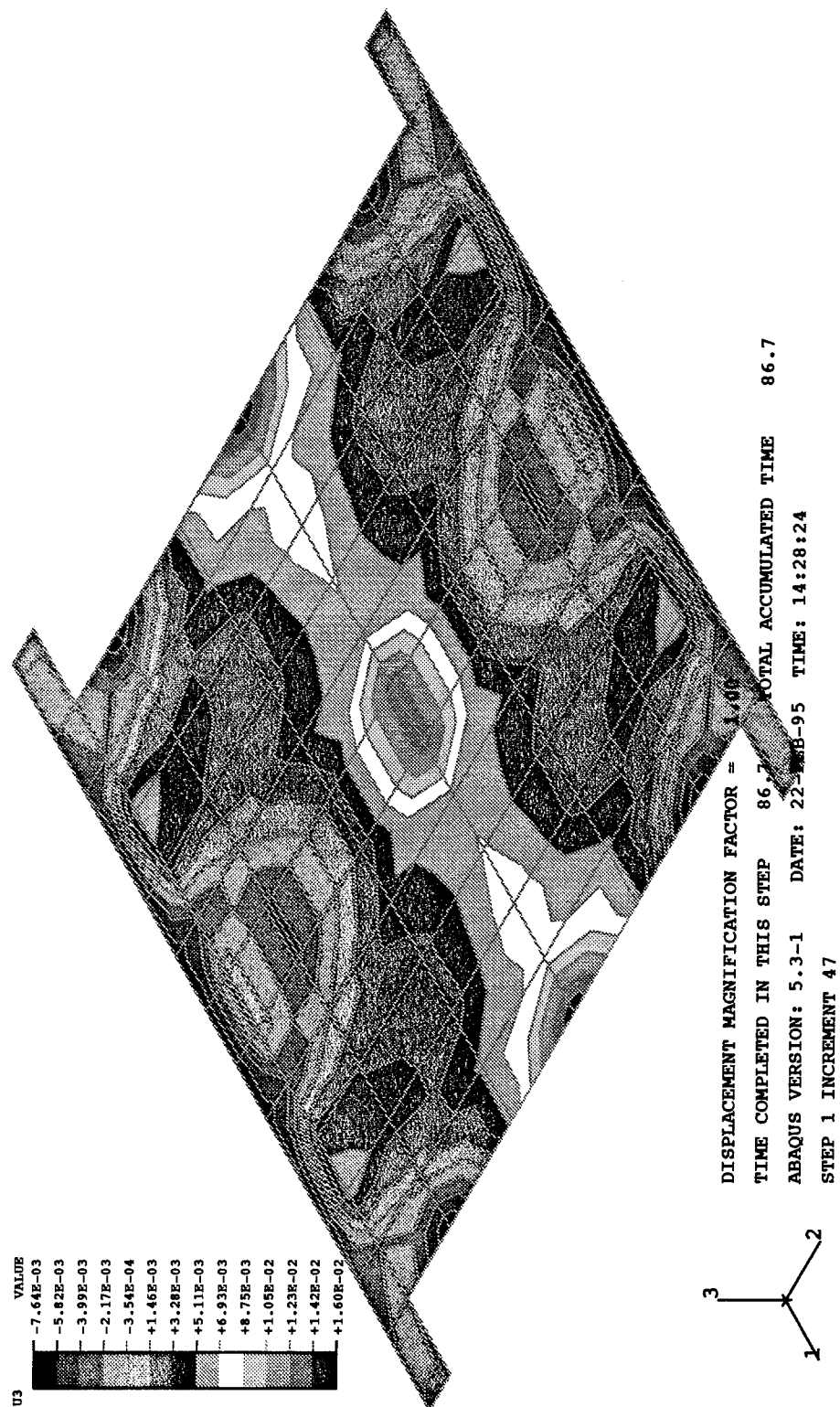
Figure 4.10:    FEA Results: vertical displacement contour plots (u3).
(units in inches).

# 5  Structural Reliability - Partial Safety Factors

Structural reliability has its roots in civil and aerospace engineering. Most engineering design practices are based upon simplified, deterministic relationships. The limitations to the current practices are readily apparent when one tries to quantify the level of safety associated with an entire ship's structure in a seaway. Currently in the field of naval architecture, there is a great interest in developing and implementing some form of reliability-based structural design into the design codes and methods (Mansour, et. al, 1984, White, et. al., 1987, Hughes, et. al., 1994). These reliability methods will allow the naval architect to design a tanker or warship to some acceptable limits and desired degrees of safety depending upon the differing operational, environmental, political, and economic requirements imposed upon each particular vessel.

In principle, reliability-based design is easy to understand; the structure has some value for strength and it is subjected to some value of load. The load (Q) and strength (S) can each be represented by a statistical probability density function. The strength should exceed the load for the structure to be safe. However, in almost all cases the extreme values of load and strength overlap and failure may occur (Figure 5.1). The region of overlap represents the probability of failure, $P_f$.

$$P_f = P(S < Q) \qquad (5.1)$$

where probability of failure is:

$$P_f = \int F_s(x) f_Q(x)\, dx$$
$$(CDF)\ (PDF) \qquad (5.2)$$

Probability of failure is not equal to the area of the overlap, but is qualitatively

represented. The greater the distance between load and strength, the safer the structure

will be. An engineer can never design a structure that is 100% safe. The probability of

failure for engineering structures typically range from $10^{-2}$ to $10^{-9}$ (Mansour, et. al., 1984).

An appropriate value of probability of failure is determined by the acceptable level of

safety associated with the structure.
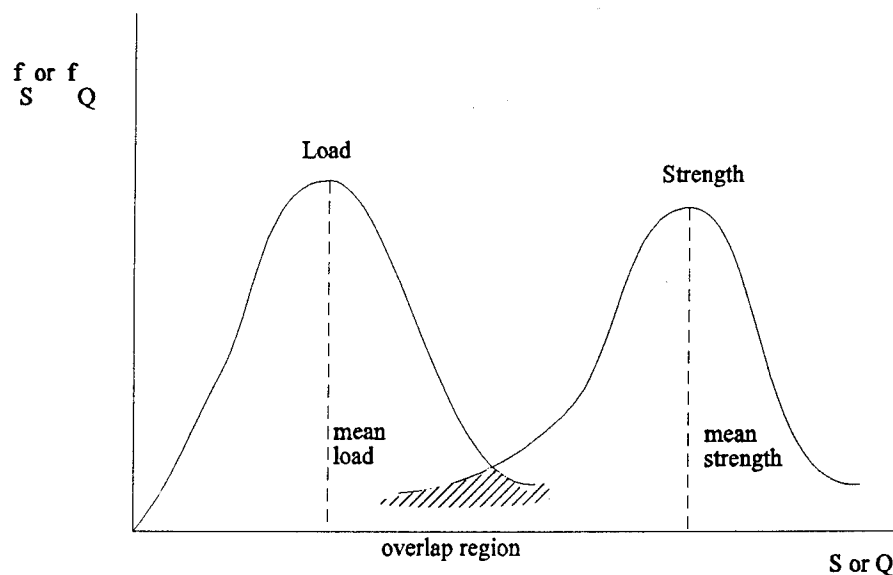


Figure 5.1: Statistical overlap of load and strength distributions.

There are many uncertainties which enter into the strength of a structure: material

yield stress, initial deformations and imperfections, modulus of elasticity, effects of

welding, manufacturing errors, etc. Reliability-based design attempts to quantify the

uncertainty associated with each of these design variables. Those variables which have

little or no variation often may be treated as deterministic, i.e. they have only a mean

value and no deviation.

One way to affect the region of failure in order to bring the structure to a desired degree of safety is to assign partial safety factors which force the load and strength curves to a acceptable limits of failure. In order for the developers of reliability-based design codes to tabulate these partial safety factors, they must know the distribution type and variance of both the load and strength. In design, the naval architect knows the operational geographic region for the ship. This operational area determines what type of loading the ship will encounter. For example, the Navy uses the winter North Atlantic as a worst case operational area. Naval architects have become proficient at statistically characterizing the distribution type and variance of different seaways. The strength, however, relies on two types of uncertainty: statistical and modeling. Engineers have been able to quantify the statistical uncertainty; the variability of factors such as material yield strength, sizing uncertainty, and modulus of elasticity have been quantified and/or are relatively easy to find. The modeling uncertainty, the quantification of the uncertainty and bias associated with the standard algorithm, is the missing piece in reliability-based design. With this information, partial safety factors can be determined and tabulated through First Order Reliability Methods(FORM)[1].

The final step in this section was to use the information from the data analysis of 86 stiffened panel tests to determine the modeling bias associated with the standard theoretical algorithm defined in Hughes (1988). Ultimately, this information could be used

---

[1]

A Ship Structures Committee (SR1345)project is currently working on using First Order Reliability Methods (FORM) to develop and tabulate partial safety factors.

by reliability-based design code developers to assign a partial safety factor to compensate for the modeling uncertainty.

The data analysis considered the results of all the tests and also broke the tests down into categories: the categories investigated were lateral and axial loaded panels only, Mode II predicted failures only, multi-bay tests only, single bay, fixed-end tests only, and single bay, pinned-end tests only. The purpose of these sub-groups was to try to determine the bias associated with various parameters that could be attributed to the variation on the theoretical versus experimental strength plot in Figure 3.21. The results of the overall analysis of all the tests and the sub-groups are given in Table 5.1.

| Table 5.1 | | | | | | |
|---|---|---|---|---|---|---|
| | all data | lateral and axial load only | mode II predicted failure only | multi-bay tests only | single bay: fixed-end | single bay: pin-end |
| mean | 0.916 | 0.916 | 0.938 | 0.878 | 0.946 | 0.850 |
| COV | 0.159 | 0.126 | 0.129 | 0.103 | 0.166 | 0.053 |
| distribution type | normal | inconclusive | log-normal | normal | log-normal | normal |
| # tests in set | 86 | 8 | 75 | 14 | 17 | 55 |

The statistical analysis considered the probability distribution function (PDF) and cumulative distribution function (CDF) of each group. Normal and log-normal distributions were fitted over the data. Chi-squared and Kolmogorov-Smirnov (K-S) tests were performed on the PDF and CDF functions, respectively, to determine relative goodness of fit (Ang, et. al., 1975). All goodness of fit tests had a 95% confidence level.

The statistical results of all the tests showed the bias to be normally distributed with a mean of 0.916 (theoretical strength over the experimental strength) and a COV of 0.159. These results confirm the general trend in Figure 3.21 and a similar data set in SSC-375 (Hughes, et.al., 1994); the theory tends to be conservative but there is still considerable scatter about the one-to-one correlation line (almost 16% variation). By comparing the mean values of the single bay tests, the results suggest that the actual edge condition is closest to simply-supported, somewhere between a fixed and pinned-end edge constraint. Furthermore, the multi-bay tests are more conservative than single bay tests, with a mean of 0.878. As was discussed in Section 3.7, the algorithm grossly underpedicted some failures as Mode I. By considering the tests predicted as Mode II only, the data points that fall significantly below the correlation line on Figure 3.21 are discounted, and the mean increases to 0.938.

Three groups had a small number of data points which tends to make their results less reliable: lateral and axial load only, multi-bay tests only, and fixed-end, single bay. As would be expected in these cases, the PDF and CDF functions did not show particularly good fits to the data histograms. In particular, the lateral and axial load only and single bay, fixed-end groups showed relatively poor PDF and CDF fits. The multi-bay PDF did not fit the data well due to an insufficient number of data points. More multi-bay tests would probably validate the conclusion of a normally distributed relationship between theory and experiment. The results of the lateral load are presented in Table 5.1, but are too inconclusive, due to an insufficient amount of data, to make any comment.

The most important result of this statistical analysis is the normally distributed

relationship for all of the 86 tests considered in this parametric study. This and larger databases will be used to determine the partial safety factors used to account for the biases associated with the theoretical model. Multi-bay tests come the closest to modeling the behavior of a failed panel section in a much larger hull structure; more multi-bay tests will model the actual behavior of a single panel in a continuum of panels better than the many single bay tests found in the literature. More data from lateral load tests will help quantify the bias that is the result of the effective strengthening of a panel under lateral and axial load. These data will be especially useful because indications are that the standard theoretical model tends to underpredict the strength of a stiffened panel under combined loading.

## 6 Conclusions

The objective of this project was to determine the level of uncertainty associated with the ultimate strength predictions generated by the standard algorithm used in stiffened panel design of ship structures. The measure of modeling uncertainty and bias is an important piece in the development of reliability-based design codes for ship structural design. The three approaches used to achieve this objective were experimental testing of stiffened panel grillages, historical data analysis, and non-linear finite element analysis (FEA). Several important conclusions can be made from these analyses about the bias and uncertainty in stiffened panel design and testing. These conclusions will lead to improved methods of stiffened panel testing, prediction, and eventually, ship structural design.

1.      The statistical analysis of the database of stiffened panel tests showed that the standard algorithm underpredicts the strength of a stiffened panel most of the time. There is, however, a large amount of scatter between the experimental and theoretical strength relationships. A statistical analysis indicates that the bias is a normally distributed relationship. This information on the modeling bias could be used by the developers of reliability-based design codes to determine and tabulate partial safety factors to account for the modeling bias associated with the theoretical algorithm. In turn, this partial safety factor, as well as many others, could be used to shift the the means and variations of load and strength to bring the probability of failure to a desired degree of safety.

2.      There were only a few tests which considered the effects of combined axial and lateral loading on stiffened panel strength. This limited number of data points indicates that the standard algorithm underpredicts the strength of a panel under combined loading.

The standard algorithm assumes that the lateral load induces a single longitudinal half-wave deflection pattern. In reality, the grillage adopts a more complex pattern of multiple half-waves; its net effect is a strengthening of the panel well past its predicted failure point. Combined loading is not at all uncommon in a ship structure. All of the outer hull structure below the waterline is subjected to this type of loading. An increased database of combined loading will allow the designer to assign a partial safety factor to account for the modeling bias associated with the combined axial and lateral loading condition.

3.      The experimental testing conducted in the USNA Ship Structures Laboratory added three additional tests to the database of stiffened panel tests. More importantly, the data collected from these tests provide an important numerical description of stiffened panel collapse and failure mechanisms. This numerical description proved useful for validating a method of FEA prediction for stiffened panel grillages.

4.      The historical data analysis showed the relative merits of stiffened panel testing methods. Single bay tests are particularly sensitive to the type of boundary end conditions: either fixed or pinned-end. Multi-bay tests, on the other hand, provide more realistic end-conditions on the center bay(s). This type of testing may be more costly, but is more accurate than the approximations seen in pinned-end and fixed-end single bay tests.

5.      The small amount of data on the effects of residual weld stresses seem to confirm the modeling assumption of residual stress equal to ten-percent of the yield stress. More tests should consider the effects of weld-induced residual weld stresses in order to validate this assumption. The variation in weld stresses can be quite large when such variables as

weld procedure, environmental conditions, manufacturing tolerances, etc. are factored into the design. As such, statistics from a larger database of residual weld tests can be used to weight the partial safety factors for strength to account for the statistical variation in the residual weld stresses on stiffened panels.

6.     Non-linear FEA shows promise as being a cost-effective method of building upon the stiffened panel test database. The numerical predictions of the stress-displacement relationships for the panel to its buckling point are very near the actual tests conducted in the USNA test fixture. More data is still needed to verify the vertical displacement predictions. However, this information is not as important as the stress-displacement predictions. More FEA models must be compared to experimental results to validate this method of prediction. Once sufficient confidence is gained in the ability of the method to predict the ultimate strength of stiffened panels accurately, it can be used to effectively "test" other stiffened panel configurations.

## 7 Recommendations for Future Work

The following recommendations are made:

1.      More combined lateral and axial load tests need to be conducted. The small number of tests reported in the literature are insufficient to make any definitive conclusions about the effects of this type of loading. An increased data base of these types of tests is necessary and should be the number one priority of future testing.

2.      Work should also be concentrated on ammeding the standard algorithm for combined loading conditions. The assumption that the plate will buckle in a single half-wave has been shown to be consistently inaccurate. A revised formula should consider the more complex mutli-half wave failure pattern.

3.      More multi-bay tests need to be conducted. Multi-bay tests are necessary to model what actually happens in a ship's structural grillage. Multi-bay tests are costlier than single bay tests. However, it was shown in the parametric analysis that it usually takes a combined analysis of the behavior of two single bay tests (one pinned-end and one fixed-end) to model the simply supported behavior of an actual ship's grillage because one tends to overpredict the mean and the other, to undepredict the mean. Therefore, the net cost of a multi-bay test may be less than the total cost of two single-bay tests.

4.      Digital dial gages are needed as a part of the data acquisition system. These gages provide displacement relationships which can be directly correlated to corresponding stresses and loads. This information will prove useful in validating the FEA vertical displacement predictions.

5.      More FEA models need to be constructed of different tests found in the literature and their stress-displacement results need to be compared to the known data. The net

result will either validate/invalidate this method of prediction. Provided the method is

validated, a large database can be built by the relatively inexpensive FEA predictions.

# References

ABAQUS, 1993, Analysis of Snap Through, Post-Buckling, and Structural Collapse Analysis, Hibbitt, Karlsson, and Sorenson, Inc.

ABAQUS, 1994, Users Manual: Volume II, Version 5.4, Hibbitt, Karlsson, and Sorenson, Inc.

ABAQUS, 1994, Theory Manual, Version 5.4, Hibbitt, Karlsson, and Sorenson, Inc.

Ang, A.H.S., Tang, W.H., 1975, Probability Concepts in Engineering Planning and Design: Volume 1 - Basic Principles, John Wiley and Sons, New York.

Antoniou, A.C., 1980, "On the Maximum Deflection of Plating in Newly Built Ships", Journal of Ship Research, Vol. 24, No. 1, pp. 31-39.

Chatterjee, S, Dowling, P.J., 1976, "Design of Box Girder Compression Flanges", Steel Plated Structures, Crosby Lockwood Staples, Paper No. 8.

Cook, R. D., 1995, Finite Element Modeling for Stress Analysis, John Wiley and Sons, Inc., New York.

Faulkner, D., 1977, "Compression Tests on Welded Eccentrically Stiffened Plate Panels", Steel Plate Structures, ed. Dowling, P.J., et. al., Crosby Lockwood, pp. 581-617.

Frankland, J.M., 1940, "The Strength of Ship Plating Under Edge Compression", United States Experimental Model Basin, Washington, D.C.

Horne, M.R. and Narayanan, R., 1976, "The Strength of Straightened Welded Steel Stiffened Plates", The Structural Engineer, No.11, Vol. 54, pp.437-43.

Horne, M.R., Montague, P., and Narayanan, R., 1977a, "Influence on Strength of Compression Panels of Stiffener Section, Spacing, and Welded Connection", Proceedings of Institute of Civil Engineers, Part 2, 63.

Horne, M.R. and Narayanan, R., 1977b, "Design of Axially Loaded Stiffened Panels", Journal Structural Division, ASCE, Vol. 103, pp 2243-2257.

Hughes, O.F., 1988, Ship Structural Design, SNAME, Jersey City, N.J.

Hughes, O., Nikolaidis, E., Ayyub, B.M.,White, G.J., Hess, P., 1994, "Uncertainty in Strength Models for Marine Structures", Ship Structures Committee Report, SSC-375, Washington, DC.

Kondo, J., Ostapenko, A., 1964, "Tests on Longitudinally Stiffened Plate Panels with Fixed Ends - Effect of Lateral Loading", Fritz Engineering Laboratory Report No. 248.12.

Mansour, A.E., Jan, H.Y., Zigelman, C.I., Chen, Y.N., Harding, S.J., 1984, "Implementation of Reliability Methods to Marine Structures", SNAME Annual Meeting, Paper No 13.

Merrison Committee, 1973, "Inquiry into the Basis of Design and Method of Erection of Steel Box Girder Bridges", Her Majesty's Stationary Office, London.

Murray, N.W., 1975, "Analysis and Design of Stiffened Plates for Collapse Load", *The Structural Engineer*, No.3, Vol. 53, pp. 153-8.

Rampetstreiter, R.H., Lee, T., Ostapenko, A., 1962, "Tests on Longitudinally Stiffened Plate Panels - Effect of Residual Stresses and Rotational Restraint by Stiffeners", Fritz Engineering Laboratory Report No. 248.5.

Robertson, A, 1925, "The Strength of Struts", *Institute of Civil Engineers*, selected paper no. 28.

Rockey, K.C., Evans, H.R., Griffiths, D.W., Nethercot, D.A., 1975, The Finite Element Method, Crosby Lockwood Staples.

Smith, C.S., 1968, "Elastic Buckling and Beam Column Behavior of Ship Grillages", Ministry of Defence, Navy Department.

Smith, C.S., 1975, "Compressive Strength of Welded Steel Ship Grillages", *Transactions RINA*, Vol. 117, pp.325-359.

Soares, C.G. and Soreide, T.H., 1981, "Behavior and Design of Stiffened Plates Under Predominantly Compressive Loads", Annual Meeting of the Portuguese Association of Engineers, Lisbon, pp 13-27.

Steen, E. and Valsgard, 1984, "Simplified Buckling Strength Criteria for Plates Subjected to Biaxial Compression and Lateral Pressure", SNAME Ship Structure Symposium, Arlington, Virginia, pp. 257-272.

Sweeney, R.J., 1933a, "The Strength of Hull Plating Under Compression: Progress Report No. 1", Experimental Model Basin.

Sweeney, R.J., 1933b, "The Strength of Hull Plating Under Compression: Progress Report No. 2", Experimental Model Basin.

Vasta, J., 1958, "Full Scale Ship Structural Tests", *SNAME Transactions*, Vol. 66.

White, G.J., Ayyub, B.M., 1985, "Reliability Methods for Ship Structures", *Naval Engineers Journal*, pp. 86-96.

White, G.J., Ayyub, B.M., 1987, "Reliability-Based Design Format for Marine Structures", *Journal of Ship Research*, Vol. 31, No. 1.

White, G.J., Ayyub, B.M.,Nikolaidis, E., Hughes, O.F., 1995, "Applications in Ship Structures", Probabilistic Structural Mechanics Handbook - Theory and Industrial Application, ed. Sundararajan, C.R., Chapman and Hall, New York.

Zienkiewicz, O.C., 1977, The Finite Element Method, McGraw Hill Book Company (UK) Limited, New York.

Appendix A1 - Tripping

Under axial loading a stiffener may buckle (trip) by twisting about its line of attachment of the plating. The plating may rotate with the stiffener to some extent; however, the plating also provides resistance to the rotation. The rotation of the plate with the stiffener does not necessarily constitute plate buckling. However, there is an interaction between plate buckling and tripping. It should be noted that one does not necessarily occur before the other (mostly dependent upon structural scantlings). Tripping can lead to a catastrophic mode of collapse. After tripping occurs, the plating loses much of its stiffness and overall buckling follows soon thereafter. Hence, tripping is a very real danger in ship structure failure and must always be considered.

For typical ship structures the dimensions of the beams are essentially thin-walled members. As a result, the rotation resulting from the torsion in the beams is described by the differential equation:

$$EI_{rz}d^2\frac{d^4\phi}{dx^4} - (GJ - \sigma_a I_{sp})\frac{d^2\phi}{dx^2} + K_\phi\phi = 0 \qquad (A1-1)$$

The ends of the stiffener are assumed to be simply supported. The resulting solution for $\phi$ (x), the rotation, is a sinusoidal buckled shape in *m* half waves over the length of the stiffener. The applied in-plane stress which causes tripping according to elastic theory is denoted as $\sigma_{a,T}$. The solution to the differential equation for rotation, $\phi(x)$, is the minimum value for the applied in-plane stress, $\sigma_a$, that satisfies the following equation:

$$EI_{sz}d^2\frac{m^4\pi^4}{a^4} + (GJ - \sigma_a I_{sp})\frac{m^2\pi^2}{a^2} + K_\phi(\sigma_{a,m}) = 0 \qquad \text{(A1-2)}$$

The critical mode for tripping corresponds to the integer value of m which produces the minimum value of $\sigma_a$. The expression for rotation, $K_\phi$ is a function of $\sigma_a$, the critical stress, and m, the number of half waves. If the critical buckling stress is large enough to cause local plate buckling, then tripping will not occur and the rotation will go to zero or become negative. If the number of half waves in the stiffener matches that of the plating, then this too will have an effect on reducing the rotation, $K_\phi$ to zero. The other important term in this equation is the flexural rigidity of the plating, GJ.

Hughes (1988), provides a method for explicitly solving for the critical tripping stress. As was discussed above, the importance of $m$, $K_\phi$, and $\sigma_a$ are underscored in this solution. First, an approximation of the number of half waves, $m$, which the stiffener will adopt will be found and defined to be $r$:

$$r = \frac{a}{\pi}\sqrt[4]{\frac{4DC_r}{EI_{sz}d^2b}} \qquad \text{(A1-3)}$$

$C_r$ is the factor by which the plate rotational restraint is reduced by web bending:

$$C_r = \frac{1}{1 + \frac{2}{3}(\frac{t}{t_w})^3\frac{d}{b}} \qquad \text{(A1-4)}$$

For each of the integer values of $m$ above and below $r$, the following equation is used to

determine $\sigma_{a,T}$.

$$\sigma_{a,T} = MIN \; m = 1,2,... \; \frac{1}{I_{sp} + \dfrac{2C_r b^3 t}{\pi^4}} (GJ + \frac{m^2 \pi^2}{a^2} EI_{sz} d^2 + \frac{4DC_r}{\pi^2 b}(\frac{a^2}{m^2} + b^2))$$

(A1-5)

When $r$ approaches 1, a simpler form of Equation A1-5 can be used:

$$\sigma_{a,T} = \frac{1}{I_{sp} + \dfrac{2C_r B^3 t}{\pi^4}} (GJ + \frac{\pi^2 EI_{sz} d^2}{a^2} + \frac{4DC_r}{\pi^2 b}(a^2 + b^2))$$

(A1-6)

Appendix A2 - Formation of a Plastic Hinge

The collapse of a panel due to large plastic deformations can be explained by plastic theory. Fundamentally, the theory is based upon materials that exhibit an idealized stress-strain curve that is perfectly elastic and then perfectly plastic (Figure A2.1). For a panel in tension, this assumption tends to be on the conservative side because the model does not account for strain-hardening of the material. However, in compression the "elastic/perfectly plastic" relationship is almost the exact behavior exhibited in most mild steels (Figures 4.5a, 4.5b, and 4.5c).
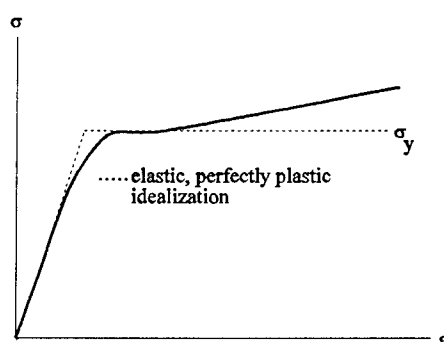


Figure A2.1: Idealized elastic-plastic stress-strain curve.

As a simple case, consider a beam simply supported on both ends (Figure A2.2). The beam is loaded laterally and a bending moment is induced. By neglecting the effects of axial loading and shear, the pure bending and deflection of the beam, $\delta$, is directly proportional to the moment, M. As the load, or moment, is increased the value of M will approach the moment required to bring the material to its yield stress, $M_Y$. As the moment increases to a value greater than $M_Y$, plasticity spreads throughout the beam. The stress in

any fiber that has yielded will remain at or very near to the value for the yield stress of the section, $\sigma_Y$. At the point where the section is entirely plastic (where the stress in the entire section has reached the yield stress), the moment is defined to be the full plastic moment of the section, $M_P$ (Figure A2.3). Every part of the beam has now yielded and the beam is no longer capable of carrying a load. The failure is analagous to placing a hinge in the beam, making it vulnerable to any form of collapse. This is an idealized model and in reality, the beam would exhibit more strength as factors such as strain hardening of the material would also contribute to the strength of the beam.
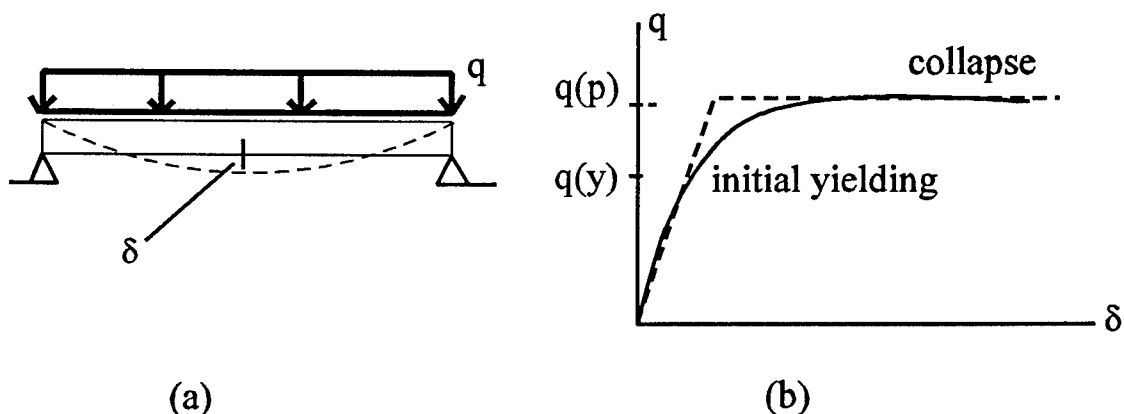


(a)                              (b)

Figure A2.2: Plastic bending of a beam. (a) An applied lateral load, q, causes a bending moment and deflection. The relationship between the load and deflection is linear until yield. (b) The applied load to cause yield, q(y) is the point of non-linearity until eventual collapse, q(p) (Hughes, 1988).

At the point in which one fiber of the material reaches yield, it can be assumed that none of the subsequent stresses in the material significantly exceed the yield stress of the material. As such, it is necessary that the stresses in a plastic hinge condition be equal and opposite in the upper and lower portions of the cross section. This condition leads to the formation of a plastic neutral axis (PNA), the line which divides the stresses of the section

into two equal areas. In a symmetric section, the PNA should coincide with the elastic neutral axis. In an asymmetric section, the PNA will not coincide with the elastic neutral axis (Figure A2.3).
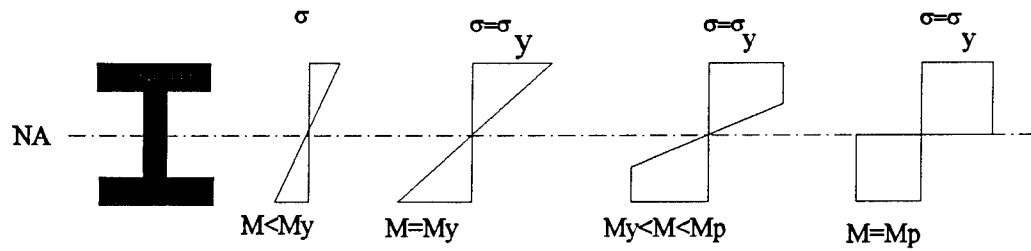


(a) Symmetric section
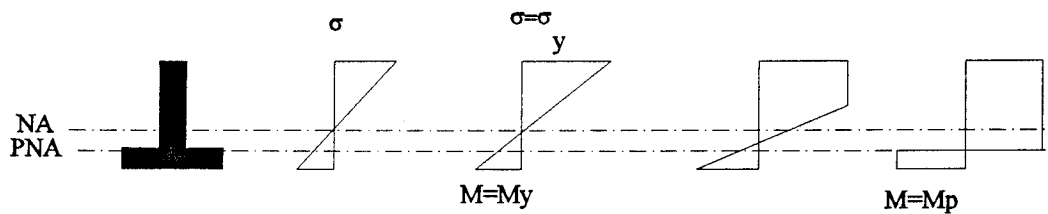


(b) Unsymmetric section

Figure A2.3: Plastic hinge formation in beam sections (Hughes, 1988).

## Appendix A3 - Perry-Robertson Formula

The Perry-Robertson formula is a simple method to predict ultimate compressive

collapse of a column. This method assumes that the column will collapse when the

maximum compressive stress reaches the yield stress. The method also accounts for the

importance of initial eccentricities in the column strength. The eccentricity factor, $\eta_e$,

utilizes the mean value of the eccentricity/residual stress factor, $\alpha$, proposed by Robertson

(1925).

The underlying theory behind this method is very similar to the collapse theory for

a stiffened panel, where:

$$\sigma_{max} = \frac{P}{A} + \frac{P\Phi\Delta}{Z}$$

$$= \frac{P}{A}(1 + \Phi\frac{\Delta}{r_c}) \quad \text{(A3-1)}$$

The first term in the equation is the applied stress or load and the second term accounts

for the loading eccentricities, $\Delta$, and the magnification effect due to column buckling, $\phi$

(Euler column buckling). An expansion of this relationship when applied to yielding gives

the following equation:

$$\sigma_Y = \sigma_{ult}(1 + \frac{\frac{\alpha L}{\rho}}{1 - \frac{\sigma_{ult}}{\sigma_E}}) \quad \text{(A3-2)}$$

This relationship is a quadratic and can be factored and expressed in a non-dimensional

form. The resulting relationship, accounting for all the terms in equation (A3-2), is:

$$R_\sigma = \frac{1}{2}(1 + \frac{1 + \eta_e}{\lambda_c^2}) - \sqrt{\frac{1}{4}(1 + \frac{1 + \eta_e}{\lambda_c^2})^2 - \frac{1}{\lambda_c^2}} \qquad (A3\text{-}3)$$

and $\lambda_c$ is the column slenderness parameter $= \dfrac{L}{\pi \rho}\sqrt{\dfrac{\sigma_Y}{E}}$

As was stated previously, the eccentricity ratio relies upon the $\alpha$ term. This term accounts

for the eccentricities and residual stresses in the column. Robertson found a mean value

for $\alpha$ of 0.003 for mild steel. The remaining parameters in the Perry Robertson formula

are geometry or material dependent.

## APPENDIX B1 - RIKS Method

The RIKS method is based upon proportional loading. The algorithm solves simultaneously for load and displacement. The load magnitude controls the increments taken along the load displacement response curve (Figure B1-1). RIKS analysis is performed as a separate loading function on ABAQUS. As the analysis proceeds through the desired stepping procedures, the load follows the expression:

$$P_{total} = P_o + \lambda (P_{ref} - P_o) \tag{B1-1}$$

The load proportionality factor, $\lambda$, defines the current local magnitudes of the load. The value of $\lambda$ is determined by ABAQUS based upon the static equilibrium path followed during the solution process. The RIKS method works in a scaled solution space where the load and displacement dimensions are scaled to make the axes on the load-displacement curve the same magnitude. The length along the equilibrium path is defined to be the "arc length". The arc length, $l$, measures the progress of the solution. Once the computer finds the proper arc length, the load proportionality factor is automatically derived, not allowing the user any control over the load magnitude. RIKS method only works well if the equilibrium path in the load-displacement space is smooth and does not branch.
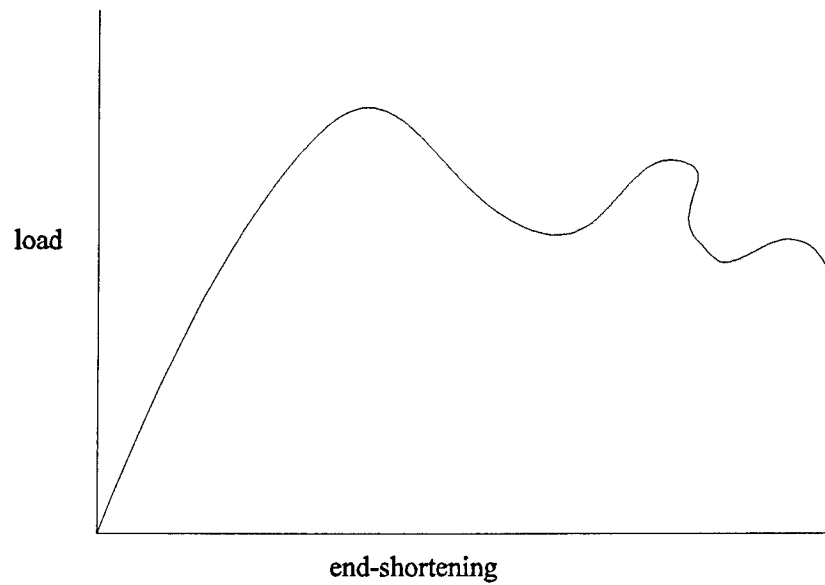
Figure B1.1: Typical load versus displacement relationship where a RIKS analysis would be necessary.